DEVELOPMENT AND BENCHMARKING OF NEW HARDWARE
ARCHITECTURES FOR EMERGING CRYPTOGRAPHIC TRANSFORMATIONS

by

Marcin Rogawski
A Dissertation
Submitted to the
Graduate Faculty
of
George Mason University
In Partial fulfillment of
The Requirements for the Degree
of
Doctor of Philosophy
Electrical and Computer Engineering

Committee:

_____   Dr. Kris Gaj, Dissertation Director

_____   Dr. Jens-Peter Kaps, Committee Member

_____   Dr. Qiliang Li, Committee Member

_____   Dr. Massimiliano Albanese, Committee Member

_____   Dr. Andre Manitius, Department Chair

_____   Dr. Kenneth S. Ball, Dean, Volgenau School
                                      of Engineering

Date: _____   Summer Semester 2013
                                  George Mason University
                                  Fairfax, VA

Development and Benchmarking of New Hardware Architectures for Emerging
Cryptographic Transformations

A dissertation submitted in partial fulfillment of the requirements for the degree of
Doctor of Philosophy at George Mason University

By

Marcin Rogawski
Master of Science
Military University of Technology, 2003

Director: Dr. Kris Gaj, Associate Professor
Department of Electrical and Computer Engineering

Summer Semester 2013
George Mason University
Fairfax, VA

Dedication

I dedicate this dissertation to my beloved wife and constant advocate, Kasia. Her patience, trust and support during these years in withstanding all the hours lost to my studies was critical to my success. To my mother Danusia and my stepfather Bohdan, who gave me the character and goal-oriented attitude, which has enabled me to get this far. To my parents-in-law Jadwiga and Czesław, who always believe, that my crazy ideas will work. Finally, I dedicate this thesis to the memory of my father Stanisław.

Acknowledgments

It is my great pleasure, but also a must, to acknowledge multiple individuals who supported me directly or indirectly in closing successfully this important chapter of my life.

First of all, I want to thank my advisor, Prof. Kris Gaj. I owe a lot to him for his precious guidance, support, encouragement, and always friendly atmosphere. His open mind, broad spectrum of knowledge, and accurate thinking helped me accomplish my goals. He has been a great mentor as well as a source of inspiration throughout my PhD study.

Furthermore, I like to thank Prof. Jens-Peter Kaps for his very valuable time, remarks, and comments. All of them were always delivered in a very constructive, but also cheerful form.

I also thank other dissertation committee members, Prof. Qiliang Li and Prof. Massimiliano Albanese. They provided sustained guidance, comments, advice and made my defense in almost relaxed atmosphere.

I would like to thank Prof. Andre Manitius for everything he has done for me an my wife. He made my GMU study time almost stress-free!

The role of supportive and welcoming friends and colleagues in the life of a researcher can not be forgotten. I would like to thank all the present and former members of Cryptographic Engineering Research Group, with a special distinction for Ekawat Homsirikamol for our model cooperation.

Finally, I would like to thank my wife, my parents, my brothers, and my big family for their unconditional support and for taking care of me more than I sometimes deserved.

Table of Contents

List of Tables

List of Figures

Abstract

DEVELOPMENT AND BENCHMARKING OF NEW HARDWARE ARCHITECTURES
FOR EMERGING CRYPTOGRAPHIC TRANSFORMATIONS

Marcin Rogawski, PhD

George Mason University, 2013

Dissertation Director: Dr. Kris Gaj

Cryptography is a very active branch of science. Due to the everlasting struggle between cryptographers, designing new algorithms, and cryptanalysts, attempting to break them, the cryptographic standards are constantly evolving. In the period 2007-2012, the National Institute of Standards and Technology (NIST) held a competition to select a new cryptographic hash function standard, called SHA-3. The major outcome of this contest, apart from the winner - Keccak, is a strong portfolio of cryptographic hash functions. One of the five final SHA-3 finalists, Grøstl, has been inspired by Advanced Encryption Standard (AES), and thus can share hardware resources with AES. As a part of this thesis, we have developed a new hardware architecture for a high-speed coprocessor supporting HMAC (Hash Message Authentication Code) based on Grøstl and AES in the counter mode. Both algorithms provide efficient hardware acceleration for the authenticated encryption functionality, used in multiple practical security protocols (e.g., IPSec, SSL, and SSH). Our coprocessor outperforms the most competitive design by Jarvinen in terms of the throughput and throughput/area ratio by 133% and 64%, respectively.

Pairing-based cryptography has emerged as an important alternative and supplement to traditional public key cryptography. Pairing-based schemes can be used for identity-based

encryption, tripartite key exchange protocols, short signatures, identity-based signatures, cryptanalysis, and many other important applications. Compared to other popular public key cryptosystems, such as ECC and RSA, pairing-based schemes are much more computationally intensive. Therefore, hardware acceleration based on modern high-performance FPGAs is an important implementation option. Pairing-schemes over prime fields are considered particularly resistant to cryptanalysis, but at the same time, the most challenging to implement in hardware. One of the most promising optimization options is taking advantage of embedded resources of modern FPGAs. Practically all FPGA vendors incorporate in modern FPGAs, apart from basic reconfigurable logic blocks, also embedded components, such as DSP units, Fast Carry Chain Adders, and large memory blocks. These hardwired FPGA resources, together with meticulously selected prime numbers, such as Mersenne, Fermat, or Solinas primes, can serve as a basis of an efficient hardware implementation. In this work, we demonstrate a novel high-speed architecture for Tate pairing over prime fields, based on the use of Solinas primes, Fast Carry Chains, and DSP units of modern FPGAs. Our architecture combines Booth recoding, Barrett modular reduction, and the high-radix carry-save representation in the new design for modular multiplication over Solinas primes. Similarly, a low-latency modular adder, based on high-radix carry save addition, Fast Carry Chains, and the Kogge-Stone architecture, has been proposed. The modular multiplier and adder based on the aforementioned principles have been used as basic building blocks for a higher level application - a high-speed hardware accelerator for Tate pairing on twisted supersingular Edwards curves over prime fields. The fastest version of our design calculates Tate pairing at the 80, 120 and 128-bit security level over prime fields in 0.13, 0.54 and 0.70 ms, respectively. It is the fastest pairing implementation over prime fields in the 120-128-bit security range.

Apart of the properly designed architectures for cryptographic algorithms, one more ingredient contributes to the success of a hardware coprocessor for any application - an

electronic design automation software and its set of options. Concerning this issue, Cryptographic Engineering Research Group (CERG) at Mason has developed an open-source environment, called ATHENa (Automated Tool for Hardware EvaluatioN), for fair, comprehensive, automated, and collaborative hardware benchmarking and optimization of algorithms implemented in FPGAs. One of the contributions of this thesis is the design of the heart of ATHENa: its most efficient heuristic optimization algorithm, called *GMU_Optimization_1*. As a basis of its development, multiple comprehensive experiments have been conducted. This algorithm has been demonstrated to provide up to 100% improvement in terms of the throughput to area ratio, when applied to 14 SHA-3 Round 2 candidates. Additionally, our optimization strategy is applicable to the optimization of dedicated hardware in any other area of science and engineering.

Keywords: Cryptography, High-performance hardware architectures, Pairing-based cryptography, modular arithmetic, authenticated encryption, heuristic methods for electronic design automation.

Chapter 1: Introduction

1.1 Motivation

New directions in Cryptography, namely Public Key Cryptography (PKC) discovery in 1976 by Diffie and Hellman [23], were introduced to solve the security problems such as confidentiality, authenticity, integrity, non-repudiation and also secure key exchange during communications in insecure networks. The first practical realization of PKC was RSA, proposed by Ron Rivest, Adi Shamir and Len Adleman in 1977 [24].

A digital signature scheme is a mathematical algorithm for demonstrating the authenticity of a digital message. Typically, digital signature is represented by a string of bits which is dependent on some secret known only to the signer (known as the signer's private key) and the content of the document being signed. Signatures have to be easily verifiable in case of a dispute about the origin of the document. An unbiased third party should be able to resolve this issue undeniably, without accessing signer's private key. Digital signatures are used to implement three major security services: authentication, integrity, and non-repudiation. Digital signatures are based on two main cryptographic transformations:

- a hash function, which takes an arbitrary size message and transforms it into a fixed-size hash value (also known as message digest), and

- a digital signature scheme, which takes: a private key of the signer and a hash value of the message to generate digital signature, and a public key of the signer, a hash value of the message, and a digital signature to verify whether a given digital signature is valid.

There are several security requirements for both algorithms: a hash function must be

0
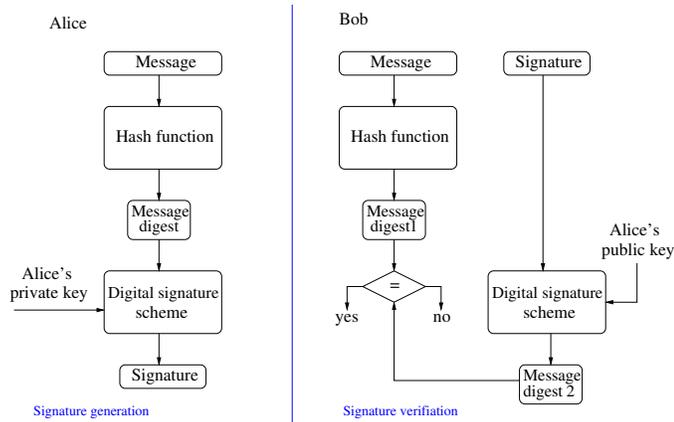
Figure 1.1: Digital signature generation and verification

irreversible and collision free and a digital signature scheme must be computationally infeasible to break. Digital signatures, key exchange and encryption schemes are used in a wide variety of Internet security protocols, such as Secure Socket Layer (SSL), Internet Protocol Security (IPSec), Domain Name System Security Extensions (DNSSec), Secure Border Gateway Protocol, etc. For example SSL uses digital signatures to authenticate secure web servers to their clients all over the world.

In IPSec the most important handshaking mode for the Internet Key Exchange protocol, apart from the key exchange support, is also based on a digital signature concept. The Domain Name System Security Extensions (DNSSec) is a new protocol for binding IP addresses and their domain names. The DNSSec requires digital signatures to provide strong authentication within the chain of trust. An aggregate signature is useful for reducing the size of certificate chains and for reducing message size in secure routing protocols such as Secure Border Gateway Protocol. These are just a few high level protocols, which are the basis of the security of any electronic information and in particular digital fund transfers used in on-line shopping, bank transactions and e-documents circulation.

For cryptographic hash functions, two families of algorithms, commonly referred to as SHA-1 and SHA-2, have been standardized by NIST, as described in the Federal Information

1

Processing Standard number 180 (the most current version is denoted FIPS-180-3). This standard defines the following variants of both families: SHA-1, SHA-2/224, SHA-2/256, SHA-2/384 and SHA-2/512. In 2005, a significant attack against SHA-1 was published [25]. A similarity between the SHA-1 and the SHA-2 specification raises the question about the possibility of extending this recently discovered attack to threaten the remaining four versions of Secure Hash Algorithm. This potential weakness in SHA-2 can affect the security of digital signature schemes based on this algorithm and finally, may undermine the robustness of cryptographic services using these signatures.

The National Institute of Standard and Technology (NIST) developed a memorandum with minimum key sizes for different security levels and for different underlying technologies. A sensitive data which is required to be protected at least until 2030 must be guarded by hash function SHA-2 with 256-bits output (SHA-3 will be an alternative solution), Advanced Encryption Standard with 128-bit key, and by digital signature schemes based on RSA and ECC technology with 3072 and 256-bits operands, respectively. The European Network of Excellence for Cryptology (ECRYPT) released similar recommendation for key sizes. However, it is stated in their work that the recommendations may need to be revised taking into account more efficient attacks that are known to exist for discrete logarithm over binary fields. The National Security Agency released the Fact Sheet NSA Suite B Cryptography where the aforementioned requirements were confirmed, but it also recommends a transition into elliptic curve systems instead of classical public key technology. This document provides the recommendation for the underlying modular arithmetic, the prime fields must be used, instead of binary and ternary fields.

Digital signature schemes and other cryptographic algorithms have been successfully implemented on a large spectrum of platforms: starting from dedicated smart card chips, through 8-bit microcontrollers, 32 and 64-bit microprocessors and finally, on high performance application specific security processors.

In general, software solutions demonstrate:

- relatively low performance, and large power and energy consumption,

- difficulty in terms of generation truly random keys,

- vulnerability to software malware and a big class of side channel attacks (e.g. timing attacks, cache attacks, etc.)

Contrary to software implementations, Application Specific Integrated Circuits (ASIC technology) require long development time and a very expensive computer-aided design (CAD) software. Moreover, after fabrication of an ASIC device, the designers cannot introduce any upgrades to the implementation. ASIC-based solution are very costly in low volumes, they require extensive and expensive testing, and the fabrication mistakes are unrecoverable.

Cryptographic services, based on digital signature schemes, key exchange and encryption schemes, are at the beginning of a new era. Novel basic cryptographic transformations, based on the cutting edge underlying technology, for the the aforementioned schemes were developed recently. They offer not only higher security, but also a set of new properties. It is possible to apply them to a big range of new applications.

In case of cryptographic hash functions NIST has started a public competition for a new SHA-3 function. Out of initial 51 candidates, only 5 algorithms were selected to the 3rd and final round: BLAKE, Grøstl, JH, Keccak and Skein. In December 2012 Keccak has been announced the winner of the contest.

Four major criteria were taken into account in the evaluation of these candidates are:

- security,

- performance in software,

- performance in hardware, and

- flexibility.

While security is commonly recognized as the most important evaluation criterion, it is also a measure that is most difficult to evaluate and quantify, especially during a relatively short period of time reserved for the majority of contests. So far all five SHA-3 final round
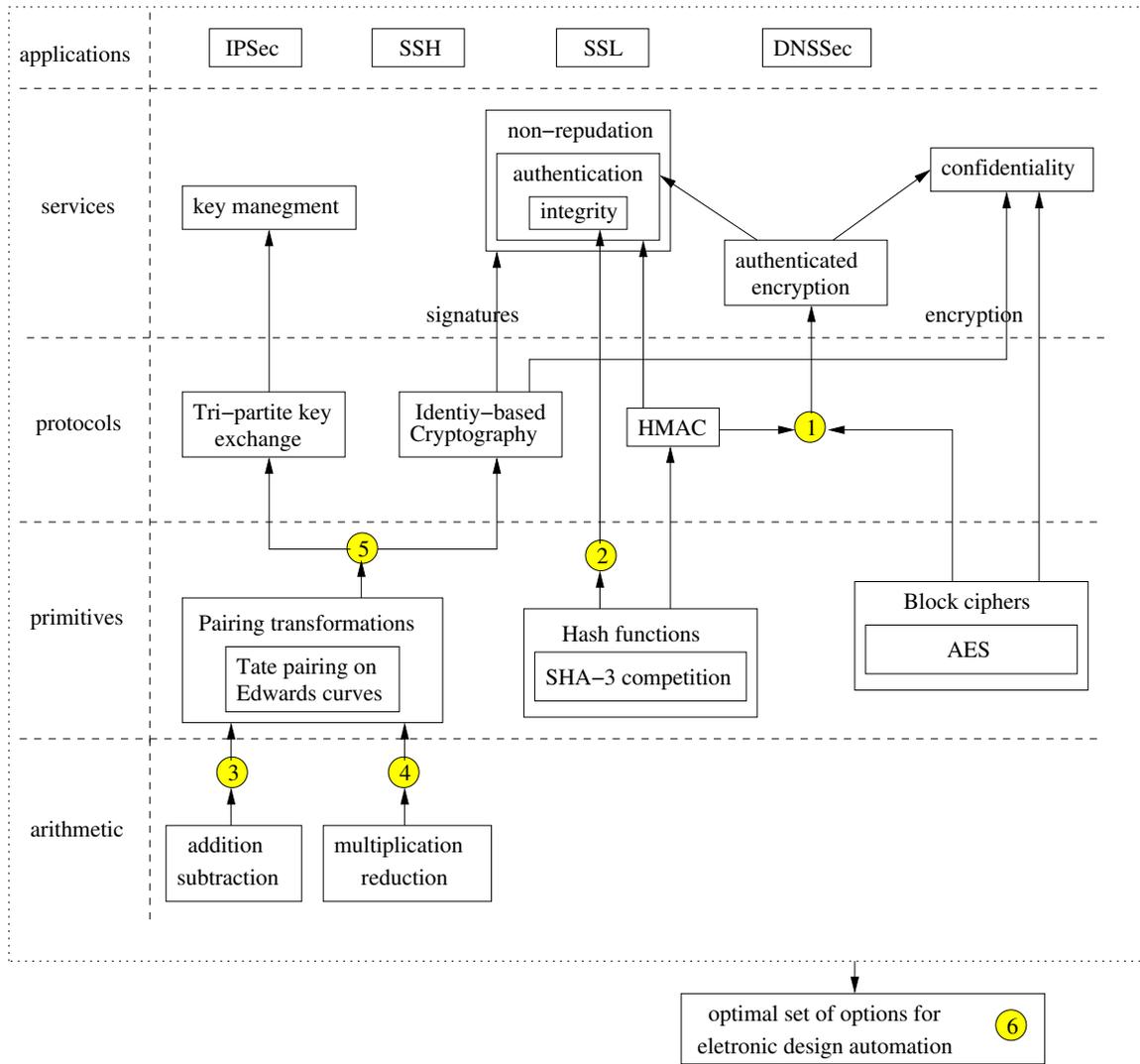
Figure 1.2: Hierarchical model of Cryptographic applications. Major contribution of this research marked with points 1-6.

candidates demonstrate higher security margin than SHA-2 algorithm. Comprehensive analysis of hardware and software implementations of final candidates was conducted by multiple cryptographic engineering research groups all over the world. These studies show potential throughput gain over solutions based on current standard. On the other hand they also show that SHA-3 will be more expensive in terms of area used in hardware.

Pairing-based schemes can be used as basic building blocks for such high level protocols like:

- identity-based encryption (identity used as a key for encryption),

- identity-based signatures (identity used as a key for signing),

- triparite key exchange (one round of computations allow the key agreement between three parties)

- group signatures (a method for allowing a member of a group to anonymously sign a message on behalf of the group),

- blind signatures (the content of a message is disguised before it is signed),

- aggregate signatures (given n signatures applied to n messages from n users, it is possible to aggregate all these signatures into a single signature which size is independent of the number of users).

This novel technology bridges the gap between the classical Public Key and the Elliptic Curve Cryptography.

In general pairing algorithms take two arguments two elliptic curve points P and Q from two different algebraic groups G_1 and G_2 and it produces an element of the third algebraic group G_T.

The most important properties of these G_1 x $G_2 \rightarrow G_T$ functions are:

- bilinearity $\forall a, b \in Z_p$: $e(aP, bQ) = e(P, Q)^{ab}$,

- non-degeneracy (function $e(P, Q)$ never returns '1')

- and efficiency in computations.

Different types of pairing functions were developed in the past, but for the prime fields the most practical are the Tate and the Optimal Ate pairing transformations. Both of them are based on the concept of iterative calculation (Miller's algorithm [27]) of a new value of pairing function for a given evaluation point, and a calculation of a new evaluation point. The Tate pairing is most efficient for the ordinary Elliptic Curves and the Optimal Ate pairing for a special class of - so called Barreto-Naehrig (B-N) curves.

In 2007 a new form of elliptic curves was discovered, so called Edwards curves. The advantages of this new form are:

- the fastest reported in the literature unified procedure for addition and doubling points,

- it is possible to embed those basic operations together with Tate pairing function evaluation,

- twisted Edwards curves with extended projective coordinates are very easy for parallelization and in fact potentially the most hardware-friendly.

In recent years implementations of cryptography on FPGAs became a popular subject in academic research and in commercial security products. Historically, FPGAs have been slower, less energy efficient and generally achieved lower physical security than their fixed ASIC counterparts. Advantages include the ability to re-program in the field to fix bugs, a shorter time to market, and lower non-recurring engineering costs. Some FPGAs have the capability of partial re-configuration that lets one portion of the device be re-programmed while other portions continue running.

In comparison to software implementations, FPGA-based cryptographic systems are faster in majority of cases, they consume less power and they offer temper resistance and overall higher security. In favor of general-purpose microprocessors software implementations have even higher flexibility and smaller development costs. Both software and FPGA

developers have an access to freely available design tools. One of the most important reasons why FPGA-based cryptographic systems are successful is the specific nature of cryptographic market and the requirements for commercial products in this sensitive area. In the developed countries, the governments require that cryptographic products pass certification process, They also demand to be involved in the design process of those solutions and to have an access to their source codes. This general policy makes the cryptographic product's market suffer from a lack of global companies. In case of relatively small companies an ideal solution for a cryptographic system, which requires high performance, capability for upgrades, low volume, and a short time to market, are the FPGA devices.

This thesis aims to answer a question: Can the recent advances in the theory of Elliptic Curves and pairing functions (namely the invention of Edwards Curves and its application to the Tate pairing) and in the theory of hash functions (namely the development of the SHA-3 standard) be exploited to develop the most efficient FPGA-based hardware architecture for the most important cryptographic services, outperforming all previously known architectures with equivalent security?

1.2   Summary of research contributions

1.2.1   Novel hardware accelerator for authenticated encryption

SHA-3 finalist, hash function Grøstl, has been inspired by the Advanced Encryption Standard (AES). This unique feature can be exploited in a large variety of practical applications (Fig. 1.2 pt. 1). In order to have a better picture of the Grøstl-AES computational efficiency (high-level scheduling, internal pipelining, resource sharing, etc.), we designed a high-speed coprocessor for the Grøstl-based HMAC and AES in the counter mode. This coprocessor offers high-speed computations of both authentication and encryption with relatively small penalty in terms of area and speed when compared to the authentication (original Grøstl circuitry) functionality only. It is almost certain that the highest quality cryptographic

algorithms, like SHA-3 finalists, will find their niche applications.

For example: this coprocessor outperforms similar hardware accelerator proposed in [1] for both IPSec modes: IP Encapsulating Security Payload (ESP) and Authentication Headers (AH) by 64% and 8%, respectively. In case of the relatively rare the ESP's encryption mode only, the coprocessor from [1] is better by 44% as compared to our results.

Extracts of this work were published as joint work with Ekawat Homsirikamol and Kris Gaj [28] and [29]

1.2.2 An adaptation of the T-box method to the AES-like hash functions

Joan Daemen, co-inventor of arguably two most important cryptographic standards - Advanced Encryption Standards (AES) and Secure Hash Algorithm (Keccak), proposed in his PhD thesis, a provably secure method of building cryptographic transformation, the *Wide Trail Strategy*. A block cipher SHARK was build upon this principle and a new, so called Table-box method for very efficient implementation of this algorithm was published in 1996. This mathod allows to redefine the round structure in a such a way, that it is friendly for FPGA memory blocks. Several researchers have proposed hardware coprocessors for AES based on the T-box method, which are the fastest [30], the most efficient [31], and implementation attacks resistant [32]. In our research we concentrated on the *Wide Trail Strategy* progeny, the AES-based hash functions: ECHO, Fugue, Grøstl-0 and SHAvite-3 ((Fig. 1.2 pt. 2)). The efficiency of the hardware accelerators for aforementioned algorithms have been improved up to 49, 173, 424 and 262 %, respectively. In this work, we have extended our work for SHA-3 finalist, Grøstl. We have demonstrated, the best hardware accelerator in terms throughput/area ratio, reported in open literature.

Extracts of this work were published as joint work with Rabia Shahid, Malik Umar Sharif and Kris Gaj [33] and [34].

1.2.3 A novel, adder/subtractor for thousand bit and more using fast carry chains of modern FPGAs

We have demonstrated a new, low latency, FPGA-oriented, hybrid adder ((Fig. 1.2 pt. 3)). This adder efficiently combines the ideas of high-radix carry save addition based on the fast carry chains, available on modern FPGA devices, and the parallel prefix network. The implementation results reveals that this hybrid adder has a great potential for the addition and modular addition of the long-size integers.

For example, our adder outperform, in terms of latency · area, both classical designs: Kogge-Stone and Brent-Kung, on 1024, 2048 and 4096-bits addition up to 50, 38 and 35%, respectively. At the same time, in terms of latency, our design is very competitive to the both, commonly accepted, as the fastest adders in open literature.

Moreover, our hybrid high-radix carry save adder with carry projection unit based on parallel prefix network have been applied to the 1024-bit modular addition circuit. The implementation results on modern FPGA devices have proven that in terms of latency, area and latency · area product, for Altera devices, have been improved over both classical designs, on average 15, 40 and 55%, respectively. In case of Xilinx devices these numbers were 50, 45 and 70%, respectively.

Extracts of this work were published as joint work with Kris Gaj and Ekawat Homsirikamol [35].

1.2.4 New approach to arithmetic based on the Solinas primes for Pairing-based Cryptography

A well known shortcut for a modular multiplication modulo a Mersenne number $(2^k - 1)$, performing modular reduction without integer division has been generalized by Jerome A. Solinas, a researcher from National Security Agency (NSA). The prime numbers generated using his method and the fast arithmetic developed for them have been named after him.

These concepts have been such a important invention, that a big class of Solinas prime numbers and their efficient arithmetic have been widely accepted, recommended and in fact they became a part of a elliptic curved-based digital signature standard.

The aforementioned reduction technique is not applicable for all Solinas primes, in particular for those which are used in Pairing-based Cryptography.

First, we have demonstrated that Solinas primes can benefit from the modified Barrett reduction algorithm and then we have proposed conditions for efficient arithmetic based on those primes. Next, we have optimized a grid method for multiplication to the geometry of the digital signal processing blocks (DSP units), embedded in the structure of modern FPGA devices.

This simple, thus very flexible design can give us some unique features - e.g.: it allows to speed up single multiplication by using two multipliers. This special feature is especially attractive in case of n multiplications, m available multipliers, and n dividing m. (e.g.: a coprocessor build upon four multipliers, and a single iteration of the final exponentiation algorithm in case of supersingular curves with embedding degree $k = 2$ requires 2 multiplications).

Finally, we have combined both concepts: grid multiplication method optimized for FPGAs and the Barrett reduction for Solinas primes, and as a result we have obtained, optimal, modular multiplier for pairing-friendly Solinas primes (Fig. 1.2 pt. 4).

Extracts of this work were published as joint work with Kris Gaj [36]

1.2.5   Novel hardware architectures for pairing on Edwards curves

We are going to demonstrate the first and the only to date, a high speed hardware accelerator for the Tate pairing on twisted supersingular Edwards curves over prime fields (Fig. 1.2 pt. 5). Our hardware architecture is based on the set of algorithms presented in [37]. It can be used directly to support emerging pairing-based protocols. This coprocessor was built upon the hardware architectures proposed for Solinas primes and the hybrid high-radix carry save

and parallel prefix network adder. We demonstrate that combining aforementioned concepts together with novel method for optimizations for final exponentiation, tight pipelining for optimal number of processing units can improve an alternative software implementation by a factor of 50 for three different security levels.

Finally, we have demonstrated, that even though Edwards curves were not optimized for pairing, they present an interesting alternative to pairing friendly Barreto-Naehrig curves. The implementation results, the hardware accelerator based on Stratix V, are elevating it, to the top of the list of the fastest, to date, pairing solution over prime fields in a security range 120-128-bits.

Extracts of this work were published as joint work with Kris Gaj [36]

1.2.6 A heuristic strategy for FPGA-oriented electronic design automation

In 2010 Cryptographic Engineering Research Group have introduced an open-source environment, called ATHENa for fair, comprehensive, automated, and collaborative hardware benchmarking of algorithms belonging to the same class. Apart from this primary use for a fair evaluation of functionally equivalent digital system designs targeting FPGAs, a major goal for this design automation system is an efficient search for the best set of options for a given optimization criterium. In this work we have demonstrated the design rationale of the most successful heuristic optimization algorithm, the ATHENa's heart, *GMU_Optimization_1* (Fig. 1.2 pt. 6). This method helps to improve up to 100% throughput/area ratio of hardware accelerators for major FPGA vendors and for functionally different digital circuits (e.g.: modular arithmetic, pairing systems, hash function and block ciphers).

Extracts of this work were published as joint work with Kris Gaj, Jens-Peter Kaps, Venkata Amriamieni, Ekawat Homsirikamol, and Benjamin Brewster in [38]. The heuristic method "GMU_Optimization_1" helped to achieve the best to date hardware implementation

results in multiple our papers, including [39], [21], [40], [33], [28], [36] and [29].

Part I

High-performance hardware architectures supporting confidentiality and integrity

Chapter 2: High-Throughput hardware architectures of AES-like Cryptographic hash functions

This chapter presents two unique hardware architectures for coprocessors supporting AES-like hash functions. First, we demonstrate an adaptation of T-table (also called T-box) method for the AES-based family of hash functions. We have used SHA-3 finalist, Grøstl, to show that this method gives the best throughput/area ratio for hardware implementations of this important class of cryptographic transformations. Finally, we have demonstrated how to use Grøstl and AES cipher similarities and convert them into a coprocessor which offers high-speed computations of both authentication and encryption.

Contents

2.1   Introduction and motivation

In the period 2007-2012, the National Institute of Standards and Technology (NIST) was holding a hash competition [41] to select a new cryptographic hash function standard, called

SHA-3, for the purpose of superseding the functions in the SHA-2 family [42]. Performance in hardware has been one of the major factors taken into account by NIST in the evaluation of Round 2 and Round 3 candidates during the SHA-3 competition [41], [43], [44]. This factor was particularly important in the final round of the contest, because the algorithms qualified to this round were not very likely to have any significant security weaknesses.

On October 2, 2012, Keccak [45] has been announced to be the winner of the NIST hash function competition [46]. This algorithm has demonstrated medium speed in software implementations [47], [48], and the best results in terms of hardware efficiency for both single stream [43] and multiple streams of data in hardware implementations [39].

Beyond any doubt, cryptographic standards for block ciphers: AES [49] and 3DES [50] and hash functions SHA-2 [42] and newly selected future standard - Keccak [45] are the most important crypto-algorithms for both Academia and Industry.

The SHA-3 competition was very similar in many aspects to the AES competition [51]: both were open and fully transparent contests, organized by NIST. They have received relatively big attention from the cryptographic community and the final result was announced after multiple years of intensive investigations in the area of security, hardware and software performance. The major outcome from both contests seems to be as well as very similar - a strong portfolio of cryptographic transformations.

Apart from the winner of AES contest, almost all finalists have been either implemented in different commercial products (e.g.: [52], [53], [54]) or they were patented [55]. It is almost certain that the highest quality cryptographic algorithms, like SHA-3 finalists, will find their niche applications.

The main objective of almost all SHA-3 related studies was to evaluate all candidates using a uniform approach, and therefore the unique features of each and every function were not deeply investigated.

There are relatively few works that discuss any distinctive hardware architectures for the SHA-3 candidates. A coprocessor supporting Skein in tree hashing mode was presented in [56]. Common architectures of the block cipher AES and the Round 2 versions of Grøstl-0

and Fugue algorithms were reported in [1]. Recently, a high-speed AES-Grøstl architecture was also reported in [57].

A compact implementation of the block cipher Threefish and the Round 3 hash algorithm Skein was demonstrated in [58]. Three outstanding low-area, resource-sharing oriented coprocessors, for combinations: Round 3 version of Grøstl/AES and ECHO/AES were proposed, designed and discussed in [59], [60] and [61], respectively.

The similarities between AES and Grøstl (or any other AES-like hash function - Fig. 2.1) lead us to two, unique and important architectures.

First of all, the majority of AES hardware accelerators implement a single round in a straightforward way or using loop-unrolling, pipelining techniques for FPGAs, utilizing a vast amount of user logic elements. This approach, based on a traditional configurable logic utilization, help to maintain platform independence, and therefore it does not exploit the full potential of modern FPGA devices. Contrary, the T-table method, described in [62], Sec. 4.2 enables the memory-oriented re-definition of AES round, and it eventually leads to the highly efficient hardware architecture of AES.

To the best of our knowledge, our work [33] was the very first one, which demonstrated a T-table-based representation of Grøstl-0 (and also ECHO, Fugue and SHAvite-3).

Second important implication of this compatibility between the current encryption standard, AES and the whole family of AES-derived hash function is their joint use for authenticated encryption. A typical application for such cryptographic service could be Secure Socket Layer [63], Transport Layer Security [64], Secure Shell [65] and Internet Protocol Security [66–68].

The rest of this chapter is organized as follows:

In Section 2.2 we discuss relevant previous work. Section 2.3 is devoted to the description of the T-table architecture of Grøstl. Section 2.4 demonstrates the design of a hardware coprocessor for authenticated encryption.

2.2 Previous work

2.2.1 Grøstl in SHA-3 competition

In January 2011, Grøstl team published tweaks to their specification of Grøstl [69], [17]. An algorithm described by the original Grøstl specification [70] has been renamed to Grøstl-0, and the tweaked version of Grøstl, described by the revised specification [17], is from this point-on called Grøstl. The proposed tweaks are aimed primarily at the increase in the algorithm resistance to cryptanalysis [69]. This increased resistance in security, typically comes together with some limited penalty in terms of performance in hardware [71].

Grøstl-0 has been implemented by several groups in FPGAs and ASICs [43]. In this chapter, we focus on implementations targeting FPGAs and optimized for high speed rather than low area. High-speed implementations of Grøstl-0 typically use two major architectures. In the first architecture, reported first in [70], permutations P and Q are implemented using two independent units, working in parallel. We call this architecture parallel architecture. In the second architecture, introduced in [72], the same unit is used to implement both P and Q. This unit is composed of two pipeline stages that allow interleaving computations belonging to permutations P and Q. We call this architecture quasi-pipelined architecture, as it is based on the similar principles as the quasi-pipelined architectures of SHA-1 and SHA-2 reported in [73], [74]. The details of the quasi-pipelined architecture of Grøstl-0 are described in [72] (Section 9), [75] (Section 3.8) and [76] (Section V).

An analysis of the influence of the Round 3 tweaks in Grøstl on the performance of this algorithm in FPGAs was conducted in [71]. Comprehensive hardware evaluation across multiple architectures for all SHA-3 finalists, including Grøstl, was investigated in [39] and [81]. The implementation results of hardware architectures, for a single stream of data, in both variants of Grøstl-256 are summarized in Table 2.1.

Table 2.1: Results of Implementations for High-Speed Architectures
of Grøstl-256, using Xilinx Virtex 5 FPGAs.

Source	Memory [BRAM]	Frequency [MHz]	Throughput [Mbps]	Area [Slice]	Throughput/Area [Mbps/Slice]
Grøstl-0 - Round 2					
Gauravaram et al. [70]	N/A	200.7	10276	1722	5.97
Jungk et al. [76]	17	295.0	7552	1381	5.46
Shahid et al. [40]	48	250.0	6098	1188	5.13
Homsirikamol et al. [75]	0	323.4	7885	1597	4.94
Gaj et al. [21]	0	355.9	8676	1884	4.61
Matsuo et al. [77]	0	154.0	7885	2616	3.01
Baldwin et al. [78]	0	101.3	5187	2391	2.17
Kobayashi et al. [79]	0	101.0	5171	4057	1.27
Guo et al. [80]	0	80.2	4106	3308	1.24
Baldwin et al. [78]	0	101.3	3242	2391	1.36
Baldwin et al. [78]	0	78.1	2498	2579	0.97
Grøstl - Round 3					
Sharif et al. [33]	18	226	5524	1141	4.84
Gaj et al. [81]	0	251	6117	1795	3.41
Homsirikamol et al. [39]	0	249	6072	1912	3.18
Homsirikamol et al. [39]	0	158	8081	2591	3.12

2.2.2 T-box method

Joan Daemen, in his PhD thesis [2], proposed the Wide Trail Strategy. It is a method of constructing highly efficient block ciphers, which are provably secure against major cryptanalytical attacks.

This Wide Trail Strategy became a design rationale of several cryptographic transformations (Fig. 2.1). Most of them demonstrate not only the hardware-software efficiency and flexibility, but also an elegance in their description.

Fig. 2.1 presents the timeline development of the aforementioned class of cryptographic transformations.

In paper [3], Shark ((Fig. 2.1 pt. 4) pt. 1) was proposed together with its efficient implementation methods. This paper demonstrated how to combine several simpler mathematical transformations into one operation equivalent to a round. This method was named table implementation, T-table or T-box implementation.

To the best of our knowledge, the first attempt of the adoption of this method for the hardware implementation of the AES round was proposed by Fischer and Drutarovsky in
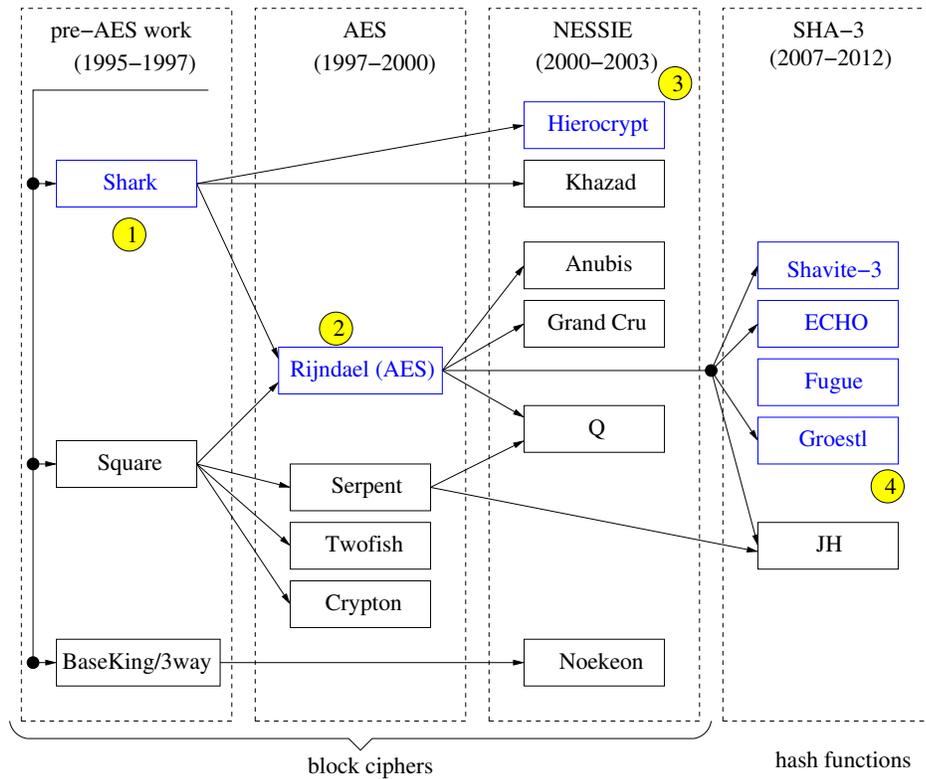
Figure 2.1: Wide Trail Strategy family of cryptographic transformations was defined in [2]. Based on this strategy several algorithms have been invented: Shark [3], Square [4], BaseKing [2], Rijndael-AES [5], Serpent [6], Twofish [7], Crypton [8], Hiercorypt [9], Khazad [10], Anubis [11], GrandCru [12], Q [13], Noekeon [14], ECHO [15], Fugue [16], Grøstl [17], SHAvite-3 [18] and JH [19]

[31] (Fig. 2.1 pt. 2). Contrary to that implementation the design, described by Drimer et al. in [30], maps the complete AES data path onto embedded elements contained in Virtex-5 FPGAs. This strategy provides most savings in logic and routing resources and results in the highest data throughput on FPGAs reported in open literature.

Taking into account the fact that the whole AES family (Fig. 2.1) is built upon similar principles, several implementational nuances can be inherited. We have proposed architectural improvements, using aforementioned technique, for block cipher Hierocrypt in [34] (Fig. 2.1 pt. 3) and hash functions: ECHO, Fugue, Grøstl-0 and SHAvite-3 in [33] (Fig. 2.1 pt. 4). Table 2.2 summarizes the geometry of the T-tables reported in open literature.

Table 2.2: Table-based hardware architectures of cryptographic transformations. T-box geometry AxB is defined by A-bit address space and B-bit words.

algorithm	T-box size	source
Block Ciphers		
AES	8x32	Fischer et al. [31], Drimer et al. [30]
Hierocrypt-3	8x32	Rogawski [34]
Hash Functions		
Grøstl-0	8x40	Shahid et al. [40]
Fugue	8x24, 8x32	Shahid et al. [40]
ECHO	8x32	Shahid et al. [40]
SHAvite-3	8x32	Shahid et al. [40]
Grøstl	8x40	ch. 2.3

2.2.3 Resource sharing

The idea of hardware resource sharing is very practical and especially attractive in industrial applications. Several companies offer so called all-in-one cryptographic solutions. For example, [82] and [83] offer customized cores, including sophisticated AES core, which supports 128, 192 and 256-bit main key and several different operational modes in a single chip. This concept was also investigated by academia: shared MD5 and SHA-1 implementation was described in [84–86], MD5 implemented together with RIPEMD-160 was reported in [87], a combined SHA-1, MD-5 and RIPEMD-160, core was discussed in [88]. Fugue with

Table 2.3: Hardware architectures supporting authenticated encryption at 128-bit security

Source	Algorytms	FPGA	Frequency [MHz]	Area [Slice/LE]	Throughput [Mbps]	Throughput/Area [Mbps/(Slice/LE)]
Balanced designs						
Rogawski et al. [28]	Grøstl-0 and AES	Cyclone III	159.9	23039	2640	0.12
Järvinen [1]	Grøstl-0 and AES	Cyclone III	53.4	13723	956[1]	0.07
Järvinen [1]	Fugue and AES	Cyclone III	59.8	4875	273[1]	0.06
Low area designs						
At et al. [90]	Grøstl and AES[2]	Virtex-6	393	169[4]	64.6[1]	0.38
Beuchat et al. [91]	ECHO and AES[3]	Virtex-6	397	155[5]	62.6[1]	0.40
At et al. [58]	Skein and Twofish	Virtex-6	276	132[5]	40.0[1]	0.30
[1] throughput recalculated for authenticated encryption based on HMAC-(hash function) and CTR-(block cipher)						
[2] this design offers Grøstl-256, Grøstl-512, AES-128, AES-192 and AES-256						
[3] this design offers ECHO-256, ECHO-512, AES-128, AES-192 and AES-256						
[4] this design uses one extra block RAM						
[5] this design uses two extra block RAMs						

AES core, and Grøstl-0 with AES core, were reported in [1]. Based on this trend, the practicality of combining different cryptographic services, confidentiality and authentication, into a single coprocessor by sharing resources as much as possible is a favored approach by the industry and academia. Table 2.3 summarizes the related work in this area.

Alternatively, a partial reconfiguration method can be used to conserve space at the cost of reconfiguration time penalty, as well as limiting hardware operating life, due to the limited number of times the chip can be configured. This approach has been demonstrated in the combined AES, SHA-2 and a modular multiplication core in [89].

A typical application for resource sharing-based coprocessor will be the IPSec protocol suite [66] for securing the Internet Protocol, which is the basis of Internet. This suite consists of the Authentication Header Protocol (providing authentication only) and Encapsulating Security Payload (providing confidentiality and optional authentication at the same time).
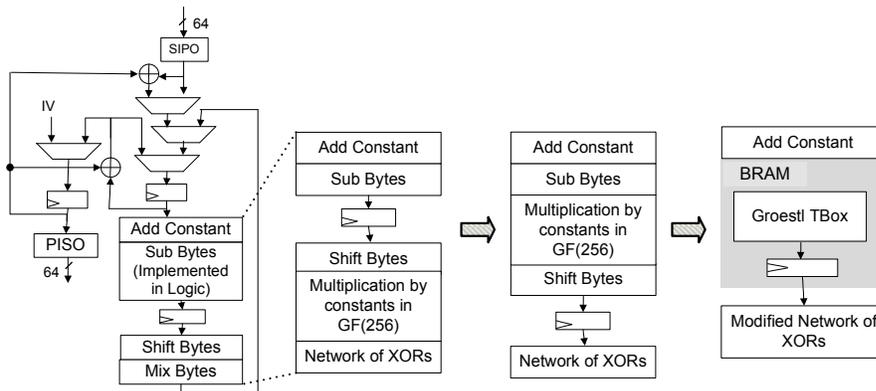
Figure 2.2: Phases in the Grøstl-0 round transformation to T-box representation.

2.3 Table-based method extension for AES-like cryptographic transformations (Grøstl case)

2.3.1 T-box-based hardware architecture of Grøstl-0 and Grøstl

In our paper [21], we have investigated SHA-3 round 2 candidates, including an investigation of a Grøstl-0 quasi-pipelined architecture, originally defined in [72]. Later on in [39], among multiple other architectures, we have extended this architecture for the Grøstl hash function. In case of this function, the quasi-pipelined architecture (together with parallel architecture) is considered the best for a single stream of data [71].

In order to represent Grøstl-0 round function, in the T-table form, there is no need to change anything in the top-level block diagram of high-speed quasi-pipelined architecture reported in [21]. The process of translating the round transformation to T-box version can be divided into three phases, and it is summarized in Fig. 2.2:

phase 1: in the MixBytes operation, represented by Fig. 2.3, we have to differentiate between: multiplication in $GF(2^8)$ by five different constants (0x02, 0x03, 0x04, 0x05 and 0x07) (Fig. 2.5) from the computation of output bytes using the Network of XORs.

22

O= MxI , I and O are 64−bit input and output, respectively.

$$
\begin{bmatrix} O[0] \\ O[1] \\ O[2] \\ O[3] \\ O[4] \\ O[5] \\ O[6] \\ O[7] \end{bmatrix} = \begin{bmatrix} 02 & 02 & 03 & 04 & 05 & 03 & 05 & 07 \\ 07 & 02 & 02 & 03 & 04 & 05 & 03 & 05 \\ 05 & 07 & 02 & 02 & 03 & 04 & 05 & 03 \\ 03 & 05 & 07 & 02 & 02 & 03 & 04 & 05 \\ 05 & 03 & 05 & 07 & 02 & 02 & 03 & 04 \\ 04 & 05 & 03 & 05 & 07 & 02 & 02 & 03 \\ 03 & 04 & 05 & 03 & 05 & 07 & 02 & 02 \\ 02 & 03 & 04 & 05 & 03 & 05 & 07 & 02 \end{bmatrix} * \begin{bmatrix} I[0] \\ I[1] \\ I[2] \\ I[3] \\ I[4] \\ I[5] \\ I[6] \\ I[7] \end{bmatrix}
$$

Figure 2.3: The Grøstl's MixBytes operation

O = MxI

$$
\begin{bmatrix} O[i] \\ O[i+1] \\ O[i+2] \\ O[i+3] \\ O[i+4] \\ O[i+5] \\ O[i+6] \\ O[i+7] \end{bmatrix} = I[i] * \begin{bmatrix} 02 \\ 03 \\ 04 \\ 05 \\ 07 \end{bmatrix} \oplus I[i+1] * \begin{bmatrix} 02 \\ 03 \\ 04 \\ 05 \\ 07 \end{bmatrix} \oplus I[i+2] * \begin{bmatrix} 02 \\ 03 \\ 04 \\ 05 \\ 07 \end{bmatrix} \oplus I[i+3] * \begin{bmatrix} 02 \\ 03 \\ 04 \\ 05 \\ 07 \end{bmatrix} \oplus I[i+4] * \begin{bmatrix} 02 \\ 03 \\ 04 \\ 05 \\ 07 \end{bmatrix} \oplus I[i+5] * \begin{bmatrix} 02 \\ 03 \\ 04 \\ 05 \\ 07 \end{bmatrix} \oplus I[i+6] * \begin{bmatrix} 02 \\ 03 \\ 04 \\ 05 \\ 07 \end{bmatrix} \oplus I[i+7] * \begin{bmatrix} 02 \\ 03 \\ 04 \\ 05 \\ 07 \end{bmatrix}
$$

Figure 2.4: The Grøstl's MixBytes operation based on reduced number of multipliers

In the MixBytes operation every single byte is multiplied by eight values in Matrix B [92], [69]. Following the idea from [31], we would represent our T-boxes as 8x64 bit substitution box tables. However, due to the fact that there are only five unique values in Matrix B (Fig.: 2.4), our proposed Grøstl-0 T-box has the dimensions 8x40 (8-bit address bus width, 40-bit words).

phase 2: the operations of Multiplication by constants in $GF(2^8)$ and S-box transformation both produce 8 bits of output for every 8 bits of input. Therefore, it is possible

S[i]

(x 02) (x 03) (x 04) (x 05) (x 07)

T[i]   i = 0,1, ... 7

S[i] − output from S−box

T[i] − input to the network of XORs in
vector multiplication by matrix
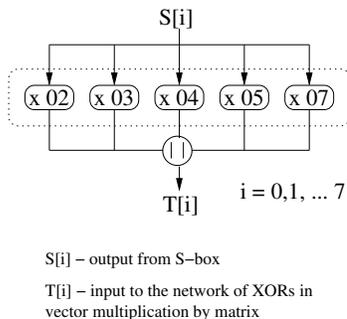
Figure 2.5: Grøstl's MixBytes single input byte multiplication by five unique values

	x02	x03	x04	x05	x07
0x00	00	00	00	00	00
0x01	02	03	04	05	07
....	....	....	....	....	....
0xFE	E7	19	D5	2B	CC
0xFF	E5	1A	D1	2E	CB

Figure 2.6: Grøstl's MixBytes table implemented as 256x40 bits ROM

	x02	x03	x04	x05	x07
0x00	C6	A5	97	F4	32
0x01	F8	84	EB	97	6F
....	....	....	....	....	....
0xFE	6D	D6	DA	61	0C
0xFF	2C	3A	58	4E	62

Figure 2.7: Grøstl's round table implemented as 256x40 bits ROM

to combine them. Since there are five different constants used in multiplications, then for every single byte there are always 5 bytes produced. We can define a look-up table with 256 words (8 bit address bus) which consist of 5-byte-wide words. One of the property of both AES and Grøstl-0 is the horizontal symmetry (every byte goes through the same set of operations) in SubBytes, ShiftBytes and MixBytes (ShiftRow and MixColumn in AES). This allows us to move the ShiftBytes operation after Multiplication by constants.

phase 3: since ShiftBytes is a simple operation, which is implemented using routing resources only in hardware, it is possible to merge this operation together with the network of XORs operation.

Such defined Grøstl-0 T-box round can be implemented in configurable logic, but due to the fact that there are 64 (in Grøstl-0-256) and 128 (in Grøstl-0-512) such 256x40 bits

loop-up tables for quasi-pipeline architecture (and this number is doubled for parallel architecture), a large number of regular logic resources is going to be occupied, and clearly there is no benefit from such a solution. However, if we implement this operation using embedded memories, both parallel and quasi-pipelined architecture can benefit from the Grøstl-0 T-box round representation. The quasi-pipelined architecture [75] was used for our T-box implementation. The pipeline register between SubBytes and ShiftBytes from this architecture was implemented as a part of the registered output from FPGA block memory. We used inference method for the implementation of the T-box in a block memory in VHDL. Because of the restrictions on the maximum word size in the Virtex 5 BRAM, we have divided a 256x40 bit memory into two memories with the dimensions, 256x32 and 256x8, respectively.

Tweaks introduced to the Grøstl specification do not affect the Grøstl T-box definition (i.e., this definition is common for both Grøstl-0 and Grøstl). The only change that have to be introduced concerned both AddRoundConstant and the Modified Network of XOR operations.

2.3.2 Implementation results

In this section, we present a comparison between the basic designs, implemented using reconfigurable logic, and embedded designs, with Block Memories. All basic designs are identical to those described in detail in [21]. All the embedded designs were, so called, T-box-based architectures with T-box tables implemented using block memories.

In Table 2.4, we demonstrate comprehensive results of throughput analysis across two high-performance (Xilinx Virtex-5 and Altera Stratix III) and two low-cost FPGA families (Xilinx Spartan 3 and Altera Cyclone II). We optimized the designs to achieve comparable throughput while replacing logic with embedded resources. However, we observed a significant drop in frequency and throughput across high-performance families. In case of the selected low-cost families the frequency, and consequently the throughput, were consistently

Table 2.4: Timing characteristics and resource utilization for basic architectures and architectures based on the T-box method in case of four selected FPGA families. Notation: Tp - throughput, Mem-bits - number of memory bits, Δ Tp - relative improvement in throughput, Δ Area - relative reduction in the number of basic reconfigurable resources, Δ Tp/Area - relative improvement in throughput/area

Algorithm	Architecture	Tp	Area	Tp/Area	Δ Tp	Δ Area	Δ Tp/Area
Altera Cyclone II [1]							
		Mbps	#LEs, #Mem-bits	Tp/#LEs	%	%	%
Fugue	Basic	1490	5825, 0	0.26	23.3	55.6	173.5
	T-box	1837	2855, 99k	0.71			
Grøstl-0	Basic	3086	18901, 0	0.16	6.9	79.2	424.4
	T-box	3300	3933, 528k	0.84			
Grøstl	Basic	2909	19176	0.15	13.0	79.1	446.7
	T-box	3288	4012, 640k	0.82			
SHAvite-3	Basic	1366	10165, 0	0.13	5.0	70.1	262.3
	T-box	1434	3044, 256k	0.47			
Altera Stratix III							
		Mbps	#ALUTs, #Mem-bits	Tp/#ALUTs	%	%	%
ECHO	Basic	13395	20754, 0	0.64	-16.8	36.6	49.8
	T-box	11146	13159, 2048k	0.96			
Fugue	Basic	3241	2391, 0	1.36	-6.8	34.2	41.6
	T-box	3022	1574, 99k	1.92			
Grøstl-0	Basic	6990	6290, 0	1.12	-33.5	63.5	82.0
	T-box	4950	2288, 528k	2.03			
Grøstl	Basic	6008	7386, 0	0.81	-2.7	62.3	158.0
	T-box	5848	2788, 640k	2.09			
SHAvite-3	Basic	3295	2930, 0	1.12	15.4	49.6	129.0
	T-box	3804	1477, 256k	2.58			
Xilinx Spartan 3 [1,2]							
		Mbps	#slices, #BRAMs	Tp/#slices	%	%	%
Fugue	Basic	1231	2493, 0	0.49	13.7	37.5	83.5
	T-box	1400	1558, 8	0.90			
SHAvite-3	Basic	1094	4017, 0	0.27	24.5	50.0	151.1
	T-box	1362	2008, 16	0.68			
Xilinx Virtex 5 [1]							
		Mbps	#slices, #BRAMs	Tp/#slices	%	%	%
Fugue	Basic	3469	712, 0	4.87	-8.8	19.4	13.1
	T-box	3165	574, 8	5.51			
Grøstl-0	Basic	8057	1629	4.95	-24.3	27.0	3.7
	T-box	6098	1188, 48	5.13			
Grøstl	Basic	6117	1795	3.41	-4.5	39.7	58.4
	T-box	5840	1083, 48	4.19			
SHAvite-3	Basic	3242	1028, 0	3.15	8.9	24.0	43.5
	T-box	3530	781, 16	4.52			
[1]ECHO did not fit entire description of T-box into embedded memory in Spartan-3, Virtex-5 and Cyclone II							
[2] Grøstl-0 and Grøstl did not fit entire description of T-box into embedded memory in Spartan-3							

improved.

This behavior can be explained as follows: In Spartan 3, basic implementation of an AES S-box costs 64 slices based on 4-input LUTs. For Virtex 5, the cost is 8 slices based on 6-input LUTs. The corresponding number of LUT levels is 5 for Spartan 3, and 2 for Virtex 5. Moving to the T-box based implementations in Spartan 3 replaces the large routing delay inside of an S-box, by a medium routing delay between logic and BRAMs. The same transition in Virtex 5, replaces the small routing delay inside of an S-box, by a larger routing delay between logic and BRAMs.

Cyclone II does not contain distributed memory (i.e., memory inside of basic Logic Elements, LE) As a result, in the basic architecture, each S-box is first converted to a set of Boolean functions, and then these functions are mapped into 4-input combinational LUTs. The result amounts to 208 Logic Elements and 7 levels of LUTs per each S-box. This transition is obviously quite costly in terms of performance. The embedded T-box based designs can take advantage of 4 kbit memory blocks present in Cyclone II, and as a result are more efficient. In Stratix III, compared to Cyclone II, larger and more flexible Adaptive Look-up Tables (ALUTs) are used for implementing S-boxes. As a result, basic designs, with a small number of ALUT levels, are relatively faster than embedded designs, which suffer from the relative large interconnect delays between reconfigurable logic and memory block.

AES-based functions, in both S-box and T-box architectures, resulted in much bigger area reduction because the functions implemented using embedded resources are a big part of the entire hash function circuit. In case of functions using round constant tables (JH, Keccak), the relative improvement is not significant because these tables are relatively small [33] and [40].

2.3.3 Conclusions

Future designers interested in using embedded resources do need to consider right FPGA family selection for their implementations because FPGA vendors have different features and architectures for embedded resources. Our results show a significant, but not consistent improvement in terms of efficiency (throughput/area) across FPGA families. From a few percents of relative improvement of throughput/area ratio in Xilinx Virtex-5 to the impressive 400% in case of Altera Cyclone II.

2.4 Hardware architecture for the authenticated encryption based on Grøstl and AES

2.4.1 Authenticated encryption in IPSec

Internet Protocol Security (IPSec) provides security against attacks on data transmitted over the Internet through security services facilitated by a set of protocols. It was designed to operate at the level of the Internet layer according to the OSI network model. This makes it completely transparent to applications and users.

The security services provided by the Internet Protocol Security (IPSec) include:

- Confidentiality - Prevents unauthorized access to the transmitted data.

- Data integrity - Ensures data was not altered during transmission.

- Authentication - Enables the identification of the information source.

The IPSec series of protocols makes use of various cryptographic algorithms, such as ciphers, hash functions and key agreement schemes, in order to provide security services. The Internet Key Exchange (IKEv2) protocol in version two has to be used to establish secure connections, so called Security Associations (SAs). The IKEv2 uses cryptographic

Table 2.5: IPSec Supported Protocols and Algorithms

Protocol	Security Service Provided	Supported Algorithm
ESP	confidentiality through encryption and optional data integrity	AES in CBC or CTR mode and HMAC-SHA-256
AH	connectionless integrity and data origin authentication	HMAC-SHA1-96, AES-XCBC-MAC-96, HMAC-SHA-256
IKE	negotiates connection parameters, including keys	Diffie-Hellman scheme and AES in PRNG mode

algorithms: key exchange algorithm (Diffie-Hellman) and pseudo random function based on the Advanced Encryption Standard (AES) in XCBC mode (AES-XCBC-PRF-128).

The Authentication Header (AH) protocol provides connectionless integrity and data origin authentication. The AH uses Hashed Message Authentication Code (HMAC) with Secure Hash Algorithm (SHA).

The Encapsulating Security Payload (ESP) protocol provides mechanisms for both confidentiality and data integrity services. In order to provide both cryptographic functions, the AES in Cipher-Block-Chaining (CBC) and/or Counter (CTR) modes of operation and HMAC based on SHA-2 are used.

To assure protection and standardization, the minimum set of cryptographic algorithms that must be supported by an implementation of IPSec for ESP, AH and IKEv2 protocols, as stated in [67], is illustrated in Table 2.5.

2.4.2 Contribution

In our paper [28], we have demonstrated that both algorithms (128-bit security level versions) can be used to build a coprocessor supporting both ESP and AH protocols. However, in case of the ESP protocol we have investigated only the case of the encryption process.

In this effort we will present that the idea of a hardware coprocessor for Grøstl and AES with a common data-path is also applicable to:

- the authenticated decryption process in the ESP protocol for 128-bit security level,

- the HMAC-Grostl for 256-bit security level in the AH protocol.

AES round   Groestl P/Q transformation
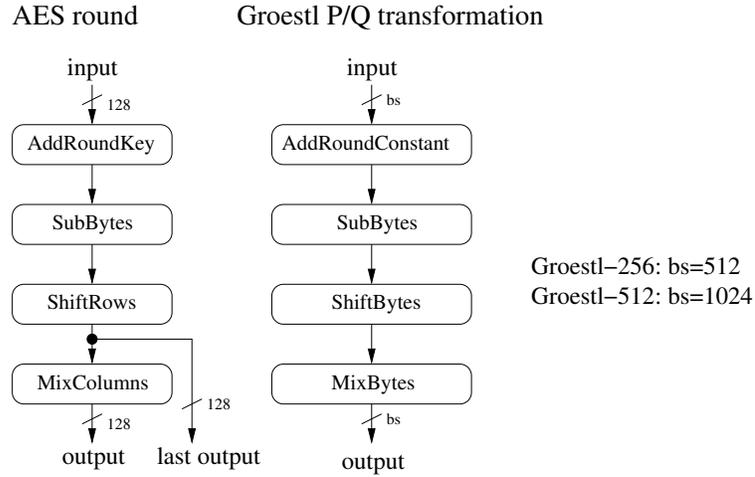
Figure 2.8: Block diagram of Grøsl and AES round

Finally, we had fully extended support to 256-bits security level. Namely, we have designed, implemented and provided results for Grøstl-512/AES-256 hardware accelerator for authenticated encryption/decryption.

The rest of this chapter is organized as follows: Section 2.4.3 is devoted to the analysis of the Grøstl-AES structure for the authenticated encryption based on the HMAC and the counter mode, respectively. Section 2.4.4 describes the proposed coprocessor. Finally, Section 2.4.5 discusses and analyzes the results and The conclusions are drawn in Section 2.4.6.

2.4.3   Authenticated encryption based on Grøstl and AES in a single coprocessor

The specifications of the block cipher AES and the hash function Grøstl are provided in [5] and [17], respectively. The round functions for both algorithms are summarized in Fig. 2.8.

The design described in [39] and [93] and the corresponding source codes from [94] will serve in this work as a starting point for our investigations.

30

Grøstl and the AES comparison

In order to extend the original Grøstl hardware architecture several facts have to be taken into consideration:

- **The basic round structures** of both algorithms are demonstrated in Fig. 2.8. All four corresponding transformations have the same order in both AES and Grøstl. Due to this fact a resource sharing between both algorithms is especially attractive. It is expected that the delay in the critical path in both cases should be very similar.

- **The SubBytes layers** in both cases are built upon the same substitution box (S-box), therefore they can be fully shared (Fig. 2.10, pt. 1). In terms of circuit area, this transformation is the most costly out of all operations of the Grøstl and AES rounds.

- **The ShiftRows and ShiftBytes transformations** in AES and Grøstl, respectively, can be implemented as a permutation of bytes (simple rewiring). However, since they are not similar, both operations have to be implemented separately and properly multiplexed (Fig. 2.10, pt. 2).

- **The AddRoundKey and the AddRoundConstant transformations** in AES and Grøstl, respectively, can be implemented as a simple network of XOR gates. However, since they are not similar, both operations have to be implemented separately and properly multiplexed (Fig. 2.10, pt. 3).

- **The MixColumns and the MixBytes** (Fig. 2.10, pt. 4) in AES and Grøstl, respectively, share the $GF(2^8)$ multiplication by constants: 0x02 and 0x03. Therefore they can be merged together (Fig. 2.9, pt. 1). The networks of output XORs require two separate paths (Fig. 2.9, pt. 2-3) for both algorithms. The MixColumns and MixBytes operations have to be multiplexed accordingly (Fig. 2.9, pt. 4).

- **The last round** of the AES block cipher is different than the regular round. Therefore

i[7]

8

x2

x3

x4

x5

x7

m[7][5]
m[7][4]
m[7][3]
m[7][2]
m[7][1]
m[7][0]

$cm_{\#7}$

||

48

m[7][5..0]

i[0]

8

· · ·

$cm_{\#0}$

48

m[0][5..0]

1

i[7..0] − 64−bit input to MixColumns/MixBytes
o[7..0] − 64−bit output from MixColumns/MixBytes
a[7..0] − 64−bit output from MixColumns
g[7..0] − 64−bit output from MixBytes
m[i][5..0] − i−th byte results of multiplication
by constants

m[7][4..0]

40

· · ·

m[0][4..0]

40

Network of XORs
in Groestl MixBytes

· · ·

g[7]

g[0]

3

m[7][5..3]   m[5][5..3]
m[6][5..3]   m[4][5..3]

24

Network of XORs
in AES MixColumns

· · ·

a[7]   a[4]

2

m[3][5..3]   m[1][5..3]
m[2][5..3]   m[0][5..3]

24

Network of XORs
in AES MixColumns

· · ·

a[3]   a[0]

a[7..0]   g[7..0]

64

o[7..0]

4

Figure 2.9: Shared MixColumns/Bytes

32

All buses are b−bit wide
unless specified otherwise.

Groestl−256 : b=512
Groestl−512 : b=1024
AES: ks=b/4
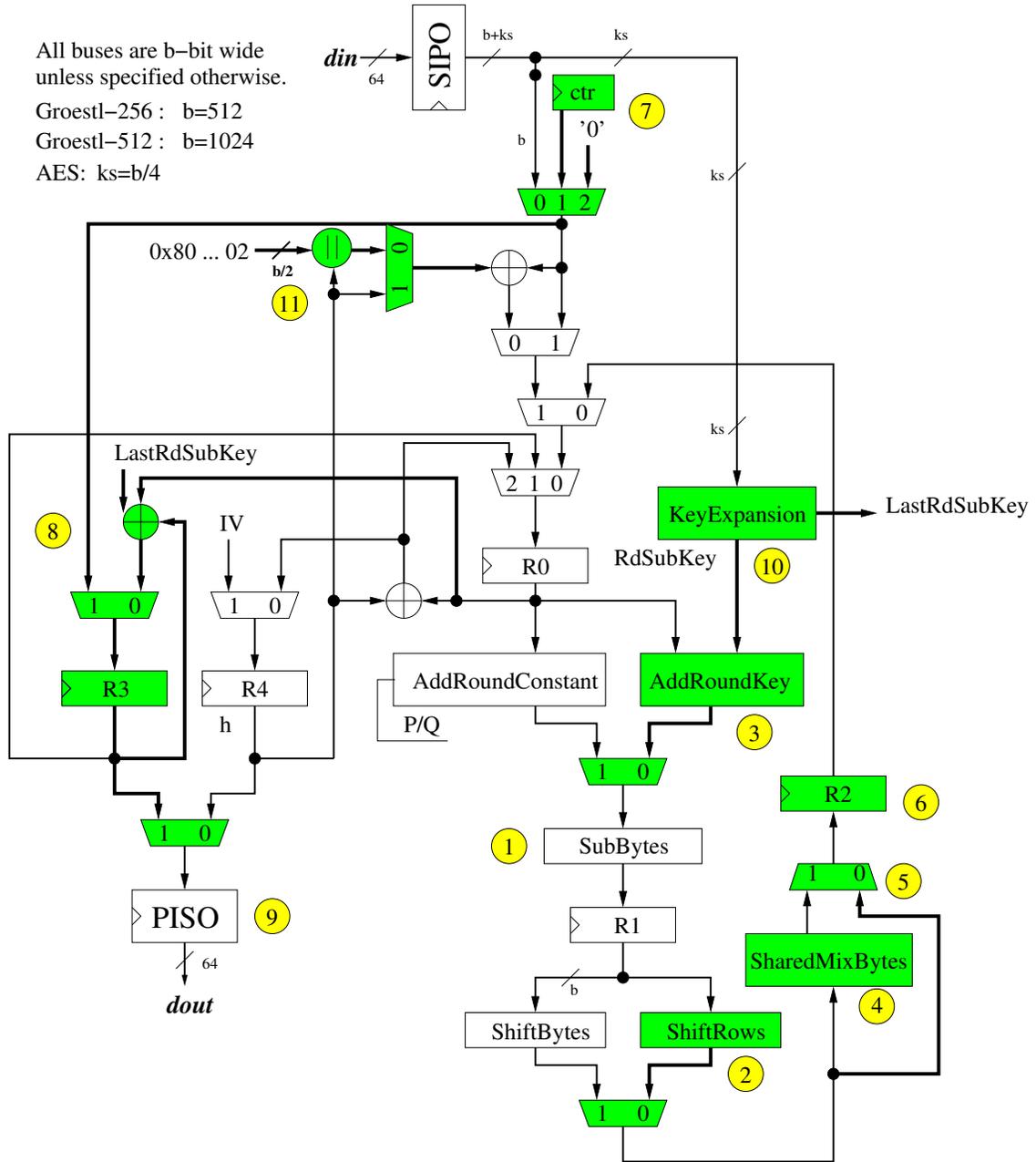
Figure 2.10: Block diagram of Grøstl/AES core

33

Table 2.6: Number of rounds and the security level relations
for Grøstl and AES

Security level	Grøstl	AES
128-bit	(Grøstl-256) 10	(AES-128) 10
192-bit	(Grøstl-384) 14	(AES-192) 12
256-bit	(Grøstl-512) 14	(AES-256) 14

we need to build a bypass bus and multiplex it with the round's regular output (Fig. 2.10, pt. 5).

- For 128 and 256-bit security level both Grøstl and AES require **the same number of rounds**. This dependency is summarized in Table 2.6. This fact helps to achieve a full synchronization of input data between the HMAC and Encryption.

- **The Grøstl double data flow pipe (P and Q transformations) vs. the AES one data flow pipe** determines the optimal number of pipeline stages. The high-speed single stream of data quasi-pipelined hardware architecture of Grøstl, demonstrated in [75], [76], [72], requires two pipeline stages for the P and Q permutations intermediate values. The third pipeline stage is required for the AES intermediate data (Fig. 2.10, pt. 6).

- **Both algorithms input block sizes differ**. They are 128-bit, 512-bit and 1024-bit for AES, Grøstl-256 and Grøstl-512, respectively. The encryption/decryption of 512-bit (1024-bit) single stream of data, by four (eight) instances of algorithm which can accommodate 128-bit input only, prohibits the feedback mode utilization. In order to increase the security level of non-feedback mode based encryption/decryption, the counter mode (Fig. 2.10, pt. 7) was applied (Fig. 2.12).

- The encryption/decryption process requires **an extra storage space** for the plaintext/ciphertext (Fig. 2.10, pt. 8).

- For a given security level **the output block** of both algorithms is different. This fact implies the size extension (doubling) of the Parallel Input Serial Output (PISO)

module for both Grøstl-256 and Grøstl-512 (Fig. 2.10, pt. 9).

- **The Key scheduling algorithm** for the AES algorithm requires an additional circuitry (Fig. 2.10, pt. 10).

- **Second hashing in the HMAC** requires message padding (Fig. 2.10, pt. 11).

Motivated by the above observations, we will show how to efficiently share the resources between corresponding versions of Grøstl and AES (Grøstl-256/AES-128 and Grøstl-512/AES-256) in our coprocessor for an authenticated encryption.

HMAC-Grøstl

A mechanism for message authentication using cryptographic hash functions, the HMAC (The Keyed-Hash Message Authentication Code) was originally defined in [95] and adapted for the IPSec in [96]. Recently this last document was updated in [97]. HMAC has a generic form and it can be used with any iterative cryptographic hash function, e.g. Grøstl, in combination with a secret shared key. The HMAC cryptographic strength rely on the properties of the underlying hash algorithm. Fig. 2.11 demonstrates the HMAC generation process.

Since the combination of HMAC with a current standard SHA-2 is denoted as HMAC-SHA-2, we are using corresponding notation for Grøstl algorithm (HMAC-Grøstl).

In order to compute the HMAC value for a given message (data) and a key (hkey) the selected hash function has to be used twice. The output from the first computations is a function of the ipad constant, padded key, and a given message. The output from the second computations (the hmac-value) is a function of the opad constant, padded key, and the result of the first computation. For the sake of simplifying our circuit (padding of the second hash computation) we restricted the range of key sizes up to the Grøstl block size.

This assumption leads us to the relation between the throughput of HMAC-Grøstl and the throughput of Grøstl:
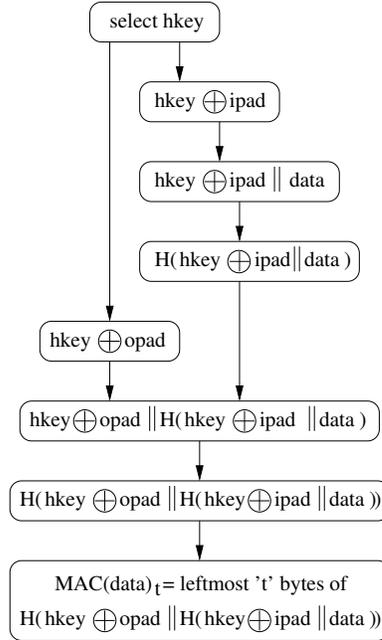
Figure 2.11: HMAC generation

$$\frac{throughput_{HMAC/Grøstl}}{throughput_{Grøstl}} = \frac{\#blocks}{c + \#blocks} \qquad (2.1)$$

where:

$\#blocks$ is the number of data blocks for a given message and $throughput_{Grøstl}$ is the maximum Grøstl hardware architecture throughput calculated for long messages.

The constant c in the denominator is an overhead from HMAC-Grøstl and it is equal to 6 and 5 in case of encryption and decryption, respectively. The following operations contribute to the value of the c constant:

- two HMAC key injections,

- two Grøstl message finalizations,

- an injection of a message digest from the first to the second hash computation,

- decryption of the first block of data (encryption process only).

36
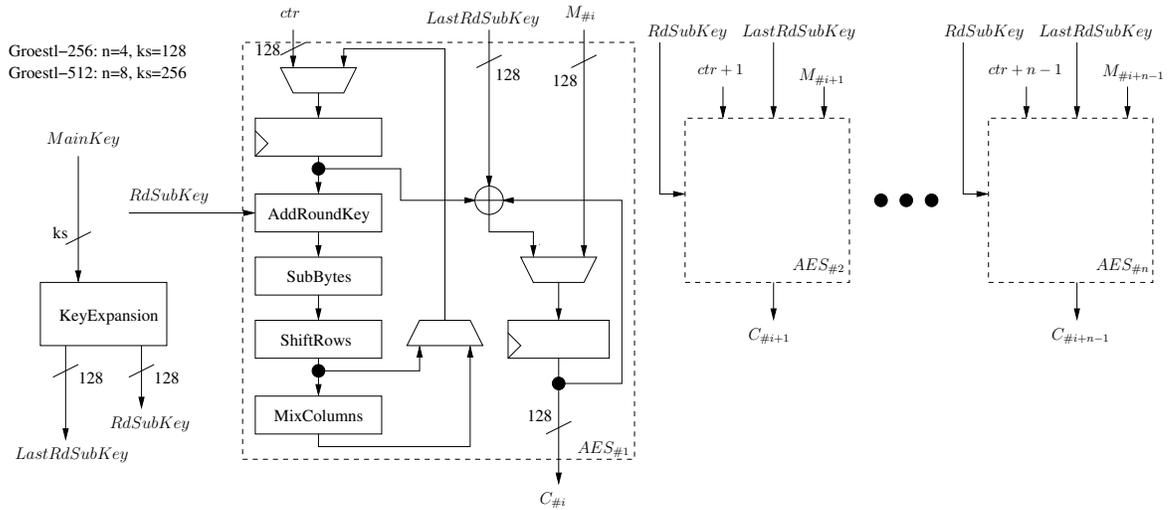
Figure 2.12: Block diagram of AES-CTR where n is the number of AES cores

In case of long messages the effect of HMAC-Grøstl overhead is marginal, and it can be omitted in the throughput calculations.

AES in Counter mode

NIST has defined five confidentiality modes of operation for use with an underlying symmetric key block cipher algorithm: Electronic Codebook (ECB), Cipher Block Chaining (CBC), Cipher Feedback (CFB), Output Feedback (OFB), and Counter (CTR) [98]. Two of the aforementioned modes of operation, namely ECB and CTR, allow parallel computations. In ECB mode, for a given key the same plaintext block is always encrypted to the same ciphertext block. This property is undesirable in a predominant number of applications, and due to this fact the ECB mode should not be used. The computations of the CTR mode in our architecture of AES is presented in Fig. 2.12.

To encrypt using AES in the counter mode with n-blocks processed in parallel, one starts with an arbitrary plaintext, a session key, and an init value for a 128-bit counter. The input plaintext M is divided into n-block chunks $M = \{M_{\#i}, M_{\#i+1}, ..., M_{\#i+n-1}\}$. In our architecture, for compatibility with Grøstl, we choose n=4 for AES-128 and n=8

for AES-256. The output ciphertext $C = \{C_{\#i}, C_{\#i+1}, ..., C_{\#i+n-1}\}$ is the XOR of the corresponding plaintext chunks (in Fig. 2.12 and the results of encryption of $E_{key}(ctr)$, $E_{key}(ctr + 1)$, ..., $E_{key}(ctr + n - 1)$. The decryption process is the same as encryption with M and C interchanged.

2.4.4 Coprocessor description

Block diagram description

A block diagram presented in Fig. 2.10 shows the datapath used in the proposed Grøstl/AES coprocessor. The non-shaded components represent the original Grøstl design, available in [94]. The original Grøstl quasi-pipelined structure has one pipeline register inserted between SubBytes and ShiftBytes operations.

In order to perform in parallel encryption and hash function computation the quasi-pipeline architecture was extended by several extra elements. The shaded components show which elements have to be added in order to accommodate HMAC-Grøstl and AES-CTR functionality.

An additional pipeline register after the Shared MixColumns/MixBytes operation is added. Two of pipeline stages contain intermediate values for the P and Q functions from Grøstl, one extra stage is responsible for the AES encryption of intermediate values of the same block of data.

Grøstl and AES pipelining

For each block of data, an input message is loaded directly to the state register as an input to the operation Q in the first clock cycle. A message block is xored with an initialized chain register, R4=IV, to create an input for the operation P in the second cycle of processing.

The counter values are loaded to the state register, R0, in the third clock cycle. When the first stage of the pipeline starts executing the first phase of the AES round, the second stage of the pipeline continues the execution of the P operation and the third stage is in

block $C_{\#i}$ for AES and $C_{\#i-1}$ for Groestl

cycle	0	1	2	3	4	5		3r−1	3r	0	1
R0:	Q^0	P^0	A^0	Q^1	P^1	A^1	.....	A^{r-1}	I	Q^0	P^0
R1:	I	Q^0	P^0	A^0	Q^1	P^1	.....	P^{r-1}	A^{r-1}	I	Q^0
R2:	A^{r-1}	I	Q^0	P^0	A^0	Q^1	.....	Q^{r-1}	P^{r-1}	A^{r-1}	I

r - number of rounds   block $C_{\#i}$ for AES and $C_{\#i-1}$ for Groestl
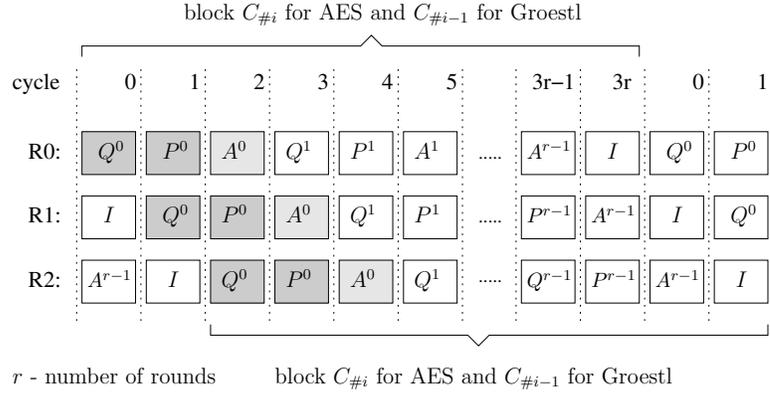
Figure 2.13: Pipelining in the Computational Unit of the Grøstl/AES core

the last phase of the Q operation.

The first stage of the pipeline consists of the Grøstl's P/Q AddRoundConstant, the AES AddRoundKey units and the fully shared SubBytes layer (in Fig. 2.14). The second stage of the pipeline consists of the ShiftBytes/ShiftRows and modified MixBytes units. The third stage of the pipeline consists of just two multiplexers.

A part of the function Q is always performed one cycle ahead of the corresponding part of the function P and two clock cycles before AES-CTR related data.

Finalization of the hash process in this design takes two clock cycles. First, the chaining value, h, is xored with the final value of Q, while P is still being processed, and the result is stored in the register R4. In the subsequent cycle the final result of P is mixed with the chaining value as well (in Fig. 2.13). In the following clock cycle, the tenth (fourteenth in case of AES-256) round of the AES-128 transformation is completed and the last AES key is xored with the output from the state register and plaintext.

When an encryption process is finished, the ciphertext is stored in the Parallel Input Serial Output (PISO) unit. The entire process is repeated until all blocks of a message are thoroughly hashed and encrypted.

It must be noted that HMAC process requires additional data in front (key xored with the constant *ipad* value) and at the end (key xored with the constant *opad* value) of the message. During the time when these pre-($M_{\#0}$) and post-($M_{\#m}$) data is processed, the

Input Interface	$I_{\#0}$	idle	key	$I_{\#1}$	idle	$I_{\#2}$	idle	$I_{\#3}$	......	idle	$I_{\#m+1}$	idle
Computational Unit	AES(idle) Groestl($I_{\#0}$)		AES($I_{\#1}$) Groestl(idle)		AES($I_{\#2}$) Groestl($O_{\#1}$)		......		AES(idle) Groestl($O_{\#m}$)		AES(idle) Groestl($I_{\#m+1}$)	AES(idle) Groestl($I_{\#m+2}$)
Output Interface	idle			$O_{\#1}$	idle		......	$O_{\#m}$		idle		HMAC (O)

$I_{\#0}$ = ipad $\oplus$ hkey   Plaintext = $I_{\#1}, I_{\#2}, ..., I_{\#m}$ HMAC(O) - HMAC value for   Groestl-256: 512-bit input block
$I_{\#m+1}$ = opad $\oplus$ hkey   Ciphertext = $O_{\#1}, O_{\#2}, ..., O_{\#m}$ a given ciphertext O   Groestl-512: 1024-bit input block
$I_{\#m+2}$ = H(ipad $\oplus$ hkey || O)

Figure 2.14: High level scheduling in the Grøstl/AES core
during encryption process

Input Interface	$I_{\#0}$	idle	key	$I_{\#1}$	idle	$I_{\#2}$	idle	$I_{\#3}$	......	idle	$I_{\#m+1}$	idle
Computational Unit	Groestl($I_{\#0}$) AES(idle)		Groestl($I_{\#1}$) AES($I_{\#1}$)		Groestl($I_{\#2}$) AES($I_{\#2}$)		......		Groestl($I_{\#m}$) AES($I_{\#m}$)		Groestl($I_{\#m+1}$) AES(idle)	Groestl($I_{\#m+2}$) AES(idle)
Output Interface	idle			$O_{\#1}$	idle		......	$O_{\#m-1}$	idle	$O_{\#m}$	idle	HMAC (I)

$I_{\#0}$ = ipad $\oplus$ hkey   Ciphertext = $I_{\#1}, I_{\#2}, ..., I_{\#m}$ HMAC(I) - HMAC value for   Groestl-256: 512-bit input block
$I_{\#m+1}$ = opad $\oplus$ hkey   Plaintext = $O_{\#1}, O_{\#2}, ..., O_{\#m}$ a given ciphertext I   Groestl-512: 1024-bit input block
$I_{\#m+2}$ = H(ipad $\oplus$ hkey || I)

Figure 2.15: High level scheduling in the Grøstl/AES core
during decryption process

AES module is not producing valid data ($AES(idle)$ in Fig. 2.14 and 2.15).

Finally, a HMAC value is calculated and it is taken from the bottom half of the chaining value, h. For a given chunk of a 512-bit data both Grøstl-256 and AES-128 cores need 31 clock cycles to complete their operations (3 pipeline stages per 10 rounds + 1 clock for the Grøstl finalization and 1 clock cycle for the final xor in the counter mode). In case of Grøstl-512 and AES-256 given chunk of 1024-bit data requires 43 clock cycles to complete their operations (14 rounds).

High-level scheduling

In order to make our implementations as practical as possible, we have followed a 64-bit interface and a simple handshaking protocol specification from [99]. Thanks to the assumptions taken from the aforementioned paper, it is possible to keep all three of the proposed coprocessor's pipeline stages busy almost all the time.

The input-output operations overlap in many cases, and therefore the separation of input/output bus and control signals is necessary.

A higher level scheduling is summarized in Figs. 2.14 and 2.15, for encryption and decryption process, respectively. The path of the very first chunk of message $I_{\#1}$ in Fig. 2.14 for the authenticated encryption is denoted by the shaded blocks.

During the computations of longer messages (more than three blocks), the coprocessor will be storing the result for the $I_{\#(i-2)}$ block, conducting HMAC-Grøstl and AES-CTR operations for the block $I_{\#(i-1)}$, and fetching i^{th} block of data ($I_{\#(i)}$) at the same time.

Throughput discussion

In the most typical scenario the speed of the hardware implementation of cryptographic transformations is understood as a throughput for long messages. The exact throughput formula is defined as follows [21]:

$$throughput = \frac{blocksize}{T * (Time_{HE}(N+1) - Time_{HE}(N))} \qquad (2.2)$$

where *blocksize* is an input block size, characteristic for each cryptographic transformation, $Time_{HE}(N)$ is a total number of clock cycles necessary to hash/encrypt (decrypt) an N-block input data and T is the clock period, characteristic for each hardware coprocessor (in Table 2.7).

In case of the Grøstl/AES-based hardware accelerator described in this chapter, the

Table 2.7: Throughput-related parameters

Algorithm	$blocksize$	$cycles$
Grøstl-256/AES-128	512	31
Grøstl-512/AES-256	1024	43
$c = 5$ (encryption) or 6 (decryption)		

throughput formula for long messages is:

$$throughput_{long} = \frac{blocksize}{cycles * T} \qquad (2.3)$$

where *cycles* is the total number of clock cycles necessary to hash a single block of message which is 31 and 43 for 128 and 256-bit security levels, respectively. T is a clock period of the coprocessor.

A potential application for an authenticated encryption-oriented, high-speed hardware coprocessor is the Encapsulating Security Payload (ESP) from the IPSec protocol suite. In this scenario the throughput has to be calculated for relatively short messages (40-1536 bytes).

Due to the fact that the HMAC-Grøstl computations take more time than the AES-CTR encryption, the throughput is considered as an effective throughput for a given message in our coprocessor. The final throughput formula is a result of both formulas: (2.1) and (2.3).

$$throughput = \frac{blocksize * \#blocks}{(c + \#blocks) * (cycles * T)} \qquad (2.4)$$

where c is the number of extra blocks processed, which is 5 and 6 for encryption and decryption, respectively.

For long messages the formula (2.4) converges to the formula (2.3).

2.4.5 Results

The HMAC-Grøstl and AES-CTR based hardware coprocessors were implemented on four high speed FPGA devices: 65nm Altera Stratix III and Xilinx Virtex 5, and 40nm Altera Stratix IV and Xilinx Virtex 6. All architectures have been modeled in VHDL-93, then synthesized, placed and routed using Xilinx ISE 13.1 and Altera Quartus II 11.1 for Xilinx and Altera FPGAs, respectively. Maximum clock frequencies have been determined using static timing analysis tools provided as a part of the respective software packages (*quartus_sta* for Altera and *trace* for Xilinx). The tool options were selected in such a way, that no embedded resources, such as block memories or DSP units, were used during implementation. This choice was made in order to enable the comparison of all implementations in terms of area and throughput to area ratio. Tables 2.8 and 2.9 summarize the results collected after the *Place-and-Route* and *Fitter*, in Xilinx and Altera, respectively.

Generally, in terms of area, the coprocessor proposed in this thesis can be implemented on the smallest device from each selected family. In case of small messages, the throughput is a function of the message size. For the smallest 40-byte packages, it is just 11% of the long messages throughput, but in case of 1536-byte messages it reaches almost 83% of long messages throughput.

Comparison to the stand-alone Grøstl implementation

In Table 2.8 and 2.9 we have summarized the implementation results of the proposed Grøstl/AES hardware accelerator for 128 and 256-bit security, respectively. We have compared these results to the implementation results of the reference Grøstl design from [81]. Additionally, we have extended the functionality of our architecture, described in [28] - our coprocessor can perform both authenticated encryption and decryption.

In case of three out of four selected FPGA families, the coprocessor investigated in this thesis requires less than 31% and 40%, respectively, of additional area compared to the basic version of quasi-pipelined architecture presented in [81], for Grøstl-256 and Grøstl-512,

respectively. In case of Altera devices, for security level = 128-bit, an extra pipeline stage reduces the critical path compared to the aforementioned design, the maximum frequency increases up to 10%. In other cases the maximum frequency is slightly worse than in the

Table 2.8: Results of shared-resources implementation for HMAC-Grøstl-256 and AES-128 in Counter Mode on modern FPGA

FPGA Family	Frequency	Area	@40Bytes	@1536Bytes	@infinity
Authenticated Encryption					
Altera					
	[MHz]	[ALUTs]	[Mbps]	[Mbps]	[Mbps]
Stratix III	271 (+10%)	9337 (+26%)	466	3704	4476 (-25%)
Stratix IV	264 (+11%)	9322 (+26%)	454	3608	4360 (-25%)
Xilinx					
	[MHz]	[CLB Slices]	[Mbps]	[Mbps]	[Mbps]
Virtex 5	261 (+4.0%)	2505 (+40%)	449	3567	4310 (-30%)
Virtex 6	276 (-6.8%)	2221 (+19%)	474	3773	4558 (-37%)
Authenticated Encryption/Decryption					
Altera					
	[MHz]	[ALUTs]	[Mbps]	[Mbps]	[Mbps]
Stratix III	263 (+6.9)	9712 (+31%)	388/452[1]	3363/3475[1]	4344 (-27%)
Stratix IV	261 (+10.1)	9699 (+31%)	385/449[1]	3337/3449[1]	4311 (-25%)
Xilinx					
	[MHz]	[CLB Slices]	[Mbps]	[Mbps]	[Mbps]
Virtex 5	233(-7.2%)	3102 (+72%)	344/400[1]	2979/3078[1]	3848 (-37%)
Virtex 6	255 (-14%)	2447 (+31%)	376/438[1]	3260/3369[1]	4212 (-42%)
[1] The encryption/decryption throughput. @infinity both values are the same The relative differences between this work and the reference Grøstl design from [81] are expressed in percentages					

Table 2.9: Results of shared-resources implementation for HMAC-Grøstl-512 and AES-256 in Counter Mode on modern FPGA

FPGA Family	Frequency	Area	@40Bytes	@1536Bytes	@infinity
Altera					
	[MHz]	[ALUTs]	[Mbps]	[Mbps]	[Mbps]
Stratix III	231 (-2.5%)	19257 (+32%)	245/286[1]	3667/3883[1]	5501 (-34%)
Stratix IV	222 (-4.3%)	19190 (+34%)	236/275[1]	3524/3732[1]	5286 (-36%)
Xilinx					
Virtex 5	190 (-12%)	6484 (+68%)	211/245[1]	3143/3328[1]	4715 (-41%)
Virtex 6	219 (-7.6%)	5074 (+40%)	233/272[1]	3477/3681[1]	5215 (-38%)
[1] The encryption/decryption throughput. @infinity both values are the same The relative differences between the reference Grøstl design from this work and [81] are expressed in percentages					

Table 2.10: Results of shared-resources implementation for Grøstl-0 (Grøstl) and AES in Altera Cyclone III

Design	Functionality	Frequency [MHz]	Area [LEs]	Latency [Cycles]	Thr. [Mbps]	Thr./Area [Mbps/Slice]
Authenticated Encryption with Grøstl-0						
[1]						
reference Grøstl-0	Grøstl-0	57.2	12086	20	1473	0.122
Design I[1]	Grøstl-0	56.0 (-2.6%)	13723 (+13.5%)	20	1434 (-2.6%)	0.104[5]
	AES	56.0	13723	10	2868	0.209
	Grøstl-0 and AES	56.0	13723	30	956[3]	0.070[4]
Design II[2]	Grøstl-0	53.4 (-7.2%)	13453 (+11.3%)	20	1366 (-2.6%)	0.102
	AES	53.4	13453	10	2049	0.152
	Grøstl-0 and AES	53.4	13453	30	911[3]	0.068
[1] Grøstl-0, 4*AES						
[2] Grøstl-0, 3*AES and Key Expansion Unit						
[3] Throughput calculated for the authenticated encryption based on HMAC-Grøstl and AES-CTR						
This work						
reference Grøstl-0	Grøstl-0	141.1	19005	21	3440	0.181
Grøstl-0, 4*AES and Key Expansion	Grøstl-0 and AES	159.9 (+13.3%)	23039 (+23.4%)	31	2640 (-23.3%)	0.115[4,5]
reference Grøstl	Grøstl	130.1	19260	21	3171	0.165
reference AES and Key Expansion	AES	129.4	4901	11	1505	0.307
Grøstl, 4*AES and Key Expansion	Grøstl and AES	144.0 (+10.7%)	23758 (+23.4%)	31	2378 (-25.0%)	0.100
[4] 64% improvement in terms of throughput/area ratio for authenticated encryption (ESP protocol)						
[5] 8% improvement in terms of throughput/area ratio for authentication (AH protocol)						
Authenticated Encryption/Decryption with Grøstl						
This work						
reference Grøstl	Grøstl	130.1	19260	21	3171	0.165
reference AES and Key Expansion	AES	129.4	4901	11	1505	0.307
Grøstl, 4*AES and Key Expansion	Grøstl and AES	134.9 (+3.7%)	25297 (+31.3%)	31	2228 (-29.7%)	0.088

reference design. The location of the 3rd stage pipeline register was investigated by moving it before the multiplexer (in Fig. 2.10, pt. 5). This change helps to improve the maximum frequency, but at the same time the throughput/area ratio decreases. This is largely due to the fact that the quasi-pipelined hardware architecture of Grøstl from [81] and triple-staged Grøstl/AES in this work requires more clock cycles, the overall throughput for long messages decreases up to 40%.

Overall, in case of Xilinx Virtex-5, the implementation results for both 128 and 256-bit security versions of our coprocessor were significantly worse. These results can be explained by the fact that the synthesis tool (XST in our experiment) behaves differently for Virtex-5 and Virtex-6.

In Tables 2.8 and 2.9, we have presented the impact of IPSec minimum and maximum size messages on the effective throughput.

In case of selected FPGA devices, the maximum throughput is restricted by slower encryption process and it varies between 340-3400Mb/s for Grøstl-256/AES-128 and 210-5500Mb/s for Grøstl-512/AES-256. The final throughput result depends on the traffic in a given network.

Additionally, the coprocessor for the 128-bit security, proposed in this work can be easily implemented on the smallest devices available in every selected high-speed family.

Comparison to the Järvinen design [1]

In order to fairly compare our hardware accelerator with the circuit described in [1], an additional implementation in Altera low-cost Cyclone III is provided (see Table 2.10). In both our work and [1], one can observe the penalty in area for introducing extra AES functionality.

In case of [1], a negligible frequency penalty was also introduced. This penalty is due to the fact that basic iterative task (P and Q Grøstl-0 functions and AES round) of the coprocessor proposed in [1] is fully combinational and extra multiplexers were added to the

Table 2.11: Throughput/Area ratio relative improvement
between this work and [1]

Functionality	Algorithms	[1]	This work	Difference
ESP authenticated encryption	Grøstl-0 and AES	0.070	0.115	+64%
AH	Grøstl-0 only	0.104	0.115	+8%
ESP encryption only	AES only	0.209	0.115	-44%

original Grøstl-0 design.

In case of our architecture, an additional pipeline stage enables frequency improvement. When both encryption and hashing for a given block of data have to be computed, the design from [1] and our core will produce output in 30 and 31 clock cycles respectively. Due to the fact that our core has three pipeline stages, ideally our circuit should have 3 times higher frequency than [1]. The obtained result, 2.85x frequency improvement, proves the validity of this concept.

A typical application for high-speed implementation of the combined confidentiality and authentication services is the coprocessor for IPSec [66]. This protocol works in two different modes: Encapsulating Security Payload (ESP) and Authentication Headers (AH). The first requires the usage of block cipher and optional hash function at the same time for a given chunk of data, second requires a hash function usage only. Table 2.10 summarizes results for both modes for our coprocessor and the coprocessor from [1]. Based on the results in Tab. 2.11, we observed 64% and 8% improvement in terms of efficiency (throughput/area) for ESP (authenticated encryption) and AH, respectively. In case of ESP in encryption mode only, the design from [1] outperforms our coprocessor by 44%.

2.4.6   Conclusions

The hash function Grøstl was one of the five finalists of the SHA-3 competition. Hardware performance of this function was investigated thoroughly over the last few years.

In this chapter we have investigated very unique feature among all SHA-3 candidates - Grøstl and the current Advanced Encryption Standard have similarities which can be exploited very efficiently in hardware. Their common structure can be utilized in the combined

datapath implementation. The coprocessor was optimized for high-speed implementation of both functions, and can find a practical application to the IPSec-based secure networks.

It outperforms similar hardware accelerator proposed in [1] for both IPSec modes: IP Encapsulating Security Payload (ESP) and Authentication Headers (AH) by 64% and 8%, respectively. In case of the relatively rare, the ESP's encryption mode only, the coprocessor from [1] is better by 44% as compared to our results.

The fully functional HMAC-Grøstl with AES-CTR hardware accelerator compared to the stand-alone quasi-pipelined architecture of Grøstl, described in [21] and improved in [39], pays the price in terms of the throughput and area on all reported devices. In case of selected Altera devices and Xilinx Virtex-6, they are up to 40% for both area and throughput for both Grøstl-256/AES-128 and Grøstl-512/AES-256 configurations.

From our point of view, the main advantage of Grøstl, apart of its excellent hardware and software implementation results, is the fact that the relatively small overhead in its hardware architecture enables a natural adoption of the most important to date block cipher - the Advanced Encryption Standard at two security levels 128 and 256-bit. As a result, our solution can provide efficient hardware acceleration for authenticated encryption used in multiple commercial applications.

Part II

Hardware architectures for public key cryptography

Chapter 3: FPGA-oriented adder for thousand bits and more

In this chapter a novel, low latency, FPGA-optimized, adder has been proposed. It efficiently combines the ideas of high-radix carry save addition and the parallel prefix network. We have demonstrated in this chapter that this idea is especially attractive once a modular addition is employed. The implementation results reveal that this hybrid adders have great potential for the addition and modular addition of the long-size integers.

Contents

3.1 Introduction

Adders are one of the most important digital circuits. They are used extensively in various branches of science and engineering, such as digital signal processing algorithms [100], computer graphics [101], [102] and cryptography [103], [104].

Multiple adder-based solutions have already been proposed, investigated and optimized for different scenarios.

Addition can also serve as a basic building block of some higher level arithmetic operations: multiplication, modular addition, and modular multiplication.

For example: Montgomery arithmetic [105], arguably the most common concept in the area of modular arithmetic, can be stripped down to three basic operations: a right shift, a least significant bit comparison, and a conditional sum. Since iterative algorithms offer a good tradeoff between computation time and circuit area, they have received considerable attention [106], [107], [108].

Several researchers proposed the utilization of carry save adders (e.g.: [109]) for this algorithm. The major advantages of a hardware architecture based on such adders are: the smallest computational latency and the fact that the time complexity is constant, regardless of the size of arguments. The biggest disadvantage of the carry save adder is the fact that its result is in a redundant form. In order to conduct operations like a comparison or a modular multiplication on such representation of arguments, a conversion to the non-redundant form has to be conducted.

Moreover, Montgomery arithmetic requires also pre- and post-processing and is of interest when a large number of consecutive modular multiplications is required.

This condition is easily fulfilled in case of the two oldest and most popular asymmetric, cryptographic algorithms: RSA [24] and the Diffie-Hellman [23] scheme.

However, compared with them, the alternative public key cryptosystems, like Elliptic Curve Cryptography [110], [111] or Pairing Based Cryptography [112] demonstrate much more irregularities in the scheduling of basic operations. Namely, a single iteration requires several modular additions, subtractions and multiplications.

Therefore, these cryptosystems are more computationally demanding and the efficient hardware architectures for both modular multiplication and addition/subtraction are equally important.

Contribution: In this effort we are going to demonstrate a novel, FPGA-optimized adder, highly applicable for the addition of very long integers. Major contributions of this chapter cover three different aspects and they are highlighted here:

- It provides a space exploration of the optimal design parameters for the fully combinational version of our adder.

- The proposed design provides the best results in terms of area · latency for 1024, 2048 and 4096-bit addition.

- Finally, this chapter presents, to the best of our knowledge the fastest and the most efficient, non-redundant, modular adder (possibly subtractor), based on the novel adder.

The rest of this chapter is organized as follows:

In Section 3.2 we discuss previous work. Section 3.3 is devoted to the description of the proposed adder. Section 3.4 demonstrates the design rationale behind the parameters selection. Section 3.5 discusses and analyzes the results, finally we draw conclusions in Section 3.6.

3.2   Previous work

In order to build efficient hardware architectures for modular arithmetic, optimized for low latency, an addition for full size arguments has to be utilized rather than any iterative approach. The most promising, in that respect, is the carry save adder introduced in [113].

A result of addition in case of both aforementioned adders is represented in the form of two vectors: sums and carries. To obtain the final result, both vectors have to be added. This carry save addition is especially attractive if the last operation can be conducted once, at the end of a sequence of multiple consecutive additions in a carry save form. An example of application for such scenario is the Montgomery multiplication, introduced in [105]. The fastest to date, a Montgomery multiplication hardware architecture for ASIC-like solutions (no special multiplication enhancing resources like DSP blocks) is based on carry save adders, as described in [109].
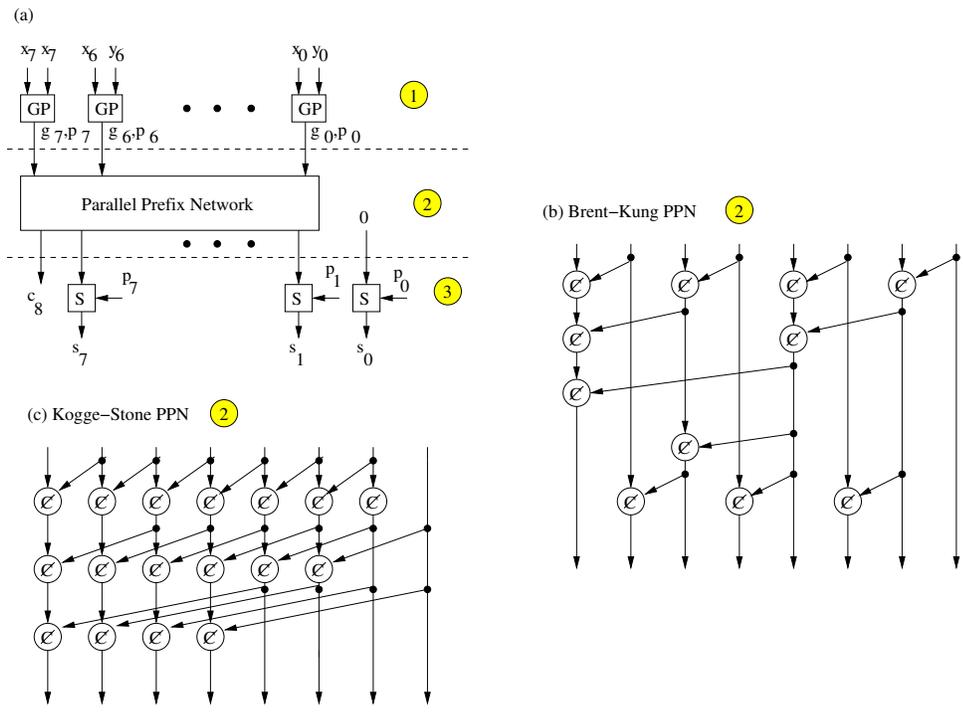
Figure 3.1: (a) General concept of the parallel prefix addition, (b) Brent-Kung adder, (c) Kogge-Stone adder. GP: $g_i = x_i \cdot y_i$, $p_i = x_i \oplus y_i$, S: $s_i = p_i \oplus c_i$, ¢: $g = g'' + g' \cdot p''$, $p = p' \cdot p''$

However, in case of ECC algorithms where addition operations are interleaved with other operations, like multiplications [114], the direct usage of carry save form is very challenging.

A high-radix carry-save addition, and its application to the modular multiplication of large operands on Field-Programmable Gate Arrays (FPGAs), was introduced in [115]. The major advantage of the high radix carry save representation over the basic radix-2 form is the possibility of utilization of hardwired fast carry chain adders available in modern FPGA. Moreover the carries vector, in the high radix carry save form, is relatively sparse and the reconstruction of the final result can be simplified.

An alternative for the high radix carry save form could be one of the adders working on full size arguments: Carry Look-Ahead adder introduced in [116], or parallel prefix network adders, such as Brent-Kung adder [117], or Kogge-Stone adder [118]. All three of those addition algorithms consist of three operational phases: first, the generate and propagate flags are calculated (Fig.: 3.1 pt. 1), then the projected carries are computed (Fig.: 3.1 pt. 2), and finally, the intermediate sums are added with the projected carries (Fig.: 3.1 pt. 3).

The time complexity of the carry signal generation in Kogge-Stone adder is O(log n). It is widely considered the fastest adder design possible. The Brent-Kung adder is expected to be slightly slower, but also a much cheaper alternative. A ripple carry adder, based on the hardwired fast carry chain, available in modern FPGA, has the best efficiency (area · latency) for relatively short arguments (less than 100-bits).

3.3 The adder

In this section we will demonstrate a hybrid high-radix carry save adder with the carry projection unit based on parallel prefix network. First of all, the hybrid adder is taking two arguments: A and B, and it is computing in non-redundant form the result - R, and the output carry - $cout$.

This circuit can be described using two parameters: n and w. They represent the size of arguments and the word size, respectively. The number of words in this case is denoted
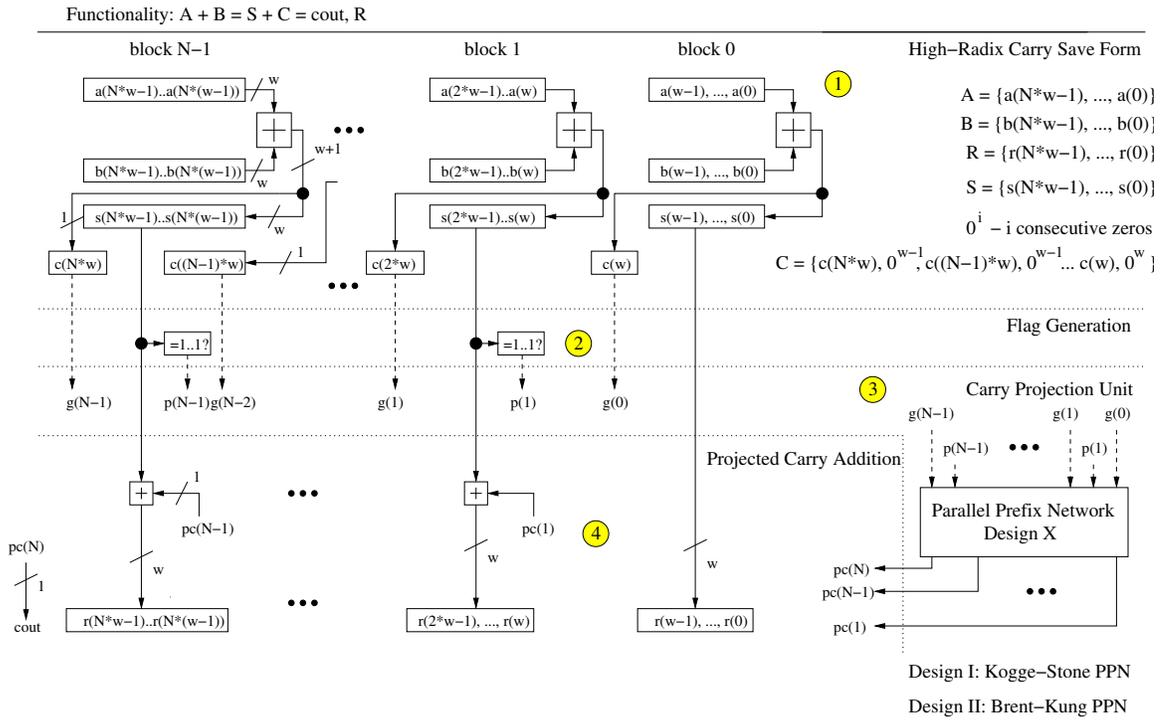
Figure 3.2: Hybrid radix-2^w carry save adder with the carry projection unit based on parallel prefix network (PPN). Design X - Design I is based on Kogge-Stone PPN and Design II is based on Brent-Kung PPN

55

as $N = \lceil \frac{n}{w} \rceil$.

The block diagram of our novel adder is shown in Fig. 3.2.

The words of A and B are added independently using the hardwired fast carry chain adders, available in modern FPGAs. The result of this operation is in radix 2^w carry save form, and it consists of a vector of sums $S = \{[s((N \cdot w - 1), ..., s((N-1) \cdot w)], ..., [s(w-1)...$ $s(0)]\}$, and sparse carry vector $C = \{c(N \cdot w), [0, ..., 0, c((N-1) \cdot w)], ..., [0, ...0, c(w)], [0,$ $0, ..., 0, 0]\}$ (Fig. 3.2 pt. 1).

For the sake of the transition of the final result in the redundant form into the non-redundant form, several observations have to be made:

- the regular addition (ripple carry like) of both vectors, S and C, results in a non-redundant form. This simple approach, although functionally correct, would not let us take any advantage of the sparsity of the vector C.

- The computation of the final result in a non-redundant form can be conducted by the iterative addition of corresponding words $c(i)$ and $s(i)$, from the least to the most significant side of both vectors.

An alternative solution for this problem is the utilization of a parallel prefix network. First, the intermediate result have to be described by two sets of flags (Fig. 3.2 pt. 2):

- propagate flags, defined by:

$$
p(i) = \begin{cases} 1, & \text{if } s(w \cdot (i+1) - 1...w \cdot i) = (1..1)_w \\ 0, & \text{otherwise} \end{cases} \tag{3.1}
$$

- generate flags (carries), defined by:

$$g(i) = \begin{cases} 1, & \text{if } c(w \cdot (i+1)) = 1 \\ 0, & \text{otherwise} \end{cases} \tag{3.2}$$

where w - word size, N - number of words, and $i \in ((N-1), ..., 0)$. Additionally, $p(N) = 0$ and $g(N) = c(w \cdot N)$.

Once, all the propagate-generate signals are computed, a carry projection unit from either Kogge-Stone [118] (Fig.: 3.1 (c)) or Brent-Kung [117] (Fig.: 3.1 (b)) adder, namely, the parallel prefix network, can start the computations of the projected carries $PC = pc(N), ..., pc(0)$ (Fig. 3.2 pt. 3).

These carries are eventually added with the corresponding words from the vector of sums (Fig. 3.2 pt. 4). This last chain of independent adders works without carries out and the concatenation of all partial, final results from them, constitutes the final output R.

The hybrid high-radix carry save and parallel prefix network adder will be called Design I or II based on the carry projection unit derived from either Kogge-Stone or Brent-Kung adder, respectively.

The total delay t_A of the adder is a sum of the delays of three building layers:

- flag generation, a delay of a comparator - t_G,

- carry projection unit, delay of the parallel prefix network - t_P,

- projected carry addition, delay of a ripple carry adder - t_C.

Therefore, the theoretical latency formula for the hybrid adder:

$$t_A \approx t_G + t_P + t_C \tag{3.3}$$

The formula 3.3 is going to be clarified, once we investigate how the generation of both flags generation is implemented in modern FPGA devices (Fig. 3.3). The comparison with
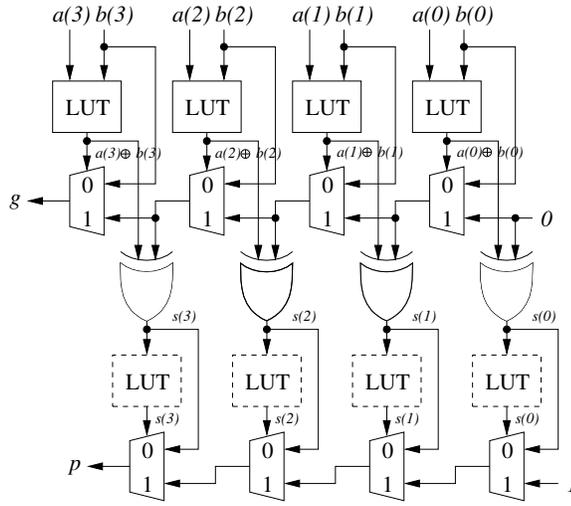
Figure 3.3: Implementation of the generate/propagate logic using fast carry chains and LUTs of Xilinx FPGAs

all ones is somehow special, and is very different than comparisons with any other numbers. An example of the case with $w = 4$-bit, shown for Xilinx FPGAs, in Fig. 3.3, provides explanations.

Only when you do the subtraction $s - 1111_b$ for unsigned numbers, then carry (the going out of range flag) is equal to 0 only if $s - 1111_b \geq 0$, which is equivalent to $s - 1111_b = 0$, and thus, $s = 1111_b$.

Therefore, in order to evaluate if certain word has propagate property, we can simply do a subtraction using fast carry chains, and look at the carry flag. Due to the fact, that the computation of the subtraction from the bottom part of Fig. 3.3 can be started once the least significant bit of the upper part addition is completed, the flag generation time, t_G is almost the same as the time of a single addition of w-bit words, at least for relatively large values of w.

The actual value of a latency of a ripple carry adder depends on the selection of the word size w. On the other hand, the numerical value of a latency of parallel prefix network is related to the number of words N.

The selection of the optimal, in terms of latency, word size w, seems to be very FPGA

n − number of bits of P
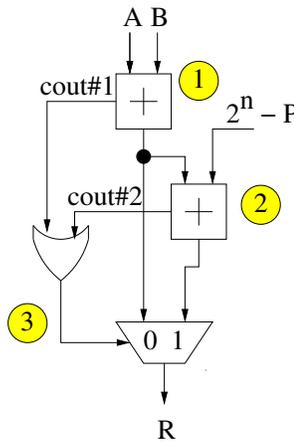
Figure 3.4: Modular adder based introduced in [20]

device dependent:

- the optimal word size is associated with the fast carry chain delay for a given length of operands w,

- the parallel prefix network delay is related to the structure of a basic FPGA logic cell, and in particula to the delay of a single look-up table.

Modular adder

In general our modular adder is an extension of the concept of an adder-based operator demonstrated in [20] (Fig. 1c). Fig. 3.4 (a) summarizes this concept. In order to compute a final result of the n-bit modular addition ($R = A + B \pmod{P}$), two intermediate values have to be computed: a result of the addition $A + B$, and a result of $A + B - P$.

Equation 3.4 demonstrates how to select the final result among both intermediate values.

$$R = \begin{cases} A + B - P, & \text{if } A + B \geq 2^n \vee A + B - P \geq 0 \\ A + B, & \text{otherwise} \end{cases} \tag{3.4}$$

59
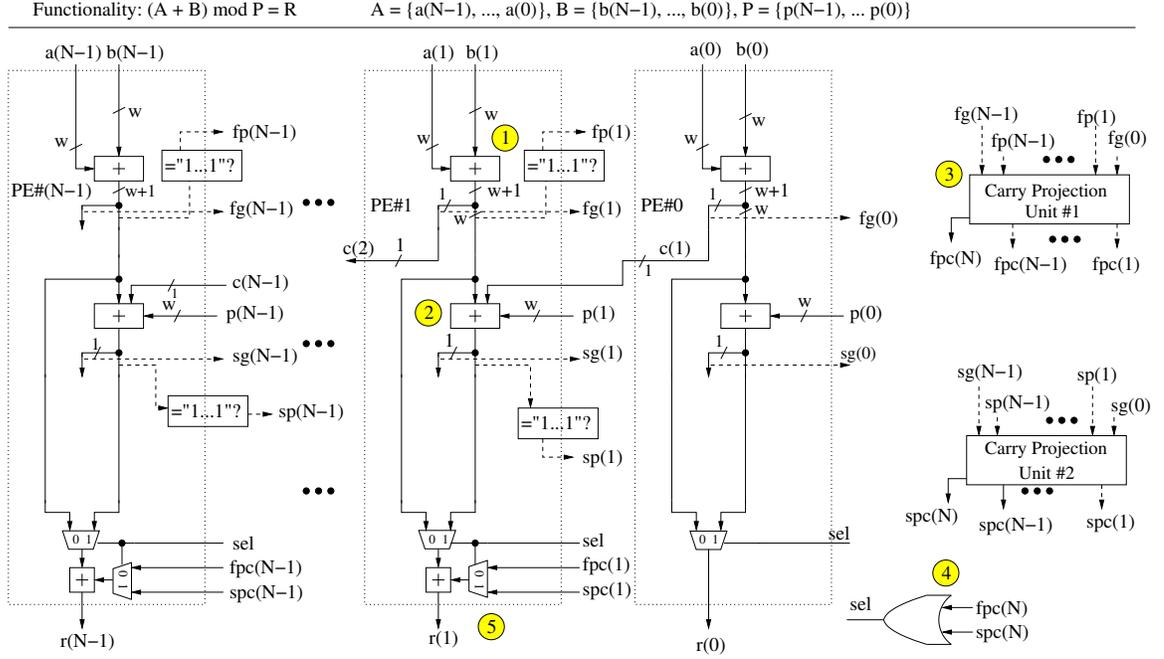
Figure 3.5: Modular adder based on the hybrid adder

Both additions in Fig. 3.4 pt. 1 and 2 can be implemented using any type of non-redundant adder: ripple carry, Kogge-Stone, Brent-Kung, and many others. The biggest advantage of the utilization of the hybrid adder in such application is the fact that the computations of the second addition can be started just after the very first phase, the high radix carry save addition, of the $A + B$ addition has been completed (Fig. 3.5). The computations of next two phases can be conducted in parallel. Once the condition for the select signal for the output multiplexer is completed, it is possible to determine which path is going to contribute to the final result of the modular addition.

Taking into account that the flag generation is conducted along with high-radix carry save addition the latency formula of the entire circuit can be approximated as

$$t_A \approx 2 \cdot t_G + t_P + t_C. \tag{3.5}$$
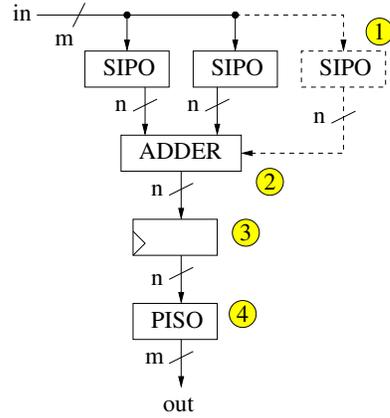
Figure 3.6: Test circuit for addition and modular addition

3.4 Parameters selection

In order to select the optimal parameters: word size - w, and the corresponding number of words N, for a given size of arguments, a simple experiment, specific to a given FPGA device, has to be conducted.

First of all, due to the fact that that our hybrid adder bridges the gap between two different type of adders: ripple carry and the parallel prefix adder, we have to find the latency characteristics of these basic adders, for different argument sizes.

Concerning two facts: limited number of pins and the delay of I/O blocks influence on the latency of any combinational circuit, we propose to use a test circuit, presented in Fig. 3.6. This figure demonstrates the combinational adder (Fig. 3.6 pt. 2) surrounded by buffers: serial input parallel output (SIPO) for the input arguments, output register (Fig. 3.6 pt. 3) and parallel input serial output (PISO) for the result of the addition (Fig. 3.6 pt. 4). Thanks to such a configuration, the critical path is ensured to be in the adder circuit itself. Moreover, in case of modular addition an extra buffer for the modulus is needed (Fig. 3.6 pt. 1).

Since the hybrid adder described in Section 3.3 consists of ripple carry adder and the basic elements of parallel prefix network adders, then the analysis of the latency of those

Table 3.1: Latency of the three major addition techniques as a function of the size of arguments

size	Ripple Carry	Kogge-Stone	Brent-Kung
	t_{RCA} [ns]	t_{KS} [ns]	t_{BK} [ns]
Altera Cyclone III (ep3c120f780c7)			
4	4.00	**4.00**	4.00
8	4.00	**4.00**	4.00
16	4.00	**4.00**	4.00
32	4.00	**4.00**	4.73
64	5.29	**5.01**	5.57
128	9.09	**6.09**	6.45
256	16.43	**7.52**	8.20
512	31.28	**9.26**	10.07
1024	N/A[1]	**10.67**	12.32
Altera Stratix III (ep3sl150f1152c2)			
4	**1.37**	1.37	1.37
8	**1.37**	1.49	1.50
16	**1.37**	1.86	1.95
32	**1.94**	2.26	2.07
64	2.86	2.84	**2.77**
128	5.01	3.56	**3.25**
256	9.09	4.21	**4.02**
512	15.54	5.02	**4.69**
1024	N/A[1]	5.90	**5.52**
Xilinx Spartan 6 (xc6slx150fgg900-3)			
4	**1.77**	1.91	1.91
8	**2.11**	2.79	2.63
16	**2.49**	3.12	3.36
32	**2.57**	4.13	4.03
64	**3.45**	5.39	4.64
128	**4.83**	6.53	6.08
256	7.48	7.61	**6.90**
512	N/A[1]	9.80	**8.25**
1024	N/A[1]		**10.35**
Xilinx Virtex 5 (xc5vlx155tff1738-3)			
4	**1.10**	1.14	1.15
8	1.64	1.70	**1.57**
16	**1.80**	2.13	2.14
32	**2.16**	2.95	2.68
64	**2.85**	3.29	3.20
128	4.16	4.20	**3.89**
256	6.91	**5.05**	5.66
512	14.13	**6.22**	7.40
1024	28.20	**7.79**	8.20
[1] did not fit			

Table 3.2: Parameters exploration for the 1024-bit addition

(w, N)	latency	area	latency · area
Altera Cyclone III (ep3c120f780c7)			
	[ns]	[LE]	[ns · LE]
Design I (8, 128)	10.67	4943	52.7
Design I (16, 64)	**10.63**	**3977**	**42.3**
Design I (32, 32)	12.18	3897	47.5
Design I (64, 16)	15.34	3904	59.9
Design II (8, 128)	14.39	3722	53.6
Design II (16, 64)	**12.49**	**3565**	**44.5**
Design II (32, 32)	13.50	3862	52.1
Design II (64, 16)	17.79	3901	69.4
Altera Stratix III (ep3sl150f1152c2)			
	[ns]	[ALUT]	[ns · ALUT]
Design I (8, 128)	6.54	3766	24.6
Design I (16, 64)	**6.42**	**3018**	**19.3**
Design I (32, 32)	7.17	2586	18.5
Design I (64, 16)	8.35	2328	19.4
Design II (8, 128)	6.15	2711	16.7
Design II (16, 64)	**6.14**	**2510**	**15.4**
Design II (32, 32)	7.12	2377	16.9
Design II (64, 16)	8.48	2268	19.2
Xilinx Spartan 6 (xc6slx150fgg900-3)			
	[ns]	[slice]	[ns · slice]
Design I (8, 128)	12.77	1893	24.2
Design I (16, 64)	**12.66**	**1304**	**16.5**
Design I (32, 32)	12.89	1187	15.3
Design I (64, 16)	12.92	1091	14.1
Design II (8, 128)	13.58	1456	19.8
Design II (16, 64)	14.27	1173	16.7
Design II (32, 32)	**13.45**	**1188**	**16.0**
Design II (64, 16)	14.49	1090	15.8
Xilinx Virtex 5 (xc5vlx155tff1738-3)			
	[ns]	[slice]	[ns · slice]
Design I (8, 128)	9.91	1655	16.4
Design I (16, 64)	10.12	1358	13.7
Design I (32, 32)	**9.79**	**1139**	**11.2**
Design I (64, 16)	9.90	1084	10.7
Design II (8, 128)	12.02	1366	16.4
Design II (16, 64)	10.96	1169	12.8
Design II (32, 32)	**9.81**	**1169**	**11.5**
Design II (64, 16)	12.90	1159	15.0

Table 3.3: Parameters exploration for the 1024-bit modular addition

(w, N)	latency	area	latency $\cdot$ area
Altera Cyclone III (ep3c120f780c7)			
	[ns]	[LE]	[ns $\cdot$ LE]
Design I (8, 128)	15.91	10253	163.1
Design I (16, 64)	**15.87**	**8324**	**132.1**
Design I (32, 32)	18.67	7596	141.8
Design I (64, 16)	22.80	7362	167.9
Design II (8, 128)	16.93	8700	147.3
Design II (16, 64)	**16.93**	**7464**	**126.4**
Design II (32, 32)	19.22	7250	139.3
Design II (64, 16)	23.61	7104	167.7
Altera Stratix III (ep3sl150f1152c2)			
	[ns]	[ALUT]	[ns $\cdot$ ALUT]
Design I (8, 128)	9.75	6655	64.9
Design I (16, 64)	**9.71**	**4916**	**47.7**
Design I (32, 32)	10.37	4106	42.6
Design I (64, 16)	13.17	3672	48.4
Design II (8, 128)	9.87	4666	46.1
Design II (16, 64)	**9.80**	**4122**	**40.4**
Design II (32, 32)	10.38	3790	39.3
Design II (64, 16)	12.91	3509	45.3
Xilinx Spartan 6 (xc6slx150fgg900-3)			
	[ns]	[slice]	[ns $\cdot$ slice]
Design I (8, 128)	16.51	2742	45.3
Design I (16, 64)	23.73	1889	44.8
Design I (32, 32)	**16.10**	**1794**	**28.9**
Design I (64, 16)	17.83	1515	27.0
Design II (8, 128)	19.15	2761	52.9
Design II (16, 64)	**17.80**	**1853**	**33.0**
Design II (32, 32)	17.99	1573	28.3
Design II (64, 16)	19.34	1489	28.8
Xilinx Virtex 5 (xc5vlx155tff1738-3)			
	[ns]	[slice]	[ns $\cdot$ slice]
Design I (8, 128)	11.44	2932	33.5
Design I (16, 64)	11.39	2037	23.2
Design I (32, 32)	**11.07**	**2075**	**23.0**
Design I (64, 16)	11.61	1803	20.9
Design II (8, 128)	14.38	2579	37.1
Design II (16, 64)	**13.18**	**1580**	**20.8**
Design II (32, 32)	13.81	1807	25.0
Design II (64, 16)	13.63	1696	23.1

adders have to be conducted.

All aforementioned adders have been plugged into our test circuit. Finally, they were implemented on two high performance FPGA devices: 65nm Altera Stratix III and Xilinx Virtex 5, and two low cost 65nm Altera Cyclone III and 45nm Xilinx Spartan 6. All architectures have been modeled in VHDL-93, then synthesized, placed and routed using Xilinx ISE 13.1 and Altera Quartus II 11.1 for Xilinx and Altera FPGAs, respectively.

Maximum clock frequencies have been determined using static timing analysis tools provided as a part of the respective software packages (*quartus_sta* for Altera and *trace* for Xilinx).

The generation of a large number of results was facilitated by an open source benchmarking environment, called ATHENa (Automated Tool for Hardware EvaluatioN), developed at George Mason University [38].

Based on the results collected in Tab. 3.1, the ripple carry addition seems to be the best choice, in terms of latency, for argument's sizes: up to 32-bits and 64-bits for Altera and Xilinx devices, respectively. However, in the case of addition for arguments in the range of 1024-bit arguments, very often the FPGA tools are not even able to complete the placement and routing successfully.

For such big precision of arguments the parallel prefix network-based adders were significantly outperforming ripple carry adder. Surprisingly, in case of the selected FPGA devices, the Kogge-Stone adder is not always faster than the Brent-Kung adder. In fact, the Kogge-Stone adder, only in case of Altera Cyclone III, is clearly superior to the Brent-Kung adder. For all other selected devices, both parallel prefix network-based adders report implementation result differences within 10% range. The Brent-Kung adder has a marginal advantage in Xilinx Spartax 6 and Altera Stratix III and the Kogge-Stone is slightly faster on Xilinx Virtex 5. This surprising outcome was a result of much higher routing delays in the case of Kogge-Stone addition.

Tables 3.2 and 3.3 summarize the result of practical search for optimal values of the word size w for 1024-bit addition and modular addition, respectively.

3.5 Results discussion

In this section, we present a comparison between the implementation results of two proposed hardware architectures, called Design I and II, and two, the best in terms of latency, classical adders: Kogge-Stone and Brent-Kung.

Table 3.4 and 3.5 summarizes the results collected after the *Place-and-Route* and *Fitter*, for addition and modular addition, respectively. All aforementioned designs were compared in terms of latency, the area utilization, and the latency · area product using four modern FPGA devices:

- **Optimal choice of parameters**

  in case of actual hardware implementations in Altera devices both novel designs have consistently achieved their best results, when the word size w was equal to 16 bits. Majority of the best reported results in Xilinx Virtex-5 were achieved when the word size was $w = 32$-bits. The only exception was the case of modular adder based on Design II, where $w=16$ appeared to be optimal. For Spartan 6, the optimal value of w was either 16 or 32 depending on the operation type: addition vs. modular addition and the design type: Design I vs. Design II.

- **Classical adders vs. novel designs.**

  For simple addition, both classical designs are very difficult to beat in terms of latency across all the selected FPGA devices. Based on Table 3.4, we can also observe that in terms of latency, there is no clear winner. In terms of latency, both novel designs demonstrate better relative results for bigger operand sizes. In terms of latency and latency · area product Design I is consistently better than classical adder for low-cost FPGA devices: Cyclone III and Spartan 6. For Virtex 5 Design I is better in terms of latency for n=2048 and n=4096, and consistently better in terms of the latency · area product. For Stratix III, the only advantage appears to be in terms of the product latency · area, and only for Design II.

Table 3.4: Implementation results for combinational versions of selected adders in the 1024-4096-bit range. Δ latency, Δ area, Δ latency · area - relative change in comparison to the best of the two classical designs in terms of latency, area and latency · area product, respectively.

size	adder (w, N)	latency	area	latency · area	Δ latency	Δ area	Δ latency · area
		[ns]	[LE /ALUT /slice]	[ns · slices ·10^3]	[%]	[%]	[%]
Altera Cyclone III (ep3c120f780c7)							
1024	Kogge-Stone	10.67	18287	195.1	-	-	-
	Brent-Kung	12.32	5169	63.7	-	-	-
	Design I (16, 64)	10.63	3977	42.3	-0.4	-23.1	-33.6
	Design II (16, 64)	12.49	3565	44.5	+17.5	-31.0	-30.1
2048	Kogge-Stone	14.33	45618	653.8	-	-	-
	Brent-Kung	14.46	10415	150.6	-	-	-
	Design I (16, 128)	12.22	8239	100.7	-14.7	-20.9	-33.2
	Design II (16, 128)	13.84	7121	98.6	-3.4	-31.6	-26.3
4096	Kogge-Stone	N/A	N/A	N/A	N/A	N/A	N/A
	Brent-Kung	18.55	20986	389.4	-	-	-
	Design I (16, 256)	14.59	17095	249.4	-21.4	-18.5	-35.9
	Design II (16, 256)	16.56	15591	258.2	-10.7	-25.7	-33.7
Altera Stratix III (ep3sl150f1152c2)							
1024	Kogge-Stone	5.90	17238	101.7	-	-	-
	Brent-Kung	5.52	3091	17.1	-	-	-
	Design I (16, 64)	6.42	3018	19.4	+16.2	-2.4	+13.5
	Design II (16, 64)	6.14	2510	15.4	+11.2	-18.8	-9.7
2048	Kogge-Stone	7.38	39188	289.1	-	-	-
	Brent-Kung	6.34	6299	39.9	-	-	-
	Design I (16, 128)	7.32	6361	46.6	+15.4	+1.0	+16.6
	Design II (16, 128)	6.72	5054	34.0	+6.0	-19.8	-15.0
4096	Kogge-Stone	9.77	88328	862.8	-	-	-
	Brent-Kung	7.39	12813	94.7	-	-	-
	Design I (16, 256)	8.31	13420	111.5	+12.4	+4.7	+17.7
	Design II (16, 256)	8.02	10130	81.3	+8.5	-20.9	-14.2
Xilinx Spartan 6 (xc6slx150fgg900-3)							
1024	Kogge-Stone	17.84	4511	80.5	-	-	-
	Brent-Kung	12.71	1898	24.1	-	-	-
	Design I (16, 64)	12.66	1304	16.5	-0.4	-31.3	-31.6
	Design II (32, 32)	13.45	1188	16.0	+5.7	-37.4	-33.8
2048	Kogge-Stone	25.51	10780	275.0	-	-	-
	Brent-Kung	15.55	3703	57.6	-	-	-
	Design I (16, 128)	14.78	2548	37.7	-5.0	-31.2	-34.6
	Design II (32, 64)	15.45	2297	35.5	-0.6	-38.0	-38.4
4096	Kogge-Stone	31.40	21097	662.3	-	-	-
	Brent-Kung	21.57	5258	113.4	-	-	-
	Design I (64, 64)	17.96	4193	75.3	-16.8	-20.3	-33.6
	Design II (16, 256)	19.32	4311	83.3	-10.4	-18.0	-26.6
Xilinx Virtex 5 (xc5vlx155tff1738-3)							
1024	Kogge-Stone	7.79	4476	34.9	-	-	-
	Brent-Kung	8.20	1988	22.4	-	-	-
	Design I (32, 32)	9.79	1100	10.8	+25.7	-44.7	-52.0
	Design II (32, 32)	9.81	1169	11.5	+25.9	-41.2	-48.9
2048	Kogge-Stone	18.05	9699	175.1	-	-	-
	Brent-Kung	10.98	3545	38.9	-	-	-
	Design I (32, 64)	9.93	2707	26.9	-9.5	-23.6	-30.9
	Design II (32, 64)	11.77	2046	24.1	+7.3	-42.3	-38.1
4096	Kogge-Stone	25.55	19677	502.7	-	-	-
	Brent-Kung	13.08	5099	66.7	-	-	-
	Design I (32, 128)	12.71	4696	59.7	-2.8	-7.9	-10.5
	Design II (32, 128)	13.34	3749	50.0	+2.0	-26.4	-25.0

Table 3.5: Implementation results for the 1024-bit modular addition. Δ latency, Δ area, Δ latency $\cdot$ area - relative change in comparison to the either one of two classical designs in terms of latency, area and latency $\cdot$ area product, respectively.

adder (w, N)	latency	area	latency·area	Δlatency	Δarea	Δlatency ·area
	[ns]	[LE /ALUT /Slice]	[ns·LE /ALUT /Slice]·10³	[%]	[%]	[%]
Altera Cyclone III (ep3c120f780c7)						
Kogge-Stone	31.76	42583	1352.3	-	-	-
Brent-Kung	23.75	11356	269.6	-	-	-
Design I (16, 64)	17.54	8474	148.6	-26.1	-25.4	-44.9
Design II (16, 64)	18.72	7699	144.1	-21.1	-32.3	-46.6
Altera Stratix III (ep3sl150f1152c2)						
Kogge-Stone	14.37	30595	439.5	-	-	-
Brent-Kung	11.43	9949	113.7	-	-	-
Design I (16, 64)	9.71	4916	47.7	-15.0	-50.6	-58.0
Design II (16, 64)	9.80	4122	40.4	-14.2	-58.6	-64.5
Xilinx Spartan 6 (xc6slx150fgg900-3)						
Kogge-Stone	35.68	9019	321.8	-	-	-
Brent-Kung	39.90	3850	153.6	-	-	-
Design I (32, 32)	16.10	1794	28.9	-59.7	-53.4	-81.2
Design II (16, 64)	17.80	1853	33.0	-55.4	-51.9	-78.5
Xilinx Virtex 5 (xc5vlx155tff1738-3)						
Kogge-Stone	41.26	7903	326.1	-	-	-
Brent-Kung	20.87	3167	66.1	-	-	-
Design I (32, 32)	11.07	2075	23.0	-47.0	-34.5	-65.3
Design II (16, 64)	13.18	1580	20.8	-36.8	-50.1	-68.5

- **Classical modular adders vs. novel designs.**

  As shown in Table 3.5 for the modular addition, both Design I and Design II significantly outperform both classical designs in terms of all three performance meassures. As a result of the relatively high area utilization in case of Kogge-Stone and Brent-Kung designs, Table 3.5 is restricted to the case of n=1024-bits only.

3.6   Conclusion

In this chapter, we have demonstrated a novel, low latency, hybrid adder based on the high-radix carry save addition and the parallel prefix network. Two different designs based on the Kogge-Stone and Brent-Kung adders, respectively, were implemented, investigated and eventually compared with their well known predecessors.

First, we have conducted an analysis for the choice of the optimal set of parameters for the proposed designs for four different FPGA families. In general, for the optimal set of parameters out best design outperforms the best classical design in terms of the prodct of

latency · area for all four investigated families. Due to this fact the latency · area, for the selected argument sizes, is always improved in comparison to the selected benchmarks.

Moreover, our hybrid high-radix carry save adders with carry projection unit based on parallel prefix network have been applied to the classical design of the modular addition circuit. The implementation results on modern FPGA devices have revealed that latency, area and latency latency · area, for Altera devices, have been improved on average 15, 40 and 55 percent, respectively. In case of Xilinx devices these average improvements amounted to 50, 45 and 70 percent, respectively.

Finally, we believe that, in order to improve the addition for a thousand bits and more in modern FPGA devices, some changes in their internal structure could have been incorporated by vendors themselves. For example, a limited number of the parallel prefix networks (of the size either 16, 32 or 64-bit) could be added. Similarly to DSP units, these carry projection units based on parallel prefix networks could be configured to operate in either combinational or pipelined mode.

For the future work we are going to investigate the application of the aforementioned concept to the high level applications like coprocessors supporting computations of cryptographic schemes based on elliptic curve and pairing transformations over primes fields.

Chapter 4: Hardware architectures for modular arithmetic based on the use of Solinas numbers and heterogenous FPGA devices

In this chapter, we demonstrate novel hardware architectures for high speed modular arithmetic based on the use of the Solinas primes and DSP units of modern FPGAs. Our goal is to show that combining the Barrett algorithm, the Booth recoding, and the high-radix carry save representation of arguments enables very efficient, parallel modular arithmetic, optimized for this important class of prime numbers.

Contents

4.1 Introduction and motivations

A well known shortcut for modular multiplication modulo a Mersenne number (2^k-1), which amounts to performing modular reduction without integer division, has been generalized by the National Security Agency (NSA) researcher - Jerome A. Solinas in [119]. In this work he discussed numbers of the following form $2^a \pm 2^b \pm 2^c \pm 1$, and $gcd(a, b, c) = word\_size$, and $word\_size = 16, 32, 64$. In [119] Solinas has also demonstrated a corresponding reduction method, based on a few additions and subtractions. A big class of Solinas prime numbers

and their efficient arithmetic have been widely accepted and recommended for the NIST standard - Elliptic Curve Digital Signature Algorithm (ECDSA) [120].

The aforementioned technique is not applicable for all Solinas primes, in particular for those primes, which are recommended for the higher security levels of pairing transformations (e.g. Solinas primes from [121] (section 7.2) or [37]).

In this chapter, we are going to demonstrate new hardware architectures for modular addition, multi-operand addition, multiplication and reduction, optimized for the use of Solinas primes.

The rest of this chapter is organized as follows:

In Section 4.2 we discuss relevant previous work in the area of modular multiplication (the addition architectures has been discussed in the previous chapter). Section 4.3 is devoted to the discussion of the hardware architectures for Solinas primes. Finally, in Section 4.4 we conclude our work.

4.2 Previous work

In 1985 Montgomery proposed modular multiplication without trial division [105]. A novel number representation and a novel basic arithmetic operation were named after his name numbers in the Montgomery domain and the modular Montgomery multiplication, respectively. It enables the multiplication and reduction to be conducted in parallel.

In 1999 Tenca et al. [106] proposed the first scalable architecture for Montgomery Multiplication. Harris et al. in [107] and Huang et al. in [122] have improved this design in terms of latency and latency · area by a factor of two.

Further improvement of the aforementioned architectures was possible when higher radixes were introduced. They were demonstrated for the Tenca et al., Harris et al. and Huang et al. designs in [123], [124] and [122], respectively.

Kaihara et al. in [125] proposed the BiPartite multiplication, a concept which enables parallel execution of the Montgomery and Interleaved multiplication. Öksüzoğlu et al. in

[126] reported DSP-based architecture for low-cost devices.

The TriPartite algorithm in [127] effectively integrates three different existing algorithms, a classical modular multiplication based on Barrett reduction [128], the modular multiplication with Montgomery reduction and the Karatsuba multiplication [129] algorithms in order to reduce the computational complexity and increase the potential of parallel processing.

Hardware architectures of modular arithmetic for parallel computing were demonstrated using Residue Number System in [130] and Spectral Modular Arithmetic in [131] and [132].

Long integers can be multiplied modulo Solinas primes using the aforementioned Montgomery arithmetic, in particular using, so called, quotient pipelining technique proposed by Orup [133].

The Orup's method has been been adapted by Suzuki in [134] and [135] to the DSP block available in Xilinx Virtex-4 and Virtex-5, respectively. To the best of our knowledge, Suzuki's hardware architecture is the fastest to date FPGA implementation of the Montgomery multiplication. Due to the internal dependencies in Orup algorithm ([134] Tab. 2), the computations of the consecutive words of the final result is separated by the interval of two clock cycles. Thus, the latency formula in case of Orup algorithm converges to $2 \cdot N$, where N denotes the number of words representing arguments.

An alternative solution is to separate both basic operations: the multiplication and reduction, and conduct the optimization on them separately. In such approach it is possible to introduce basic, two-stage pipelining into multiplication-reduction computations.

In case of the multiplication, several improvements have been analyzed in the past by Karatsuba et al.[129], Toom [136], Schönhage and Strassen [137] and recently Fürer [138]. All four aforementioned methods would require large amount of DSP units, thus we are going to use simpler, conceptually slower, yet powerful, grid (also called box) multiplication method. The latency formula in case of grid multiplication converges to N.

In case of the reduction, for a random prime number, the complexity of the classical Barrett reduction [128] is equivalent to the complexity of the multiplication method.

However for the meticulously selected Solinas primes this algorithm might be simplified to few additions and subtractions. The optimization of the Barrett reduction for Solinas primes is going to be beneficial for the scheduling of scenarios where pipelining technique can not be utilized (e.g. an exponentiation enforces the date dependency in consecutive multiplications).

A brief overview of hardware architectures for modular arithmetic is provided in table 4.1.

Table 4.1: General Purpose Modular Multiplication/Inversion architectures for GF(p)

| Algorithm	Radix-2	Higher Radix	Scalability
Montgomery Multiplication			
Binary Arithmetic			
Tenca and Koç	[106]	[123]	yes
Harris et al.	[107]	[124]	yes
Huang et al.	[122]	[122]	yes
Michalski and Buell		[139]	yes
McIvor et al.	[109]		no
Suzuki		[134]	yes
Öksüzoğlu and Savaş		[126]	yes
Residue Numbers Systems Arithmetic			
Kawamura	NA	[130]	no
Bajard et al.	NA	[140], [141]	no
Spectral Modular Arithmetic			
Saldamlı and Koç		[131], [142]	no
Baktır et al.		[132]	no
Interleaved Multiplication-Reduction			
Amanor	[143]		yes
AbdelFattah et al.	[144]		no
Mixed Montgomery-Interleaved Multiplication			
Kaihara and Takagi	[125], [145]	[125], [145]	yes
Sakayama et al.		[127]	no
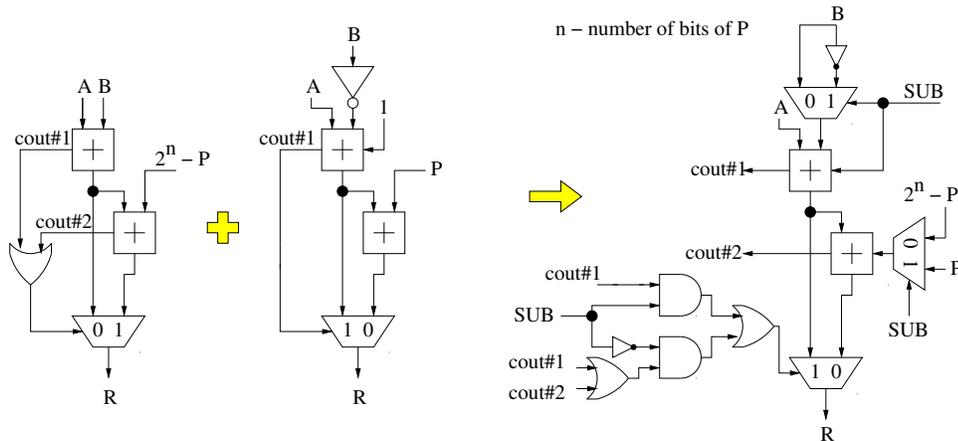
Figure 4.1: Modular adder/subtractor - high level block diagram
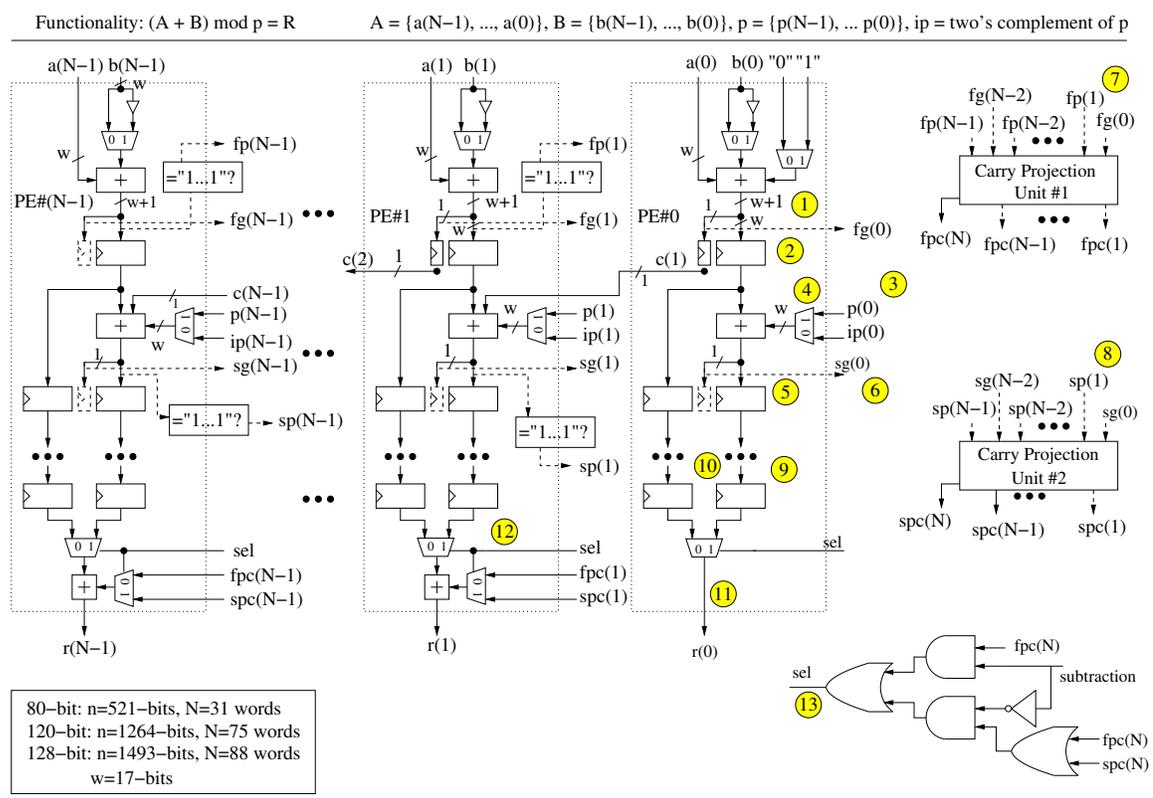
Figure 4.2: Pipelined high-radix carry save modular adder/subtractor

74

4.3 Architectures for the Solinas primes

4.3.1 Modular adder/subtractor

In general our modular adder/subtractor is an extension (Fig. 4.1) of the concept of adder-based operator demonstrated for instance in [20] (Fig. 1c). It is demonstrated in Fig. 4.2 and it supports both modular addition or subtraction (argument B has to be transformed into one's complement form and '1' has to be added to the least significant word Fig. 4.2 pt. 1).

Both A and B as well as modulus p and its two's complement value ip are split into N w-bits words. First, A and B are added (or subtracted) and the intermediate result, in 2^w radix carry save form, is computed.

Those intermediate results must be stored into registers (Fig. 4.2 pt. 2). Next in line is the addition of this partial result with either modulus or its two's complement value for subtraction and addition, respectively (Fig. 4.2 pt. 4), and again the intermediate results (vector of sums and carries) of this operation are stored into registers (Fig. 4.2 pt. 5).

Both intermediate results, represented as vectors of sums and carries, have additional sets of flags. The first and the second intermediate results produce $\{fp(n-1),...,fp(0)\}$, $\{fg(n-1),...,fg(0)\}$ (Fig. 4.2 pt. 3) and $\{sp(n-1),...,sp(0)\}$, $\{sg(n-1),...,sg(0)\}$ (Fig. 4.2 pt. 6), respectively.

The flag $fp(i)$ is set when i-th word of the first intermediate result consists of all ones (Eq. 3.2). The flag $fg(i)$ is set when the carryout from the i-th block of the first intermediate result is equal to one. The definition of flags: sp(i), sg(i) is identical except that they concern second intermediate result. Those flags are going to two separate *carry projection units* (Fig. 4.2 pt. 7 and 8), which are described in the next subsection.

A single carry projection unit computes the projected carries within a deterministic number of clock cycles. In order to increase the performance of the whole modular adder additional chains of registers were added (Fig. 4.2 pt. 9 and 10), making this circuit fully

pipelined. The number of modular additions possible to perform at the same time for a given security level are summarized in Table 5.6.

Finally, both *carry projection units* compute vectors of projected carries and also determine which intermediate result will be selected as the final result. In order to do that, we need to investigate two separate cases for the addition (Eq. 4.1) and subtraction (Eq. 4.2).

- $R = A + B \pmod{P}$

$$R = \begin{cases} A + B - P, & \text{if } A + B \geq 2^k \vee A + B - P \geq 0 \\ A + B, & \text{otherwise} \end{cases} \quad (4.1)$$

- $R = A - B \pmod{P}$

$$R = \begin{cases} A - B + P, & \text{if } A - B < 0 \\ A - B, & \text{otherwise} \end{cases} \quad (4.2)$$

In case of the addition, the conditions $(A + B \geq 2^k)$ or $(A + B - P \geq 0)$ corresponds to the values of $fpc(N)$ and $spc(N)$ (the most significant carries computed in the *carry projection units*), respectively. If any of these conditions happens the value of $A + B - P$ has to be selected, otherwise the value $A + B$ is correct. On the other hand, when the subtraction is conducted, we have to check only if the first intermediate result is negative or positive. Thus, evaluation of the flag $fpc(N)$ is sufficient for the determination which value, $A - B + P$ or $A - B$, should be chosen.

Based on the aforementioned conditions, the signal *sel* (Fig. 4.2 pt. 13) selects one of the partial results for the final addition with projected carries, and the final result (Fig. 4.2 pt. 11 and 12) is obtained.
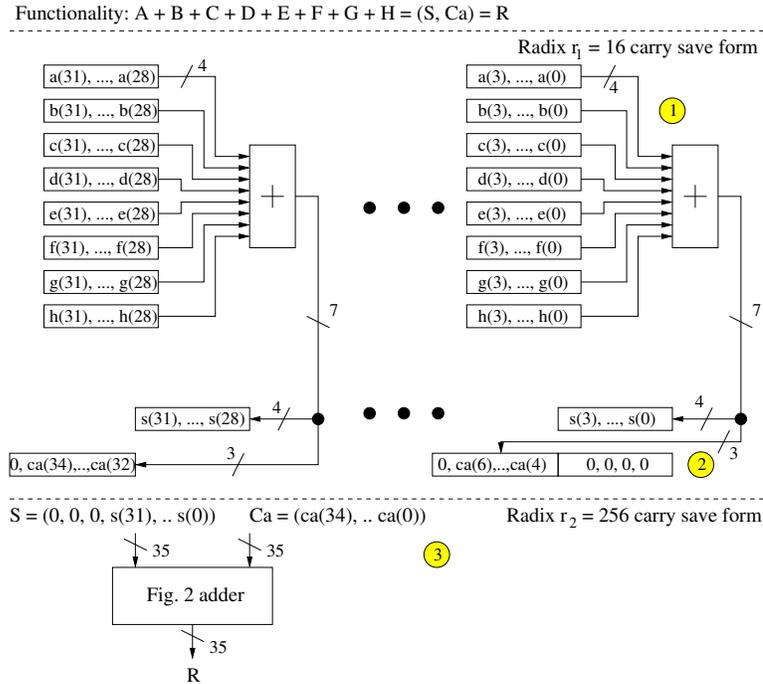
Figure 4.3: High-radix carry save multi-operand adder

4.3.2 Mixed radix multi-operand addition

The multi-operand addition can also benefit from the aforementioned hybrid adder. In Fig. 4.3 we have presented an example of an addition of eight 32-bits arguments, but this concept can be easily extended to the larger number of arguments and the wider operands as well. This adder works in two operational phases:

- The reduction of the number of arguments phase (upper part of Fig. 4.3). It is completed when all eight arguments: $A, ..., H$ (Fig. 4.3 pt. 1), are reduced to just two operands, the partial results of this operation: S and Ca (Fig. 4.3 pt. 2). The size of the significant part of every word in the carry vector: Ca, depends on dynamic range of arguments and it can be determined by the value of $\lceil log_2(M) \rceil$, where M defines the number of operands. In case of our example: eight 4-bits operands ($M = 8$) added together produce 4-bits of sum (S) and 3-bits of carry (Ca).

77

- The addition of the intermediate values: (S, Ca) (lower part of Fig. 4.3 pt. 3) is performed exactly like in case of the adder described in the previous chapter.

Due to the fact that the eight-argument addition is logically more complex than the two-argument addition, we have decided to conduct both phases using two different radices. The first phase radix r_1 is always smaller than the second phase radix r_2. In Fig. 4.3, $r_1 = 2^4$ and $r_2 = 2^8$, but the optimal ratio between these two parameters seems to be specific issue for a given FPGA family.

4.3.3 Modular multiplier with Booth recoding and Barrett reduction

4.3.4 Multiplication using DSP blocks

This circuit is based on a grid multiplication method adapted to modern FPGA structures. In order to achieve high-speed computations, DSP slices available on modern FPGA devices, have to be used. In this section Xilinx Virtex-6 devices will serve as a case study. Due to the fact that every Virtex-6 DSP unit contains 17x24 multiplier, both multiplication arguments have to be represented in two different radices (2^{17} and 2^{24}).

Every argument can be then represented by N and M words in the respective radix. The sizes of arguments at a given security level are summarized in Tab. 5.1. The number of words in a particular representation can be computed using formula $\lceil \frac{n}{w} \rceil$, where n and w correspond to the sizes of arguments and words in bits, respectively.

The argument A (Fig. 4.4 pt. 1), represented in radix 2^{17}, is constant during the particular multiplication. The argument B is scanned in 24-bit chunks and it is updated every clock cycle from the least significant to the most significant word. This configuration is optimized for low latency rather than the small DSP utilization.

Every clock cycle, every DSP block produces N (in case of 80-bit security $N=31$) 41-bit chunks of intermediate data. As a consequence of a 17-bit granulation of argument A, the neighboring 41-bit chunks contribute to the different parts of partial sum and they are

Functionality: A * B = (RR, RC), where   A = {a(N−1), ..., a(0)}, B = {b(N−1_, ...,0)}, RR = {rr(2M−1), ..., rr(0)}, RC = {rc(2M−1), ..., rc(0)}
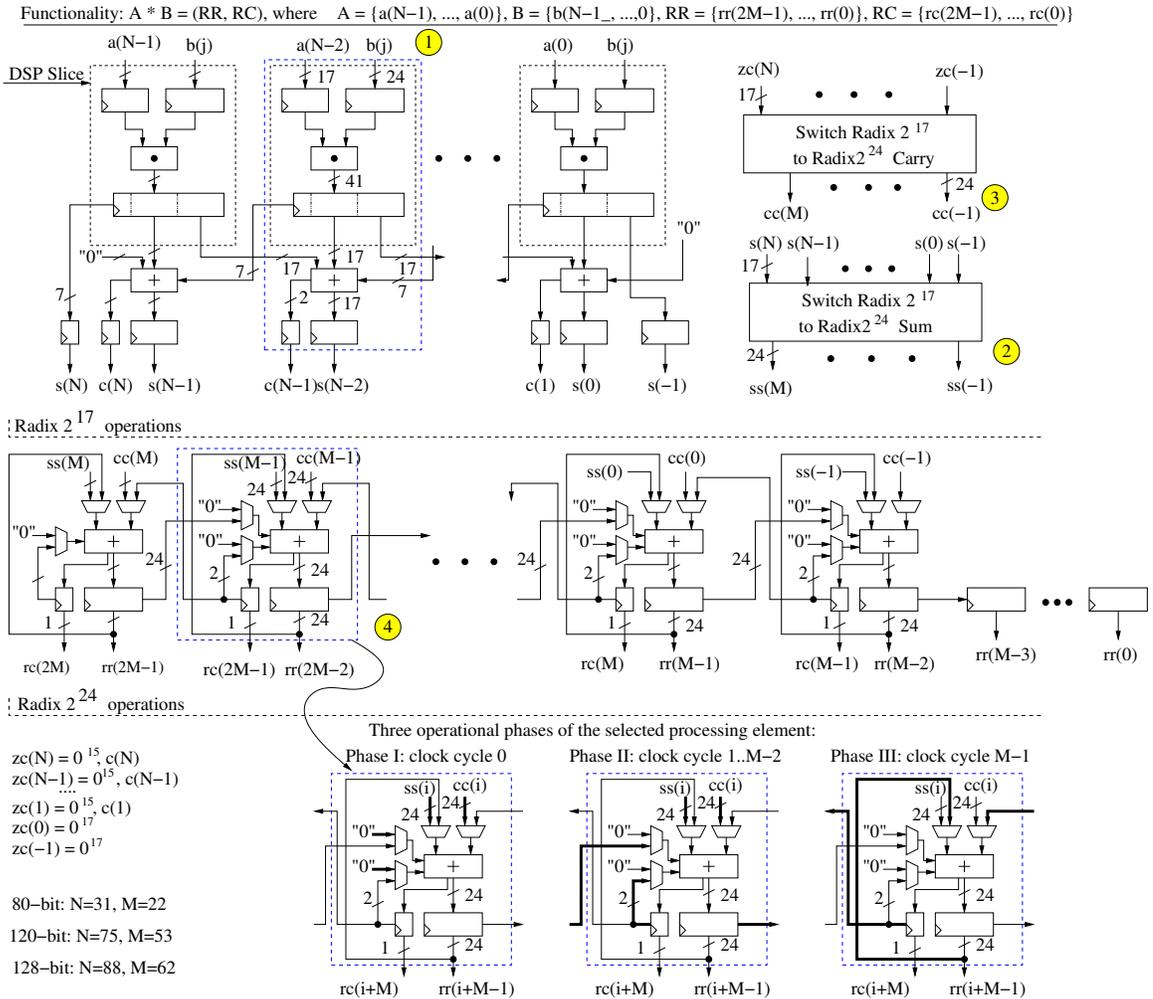
Figure 4.4: Block diagram of a multiplier based on 24x17 DSP units

79
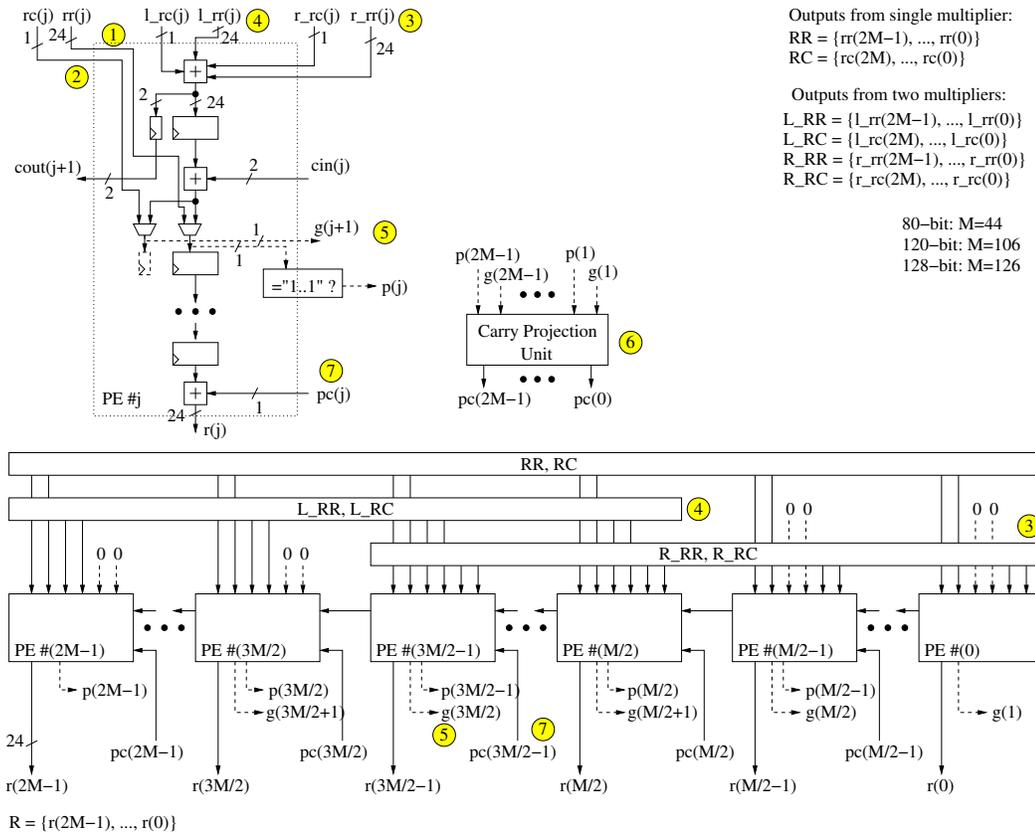
Figure 4.5: Additional circuit for the multiplier double speed mode support.
$(L\_RR = (RR << \frac{24 \cdot M}{2}), L\_RC = (RC << \frac{24 \cdot M}{2})$, for (RR, RC) from left multiplier) and $(L\_RR = RR, L\_RC = RC$, for (RR, RC) from right multiplier)

shifted by 17 positions to the right. In order to compute the final value of multiplication - all partial sums must be added.

As a result of the facts: the argument A consists of N 17-bit words and only 24-bits of argument B ($b(j)$) are used, then the size of the product $A \cdot b(j)$ is defined by $17 \cdot N + 24$. This lead us to the conclusion that $N + 2$ 17-bits words are needed for the representation of this partial product (the indices of (S, C) on Fig. 4.4 are between N and -1) .

Correspondingly, because of the 24-bit granulation of argument B, the neighboring partial sums contribute to different parts of the final result and they are shifted by 24 positions to the right (Fig. 4.4 pt. 4).

Due to the discrepancies in relative positions between 41-bit chunks of data produced by DSPs and the relative positions between partial sums, the radix changes are introduced (Fig. 4.4 pt. 2, pt. 3). They are implemented by simple rewiring.

However, every partial sum is represented by $N + 2$ 17-bit words at the input to the radix change module and it has to be transferred into $M + 2$ 24-bits words. It is a natural consequence of the fact that $\lceil \frac{(N+2) \cdot 17}{24} \rceil$ represents the number of output words.

The partial result of multiplication is obtained in a high radix carry save form: a sum vector (Fig. 4.4: RR) and a carry vector (Fig. 4.4: RC).

The numbers of clock cycles required to perform the multiplication at a given security level are summarized in Table 5.6.

Our grid multiplier could easily benefit form the Karatsuba's algorithm [129]. However, the basic step of Karatsuba's algorithm allows us to compute the product of two large numbers A and B using three multiplications of smaller numbers, each with about half as many digits as A or B, and also three additions and digit shifts. Therefore, the most basic version of parallel Karatsuba approach would result with approximately $\frac{3}{2}$x more DSP units. Further recursion would provide even higher DSP block utilization, but also it would help improve the latency of a single multiplication. In this chapter we will report result for a multiplier without the Karatsuba trick.

4.3.5 Double-speed mode

A computation of a pairing transformation consists of execution of two other algorithms: the Miller's loop and the final exponentiation. Those algorithms demonstrate different data-dependency schemes and due to that fact different number of basic arithmetic modules might be optimal for them.

The major motivation behind the introduction of the double speed mode (further improvement is possible and it depends on the application and number of multiplication units) for the multiplier was the fact that a single iterations of Alg. 4, Alg. 3 can be achieved using up to four independent streams of data and a single iteration of Alg. 7 requires two modular multiplications only. The latency-optimized design of our coprocessor (details in the next section), conducting the Miller loop computations, requires four multipliers working in parallel in a basic mode. On the other hand, a single iteration of the final exponentiation need only two multipliers working in parallel. The major motivation behind the introduction of this special double speed mode was full utilization of computational resources and thanks to this fact shortening the latency of a single iteration of the final exponentiation.

Kaihara and Takagi have introduced the Bipartite multiplication in [125]. This concept enables splitting multiplication into two parts. These two parts are then processed separately, in parallel, potentially doubling the speed of calculations. Later on, the Bi-Partite multiplication was generalized using Karatsuba [129] algorithm, and the TriPartite multiplication was introduced in [127].

A double speed mode in case of the multiplier proposed in this chapter is an idea inspired by the aforementioned concepts, however the computations in both paths are in the same integer domain (in [125] and [127] one of the domains is Montgomery and the other one is natural, integer domain.). Let A, B be $w \cdot N$-bit numbers, and $A = A_H \cdot 2^{\frac{w \cdot N}{2}} + A_L$, then the multiplication of A and B can be computed as follows

$$A \cdot B = (A_H \cdot 2^{\frac{w \cdot N}{2}} + A_L) \cdot B = A_H \cdot B \cdot 2^{\frac{w \cdot N}{2}} + A_L \cdot B. \tag{4.3}$$

Both terms, $A_H \cdot B$ and $A_L \cdot B$ are calculated using two separate multipliers in a half of the clock cycles. In order to complete the multiplication, an extra circuitry (Fig. 4.5) is needed for the addition of both partial sums.

In case of normal operational mode of the multiplier, the high-radix carry save results (RR and RC) are bypassed to the registers (Fig. 4.5 pt. 1 and 2). In case of the double speed mode, the most significant part ($L\_RR = (RR << \frac{24 \cdot M}{2})$, $L\_RC = (RC << \frac{24 \cdot M}{2})$) (Fig. 4.5 pt. 4), after a fixed shift, and the least significant part ($R\_RR = RR$, $R\_RC = RC$)(Fig. 4.5 pt. 3) have to be added and stored into registers. The generate and propagate flags are transferred to the inputs of the carry projection unit, and the corresponding carries at the foundry of each word are computed by this unit (Fig. 4.5 pt. 6). Finally, the transition between high-radix carry save form into radix two form is completed, when the projected carries are added to the corresponding words (Fig. 4.5 pt. 7).

4.3.6 Barrett reduction for Solinas primes:

Solinas proposed a method of generalization of Mersenne primes (a prime number of a form 2^p-1, where p is a prime) in [119]. He proposed an efficient arithmetic for numbers of the form $2^a \pm 2^b \pm 2^c \pm 1$, where $gcd(a, b, c) = word\_size$, and $word\_size = 16, 32, 64$. This method is not suitable for the Solinas primes recommended for supersingular curves-based pairing (Table 5.1).

Instead of previously mentioned arithmetic we decided to adopt the Barrett reduction [128] for Solinas primes. This method (Alg. 1) computes $r = x \bmod p$ for a given x and p. It requires the pre-computation of the quantity

$$\mu = \lfloor 2^{2n}/p \rfloor. \tag{4.4}$$

The algorithm is the most efficient if many reductions are performed with a single modulus. For example, a single Tate pairing requires computation of thousands of multiplications, each and every one has to be reduced by a common modulus. The pre-computation of μ takes a fixed amount of work, which is negligible in comparison to Tate pairing cost.

For a random prime number, the complexity of Barrett reduction is equivalent to the complexity of the multiplication method. However, in case of the selected Solinas prime numbers (Tab. 5.1) the multiplications by two constants: μ (ln. 2 in Alg. 1) and p (ln. 5 in Alg. 1) can be reduced to the multi-operand addition.

Two values r_1 and r_2 (computed in line 4 and 5 in Alg. 1) have a possible range between 0 and $2^{n+1} - 1$. Therefore, the result of the subtraction $r = r_1 - r_2$ (line 6 in Alg. 1) will be in a range $< -2^{n+1} - 1, 2^{n+1} - 1 >$. For a given prime modulus p the ratio $\lfloor \frac{2^{n+1}}{p} \rfloor$ defines the maximum number of iterations of the *while* loop (lines 9-11) in Alg. 1. Hence, in case of Solinas primes selected in Tab. 5.1 the number of those iterations is always in a range of $< 0, 3 >$. Additionally, the *if* condition from lines 7 to 9 in Alg. 1 duplicates number of possible scenarios for this *if-while* part of Barrett algorithm. Since 2^{n+1}, p and then $2 \cdot \lceil \frac{2^{n+1}}{p} \rceil$ parameters are known in advance, they can be precomputed and stored in a memory.

This approach allows to compute in parallel two paths in Alg. 1: the first one, consisting of lines 1-3 and 5, leads to the r_2 evaluation. The second one, consisting of lines 4 and 7 to 12, leads to the computations of $r_1 + cons(i)$, where $cons = \{0, -p, -2p, -3p, 2^{n+1}, 2^{n+1} - p, 2^{n+1} - 2p, 2^{n+1} - 3p\}$. Finally, the r is calculated by the subtraction of r_2 from all eight precomputed values, and the selection of the correct value ($r \in (0, p-1)$) is relatively simple task (see Eq. 4.5 and 4.6).

The block diagram of **Barrett reduction circuit for Solinas primes** is demonstrated
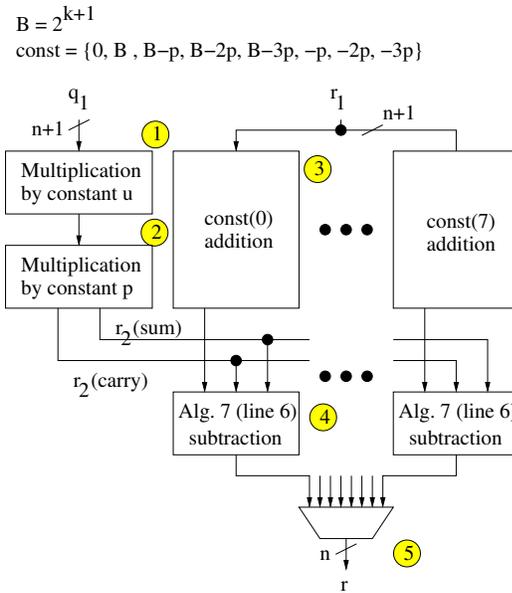
Figure 4.6: Block diagram of Barrett reduction for Solinas primes

---

Algorithm 1 Barrett modular reduction according to [146](14.42)

Require: $x = (x_{2n-1}...x_1, x_0)_2$, $p = (p_{n-1}...p_1, p_0)_2$ $(p_{n-1} \neq 0)$, $\mu = \lfloor 2^{2n} / p \rfloor$
Ensure: $r = x \bmod p$

1: $q_1 \leftarrow \lfloor x/2^{n-1} \rfloor$
2: $q_2 \leftarrow q_1 \cdot \mu$
3: $q_3 \leftarrow \lfloor q_2/2^{n+1} \rfloor$
4: $r_1 \leftarrow x \bmod 2^{n+1}$
5: $r_2 \leftarrow q_3 \cdot p \bmod 2^{n+1}$
6: $r \leftarrow r_1 - r_2$
7: **if** $r < 0$ **then**
8: $\quad r \leftarrow r + 2^{n+1}$
9: **end if**
10: **while** $r \geq p$ **do**
11: $\quad r \leftarrow r - p$
12: **end while**
13: **return** r

---

in Fig. 4.6. For the reason that it is the least parametrizable module, in terms of VHDL modeling, it is difficult to demonstrate detailed, generalized, applicable for all security levels, version of this circuit. However, every basic building block is very simple. Every pipelining stage consist of either fixed shifts, constant value addition or up to 4 operand addition (up to 8 at higher security levels).

- **Multiplication by μ - (ln. 2 in Alg. 1)** is presented in Fig. 4.6 pt. 1. Since the μ value is unique for every p, we are going to use as an example p for 80-bit security level.

  The pre-computations of μ (Eq. 4.4) and then the application of Booth recoding [147] led us to the $\mu = 2^{522}$ - 2^{365} + 2^{362} + 2^{207} + 2^{206} + 2^{202} - 2^{51} + 2^{49} + 2^{47} + 2^{45} + 2^{42} + 2^2 for 80-bit security parameters. The multiplication by this μ could be implemented by twelve fixed shifts and one twelve-operand addition/subtraction unit. Instead of that this operation was implemented in a pipelined fashion within 4 pipeline stages.

  In the first stage, the results of fixed shifts are represented in the radix-2^8 carry save form, grouped into three sets of four elements and the four operand addition is conducted. The results of this last operation are three vectors of sums and corresponding carries.

  In the second stage of pipelining of the multiplication by μ, the three vectors of sums and three vectors of carries are added in the carry save radix-2^8 form. The results of this last operation are a new vector of sums and carries in the radix-2^8 form. The radix-2^8 selection for the multi-operand addition was determined by an obvious fact that radix-2^8 offers a shorter critical path than the radix-2^{17}

  Since it is not a trivial task to conduct division on any number in a carry save form (ln. 3 in Alg. 1), a transfer to radix-2 is needed. Since the computations of projected carries are less complex in the higher radices carry save forms (smaller number of the generate and propagate flags) then the vectors of sums and carries computed in the second pipeline stage are represented in carry save radix-2^{17} form and the addition is

86

conducted. Sets of generate and propagate flags are produced and sent to the carry projection unit.

The fourth and the last pipeline stage in this module is motivated by the fact that carry projection unit for the 80-bit security level requires one clock cycle for the projected carries computation.

Once projected carries are added to the vector of sums, the final result of multiplication by μ - a q_2-value is created. The division by the power of two in ln. 3 of Alg. 1 is conducted by a simple selection of upper part of q_2

- **The Multiplication by p - (ln. 5 in Alg. 1)** is presented in Fig. 4.6 pt. 2. In case of Solinas primes for 80, 128 and 192-bit security levels, the multiplication by the modulus p in the Barrett algorithm can be implemented using three fixed shifts, one addition and two subtraction. All those operations are conducted in one clock cycle by three operand addition, where arguments and result are represented in the carry save radix-2^8 form.

- **Constant addition units** are presented in Fig. 4.6 pt. 3. Every single unit conducts, in parallel, the addition of r_1 to one of eight following constants: $const = \{c(0) = 0, c(1) = -p, c(2) = -2p, c(3) = -3p, c(4) = 2^{n+1}, c(5) = 2^{n+1} - p, c(6) = 2^{n+1} - 2p, c(7) = 2^{n+1} - 3p\}$. Due to the fact that there are five pipeline stages (for 80-bit security arguments) in the lines 1-3 and 5 of Alg. 1 then in order to keep Barrett reduction circuit fully pipelined we perform the eight constants addition within five clock cycles.

- **($r_1 - r_2$ subtraction units from line 6 in Alg. 1)** are presented in Fig. 4.6 pt. 4. All eight possible intermediate values have to be eventually subtracted from the values computed in the *Multiplication by p* circuit. Due to the fact that the r_2 is in the radix 2^8 radix carry save form, then the subtraction is conducted in two clock cycles. In the first and the second clock cycles the two's complement values of a vector of sums and a vectors of carries are added to the r_1, respectively. Finally, the *carry projection*

87

units compute the projected carries to corresponding partial results and all eight final results can be represented in radix-2 form.

- **The final result selection** is presented in Fig. 4.6 pt. 5. As a result of the fact that two non-negative values: r_1 and r_2 can have up to $(n+1)$-bits, then the possible range of $r = r_1 - r_2 \in (-2^{n+1}, 2^{n+1})$ (Alg. 1). The most significant $(n+2)$-bit, of the $r_1 - r_2$, determines if this partial result is either negative or positive.

So in the next step the final result is going to be selected from the following two sets:

- Set 1, when $r_1 - r_2$ is positive:

$$
r = \begin{cases}
a = r_1 - r_2, & \text{if } a_{(k+1..k-1)} \in \{0, 1\} \\
b = r_1 - r_2 - p, & \text{if } b_{(k+1..k-1)} \in \{0, 1\} \\
c = r_1 - r_2 - 2p, & \text{if } c_{(k+1..k-1)} \in \{0, 1\} \\
d = r_1 - r_2 - 3p, & \text{if } d_{(k+1..k-1)} \in \{0, 1\}
\end{cases}
\tag{4.5}
$$

- Set 2, when $r_1 - r_2$ is negative:

$$
r = \begin{cases}
e = r_1 - r_2 + b^{k+1}, & \text{if } e_{(k+1..k-1)} \in \{0, 1\} \\
f = r_1 - r_2 + b^{k+1} - p, & \text{if } f_{(k+1..k-1)} \in \{0, 1\} \\
g = r_1 - r_2 + b^{k+1} - 2p, & \text{if } g_{(k+1..k-1)} \in \{0, 1\} \\
h = r_1 - r_2 + b^{k+1} - 3p, & \text{if } h_{(k+1..k-1)} \in \{0, 1\}
\end{cases}
\tag{4.6}
$$

The selection within a set is always unique, it is due to the Barrett reduction (Alg. 1) prerequisite for the most significant bit $p_{k-1} \neq 0$

4.4 Conclusions

The reduction technique proposed in [119] is not applicable for all Solinas primes, in particular for those which are used in Pairing-based Cryptography.

First, we have demonstrated that Solinas primes can benefit from the modified Barrett reduction algorithm and then we have proposed conditions for efficient arithmetic based on those primes. Next, we have optimized a grid method for multiplication to match the structure of the digital signal processing blocks (DSP units), embedded in the modern FPGA devices.

This simple, but very flexible design can give us some unique features - e.g.: it allows us to speed up single multiplication by using two multipliers. This special feature is especially attractive in case of n multiplications to be executed using m available multipliers where n divides m. (e.g.: two multiplications executed using four multipliers, which is the case in our pairing coprocessor described in Chapter V).

Finally, we have combined both concepts: the grid multiplication method optimized for FPGAs and the Barrett reduction for Solinas primes, and as a result we have obtained, an optimal, modular multiplier for pairing-friendly Solinas primes.

Chapter 5: Pairing on Edwards curves for speed-oriented applications

In this chapter are going to demonstrate the fastest to date, a high speed hardware accelerator for the Tate pairing on twisted supersingular Edwards curves over prime fields. This coprocessor was built upon the hardware architectures proposed for Solinas primes and the hybrid high-radix carry save and parallel prefix network adder.

Contents

5.1　Introduction and motivation

In 1985, Koblitz [111] and Miller [110] independently discovered that elliptic curves can be used to construct public key cryptosystems. Since then, Elliptic Curve Cryptography(ECC) has been an important object of studies, leading to multiple practical applications [148], [149], [150] or [151]. Due to the performance and security reasons, different forms and types of elliptic curves have been proposed: Hessian [152], Koblitz [153], Jacobian [154],

Montgomery [155] and doubling and tripling oriented Doche-Icart-Kohel [156]. A new form of elliptic curves was recently introduced by Edwards [157]. Bernstein and Lange have demonstrated multiple improvements and applications to cryptography [158], [159], [160] and [161]. The details and explicit formulae of most important curves are summarized in [114].

An operation of bilinear pairing on elliptic curve has been introduced originally for cryptanalysis by Frey and Rück [162] and Menezes, Okamoto and Vanstone [163]. In 1986 Miller [164] proposed the first algorithm for iteratively computing the Weil and Tate pairings. Nowadays, pairing is primarily used in cryptography for constructive reasons: it is a basis of security schemes for various applications. The versatility of pairing based cryptography has made it an important object of studies. Several of pairing-based schemes, such as tripartite key exchange protocol [165], identity-based encryption [166], identity-based signatures [167], and short signatures [168], have been proposed in the last decade. Apart from the mentioned previously Weil and Tate pairing, other popular pairing types were discovered, e.g.: Eta [169], Ate [170], R-Ate [171] and Optimal-Ate [172].

5.1.1 Motivation

Compared with other popular public key cryptosystems, like Elliptic Curve Cryptography or RSA [24], pairing is much more computationally demanding. Therefore, the efficient hardware and software implementations of cryptographic pairing have also received significant attention [173], [174], [175], [176], [177], [178] and [179]. However, the hardware architectures for Edwards curves-based pairing, introduced for supersingular in [37] and ordinary forms in [180], have not been reported yet.

The National Security Agency released the Fact Sheet NSA Suite B Cryptography [181]. This document recommends a transition into elliptic curve systems instead of classical public key technology, such as RSA and DSA [120]. Finally, it provides the recommendation for the underlying modular arithmetic: the prime fields must be used, instead of binary or

ternary fields.

The computation of a pairing can be broken down into curve, group and eventually modular operations in the underlying fields (Fig. 5.1) Thus, having an efficient modular multiplier is a major component of a high performance pairing processor. In this work, we are interested in hardware implementation of pairings over large characteristic fields.

One of the possible optimizations is to take advantage of the embedded resources in the modern FPGA. Practically all FPGA vendors incorporate in modern FPGAs, apart from basic reconfigurable logic resources [182], also embedded components, such as large memory blocks [183], DSP units [184], and Fast Carry Chain Adders [182], [185]. These hardwired FPGA resources, together with meticulously selected prime numbers such as Mersenne, Fermat, or Solinas [119] primes can serve as a basis of an efficient hardware modular architecture.

A well known shortcut for modular multiplication modulo a Mersenne number (2^k-1), performing modular reduction without integer division has been generalized by Solinas in [119]. A big class of Solinas prime numbers and their efficient arithmetic have been widely accepted and recommended for ECDSA [120]. The aforementioned technique is not applicable for all Solinas primes (e.g. Solinas primes from [121] (section 7.2)).

Historically, the software implementations of cryptography have been slower than their FPGA counterparts. Pairing implementations over prime fields on general purpose processors are unique in this respect and they have been demonstrated to be as fast as the hardware architectures [177]. An efficient protection based on the prime field pairing systems for cross-platform communication is possible.

5.1.2 Contribution

In this effort we are going to demonstrate several new hardware design techniques for Tate pairing on Edwards curves over prime fields defined in [37]. Major contributions of this chapter cover four different layers of pairing computations and they are highlighted here:
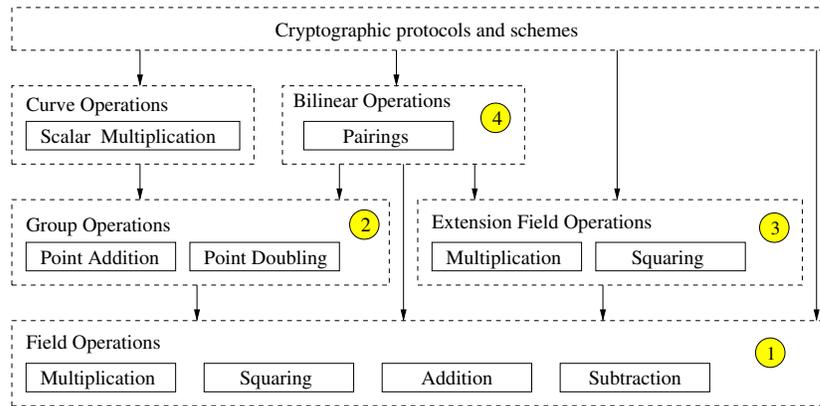
Figure 5.1: Hierarchy of functions in pairing-based cryptosystems

- This chapter presents an application of our Solinas primes-based, modular arithmetic architectures for addition and multiplication (Fig. 5.1, pt. 1) to the higher level application - Pairing-based cryptography [186] on supersingular curves.

- It further explores the parallelism in the explicite formulae of group and bilinear operations. Eventually, operation scheduling for multi-core environment is provided. (Fig. 5.1, pt. 2)

- It provides a novel approach to the final exponentiation for given parameters (Fig. 5.1, pt. 3).

- It provides first hardware architecture for 80, 120 and 128-bit pairing on Edwards curves (Fig. 5.1, pt. 4).

- Finally, the proposed design computes 80, 120 and 128-bit secure pairing over prime field in less than 0.14, 0.54 and 0.70 ms, respectively. It is the fastest pairing implementation over prime fields in 120-128-bit security range.

The rest of this chapter is organized as follows:

In Section 5.2 we discuss previous work. Section 5.3 is devoted to the Tate pairing on Edwards curves over prime fields. Section 5.4 describes the proposed coprocessor. Section 5.5 discusses and analyzes the results, finally we draw conclusions in Section 5.6.

5.2   Previous work

Baretto and Naehrig have demonstrated a pairing-friendly class of curves for prime fields in [187] (Barreto-Naehrig (BN) curves). Currently, they are considered the most suitable for 128-bits security level pairing over prime fields. Several coprocessors for the computation of pairing over aforementioned curves on 128-bit security level were demonstrated in the literature.

A pairing coprocessor, implemented in Xilinx Virtex-4, demonstrated by Ghosh et al. in [188], consumes 52 kSlices and it computes the Tate, Ate, and R-ate pairings in 34.6 ms, 24.2 ms, and 16.4 ms, respectively. A design-space exploration of an application-specific instruction-set processor (ASIP) for the computation of various cryptographic pairings over BN-curves was investigated by Kammler et al. in [189]. The Montgomery reduction in a polynomial ring, combined with a coefficient reduction phase, using a pseudo-Mersenne numbers, helped Fan et al. in [174] to speed-up pairing computation significantly and beat all previously reported hardware implementations by a factor of 5.

Finally, Cheung et al. in [178] have shown that by combining RNS and lazy reduction, the speed of pairing computation in hardware can be largely increased. The fastest version of the proposed coprocessor computes an optimal-Ate pairing at 126-bit security level in 0.573 ms.

This work concentrates on the pairing architectures for prime fields. However, it is important to underline the fact that traditionally the binary fields-based architectures are more successful in terms of hardware implementations. The fastest to date FPGA implementation of the 128-bit secure pairing architecture on supersingular curves over binary fields was demonstrated in [179].

The Tate pairing on supersingular and ordinary Edwards curves over prime field was introduced in [37] and [180], respectively.

5.3 Tate pairing on twisted supersingular Edwards curves

5.3.1 Twisted Edwards curves

Edwards in [157] has introduced the addition law for the curves $x^2 + y^2 = c^2 \cdot (1 + x^2 \cdot y^2)$ over a non-binary field K. Later on, Bernstein and Lange have demonstrated more general version of Edwards curves defined by $x^2 + y^2 = c^2 \cdot (1 + d \cdot x^2 \cdot y^2)$, where $c, d \in K$ with $c \cdot d \cdot (1 - d \cdot c^4) \neq 0$. In [158], this form was generalized to twisted Edwards form defined by

$$E_{a,d} : a \cdot x^2 + y^2 = 1 + d \cdot x^2 \cdot y^2, \tag{5.1}$$

where $a, d \in K$ with $a \cdot d \cdot (a - d) \neq 0$. Edwards curves became then a special case of twisted Edwards curves, where a is equal to 1.

A supersingular form of Edwards curves has been investigated by Das and Sarkar in [37]. They have presented the application of the supersingular twisted Edwards curves for the pairing computations in the aforementioned paper.

5.3.2 Tate pairing on supersingular Edwards curves

In general, pairing transformation e (Eq. 5.2) takes two arguments (two elliptic curve points P and Q from two algebraic groups G_1 and G_2) and produce an element F of the third algebraic group G_T.

$$F \leftarrow e(P, Q), \tag{5.2}$$

where $P \in G_1, Q \in G_2, F \in G_T$.

The most important properties of these transformations are: bilinearity ($\forall a, b \in Z_p$: $e(a \cdot P, b \cdot Q) = e(P, Q)^{a \cdot b}$), non-degeneracy (function $e(P,Q)$ never returns '1'), and efficiency

in computations [166].

Tate pairing was first introduced in cryptography in [162] and we adopt its definition from [37]. Let E be an elliptic curve defined over F_q. r is a large prime divisor of the number of points on the curve $\#E(F_q)$. The smallest positive integer k, such that r divides $(q^k - 1)$ is called an embedding degree. Let $G = E(F_q^k)$. The Tate pairing is defined as $e_r : G[r]$ x $G/rG \to F_{q^k}^* / F_{q^k}^{*r}$, with $e_r(P, Q) = f_P(Q)^{\frac{q^k - 1}{r}}$. The calculation of f_P function is conducted through two phases: so called Miller's loop, and the final exponentiation. Let $h_{P,Q}$ denote the rational function corresponding to the addition of the points: P and Q. Let $r = (r_{l-1}$ ... $r_0)$ the binary representation of r. With this setup, an algorithm for computing the Tate pairing $e_r(P,Q)$ on an elliptic curve is given below.

Algorithm 2 Miller's algorithm [110] for computing Tate pairing

---

Require: Points P and Q, prime divisor $r = (r_{l-1}$ ... $r_0)$, $r_{l-1} = 1$, field order q, and embedding degree k, $h_{P,Q}$ a rational function
Ensure: $F = e(P, Q)$
1: $F = 1$, $R = P$

2: **for** $j = l - 2$ downto 0 **do**
3:      $G \leftarrow h_{R,R}(Q)$ and $R = 2 \cdot R$ /* Algorithm 3 */
4:      $F = F^2 \cdot G$ /* Algorithm 5 and 6 */
5:      **if** $r_i = 1$ **then**

6:          $G \leftarrow h_{R,P}(Q)$ and $R = R + P$ /* Algorithm 4 */
7:          $F = F \cdot G$ /* Algorithm 6 */
8:      **end if**

9: **end for**
10: **return** $F \leftarrow F^{\frac{q^k - 1}{r}}$ /* Algorithm 7 */

The Tate pairing by itself turns out to be unsuitable for cryptographic applications because it frequently returns the value 1. The Theorem 2 from [37] defines the distortion map on the Edwards curve as

$$\phi(x, y) = (x \cdot i, \frac{1}{y}), \tag{5.3}$$

96

where i is the imaginary unit, such that $i^2 = -1$. This additional mapping prevents the Tate pairing from returning 1. The explicit formulae for particular Tate pairing parts are discussed below.

Algorithm 3 Doubling and computation of Miller value using projective Edwards coordinates

---

Require: $R = (x_R, y_R, z_R)$, precomputed values: $c_1 (Eq.5.4), c_2 (Eq.5.5), c_3 (Eq.5.6)$
Ensure: $2R = (x_{2R}, y_{2R}, z_{2R}), G = g_1 \cdot i + g_2)$
1: $b \leftarrow (x_R + y_R)^2$
2: $c \leftarrow x_R^2$
3: $d \leftarrow y_R^2$
4: $e \leftarrow c + d$
5: $h \leftarrow z_R^2$
6: $j \leftarrow e - 2 \cdot h$
7: $be \leftarrow b - e$
8: $x_{2R} \leftarrow be \cdot j$
9: $k \leftarrow c - d$
10: $y_{2R} \leftarrow e \cdot k$
11: $z_{2R} \leftarrow e \cdot j$
12: $l \leftarrow (y_R + z_R)^2$
13: $m \leftarrow l - d - h$
14: $n \leftarrow 2 \cdot h$
15: $cc \leftarrow be \cdot (n - m)$
16: $dd \leftarrow n \cdot (2 \cdot e - n - m)$
17: $ee \leftarrow m \cdot (m - 2 \cdot c)$
18: $g_1 \leftarrow c_1 \cdot cc$
19: $g_2 \leftarrow c_2 \cdot (dd - ee) + c_3 \cdot ee - dd$
20: **return** $2R = (x_{2R}, y_{2R}, z_{2R}), G = g_1 \cdot i + g_2$

5.3.3 Miller loop

Let E be an elliptic curve and the points: P and $Q \in E(F_q)$ are the arguments for the Tate pairing (Alg. 2). First, argument $P = (X_P, Y_P)$ is given using so called projective coordinates (x_P, y_P, z_P), where $X_P = \frac{x_P}{z_P}$ and $Y_P = \frac{y_P}{z_P}$. The second argument, point Q is given in affine coordinates as (x_Q, y_Q), but it can be used after the distortion map (Eq. 5.3) was applied: $\phi(Q) = (x_Q \cdot i, \frac{1}{y_Q})$.

In order to compute a pairing value for P and Q, Das and Sarkar proposed to use the dedicated addition (Alg. 4) and doubling (Alg. 3) formulae.

97

Algorithm 4 Addition and computation of Miller value using projective Edwards coordinates

Require: $P = (x_P, y_P, z_P)$, $R = (x_R, y_R, z_R)$, precomputed values: $c_1(Eq.5.4), c_2(Eq.5.5), c_3(Eq.5.6)$, curve parameter - d_E

Ensure: $R = P + R = (x_{P+R}, y_{P+R}, z_{P+R}), G = g_1 \cdot i + g_2$

1: $a \leftarrow (z_P \cdot z_R)$
2: $b \leftarrow a^2$
3: $c \leftarrow x_P \cdot x_R$
4: $d \leftarrow y_P \cdot y_R$
5: $e \leftarrow d_E \cdot c \cdot d$
6: $f \leftarrow b - e$
7: $g \leftarrow b + e$
8: $h \leftarrow (x_P + y_P) \cdot (x_R + y_R) - c - d$
9: $m \leftarrow a \cdot (d - c)$
10: $x_{P+R} \leftarrow a \cdot f \cdot h$
11: $y_{P+R} \leftarrow g \cdot m$
12: $z_{P+R} \leftarrow f \cdot g$
13: $j \leftarrow (z_P - y_P) \cdot (z_R + y_R) - a + d$
14: $k \leftarrow (x_P - z_P) \cdot (x_R + z_R) - c + a$
15: $cc \leftarrow c \cdot j$
16: $dd \leftarrow a \cdot (2 \cdot x_R \cdot y_P - h - k)$
17: $ee \leftarrow -x_R \cdot z_P \cdot j + (d + y_P \cdot z_R) \cdot k$
18: $g_1 \leftarrow c_1 \cdot cc$
19: $g_2 \leftarrow c_2 \cdot (dd - ee) + c_3 \cdot ee - dd$
20: **return** $P + R = (x_{P+R}, y_{P+R}, z_{P+R}), G = g_1 \cdot i + g_2$

In order to speed up the computation of every single iteration of the Miller loop, the following pre-computations have to be conducted:

$$c_1 = x_Q \cdot (y_Q^2 - d_E), \tag{5.4}$$

$$c_2 = y_Q, \tag{5.5}$$

$$c_3 = y_Q^2, \tag{5.6}$$

where the d_E denotes the d from the Edwards curve definition.

A single iteration of Alg. 3 requires 14 modular multiplications and 19 modular additions. For the sake of simplicity $d_E = $ -1 and thanks to this fact the multiplication in line 5 of Alg. 4 can be implemented as a simple negation. In case of this algorithm the total number of modular multiplications and modular additions are 24 and 25, respectively.

Algorithm's 2 ln. 4 and 7: Let F and G be complex numbers and they are represented by $f_1 \cdot i + f_2$ and $g_1 \cdot i + g_2$, respectively.

Algorithm 5 Squaring of two complex numbers

Require: $F = (f_1 \cdot i + f_2)$
Ensure: $F^2 = (d \cdot i + e)$
 1: $a \leftarrow f_1 \cdot f_2$
 2: $b \leftarrow (f_2 - f_1)$
 3: $c \leftarrow (f_2 + f_1)$
 4: $d \leftarrow 2 \cdot a$

 5: $e \leftarrow b \cdot c$

 6: **return** $F^2 = d \cdot i + e$

Table 5.1: Parameters of Solinas primes used for Tate pairing on supersingular twisted Edwards curves

Security	Field order - q	Prime divisor - r	Exponent - $e = \frac{q^k - 1}{r}$
80-bits	$2^{520} + 2^{363} - 2^{360} - 1$	$2^{160} + 2^3 - 1$	$2^{880} + 2^{723} - 2^{721} + 2^{720} - 2^{361}$
120-bits	$2^{1263} + 2^{1037} - 2^{1005} - 1$	$2^{258} + 2^{32} - 1$	$2^{2268} + 2^{2042} - 2^{2011} + 2^{2010} - 2^{1006}$
128-bits	$2^{1492} + 2^{1237} - 2^{1224} - 1$	$2^{268} + 2^{13} - 1$	$2^{2716} + 2^{2461} - 2^{2449} + 2^{2448} - 2^{1225}$
191-bits	$2^{3955} + 2^{3581} + 2^{3573} - 1$	$2^{382} + 2^8 - 1$	$2^{7528} + 2^{7154} - 2^{7147} + 2^{7146} - 2^{3574}$

Algorithm 6 Multiplication of two complex numbers

Require: $F = (f_1 \cdot i + f_2)$ and $G = (g_1 \cdot i + g_2)$
Ensure: $F \cdot G = (e \cdot i + g)$
 1: $a \leftarrow f_1 \cdot g_2$

 2: $b \leftarrow f_2 \cdot g_1$

 3: $c \leftarrow f_2 \cdot g_2$

 4: $d \leftarrow f_1 \cdot g_1$

 5: $e \leftarrow a + b$

 6: $g \leftarrow c + d$

 7: **return** $F \cdot G = e \cdot i + g$

Then, the computation of Alg. 2 ln. 4 requires an execution of Alg. 5 (F^2), and then execution of Alg. 6 ($F \cdot G$). In case of Alg. 2 ln. 7, an execution of Alg. 6 ($F \cdot G$) is sufficient. Finally, the ln. 4 demands 6 modular multiplications and 5 modular additions. For ln. 7 these numbers are 4 and 2, respectively.

Due to the fact that the modular addition operation is relatively cheap, in terms of circuitry and calculation's latency, then the number of modular multiplication indicates the complexity of every operation. In case of 80-bit, 120-bit and 128-bit security level the number of modular multiplications are 5036, 10584 and 11148 respectively.

5.3.4 Choice of parameters for supersingular curves with embedding degree $k=2$

The security of pairing-based cryptography for different type of curves is discussed in [121]. Choice of parameters and the generation procedure for supersingular curves with embedding degree $k=2$ was presented in section 7.2 of this paper. Koblitz and Menezes have recommended prime numbers of the form $2^{a_1} \pm 2^{a_2} \pm 1$, so called Solinas primes [119], to be used for a prime divisor r and a prime field order q.

The Pollard's rho method is the fastest known algorithm for solving the ECDLP [190]. For an implementation details of this method we recommend [191].

Function field sieve algorithm is the fastest known method for solving the DLP in the extension field. Detailed discussion about the time complexity of this method was conducted by Joux at el. in [192]. They have summarized that the FFS complexity is usually expressed using the following function:

$$L_q(\alpha, c) = exp((c + o(1))(log(q))^\alpha (log(log(q)))^{1-\alpha}, \qquad (5.7)$$

where log denotes natural logarithm. In particular, for the prime field F_p and for binary fields F_{2^n}, the number field sieve and the function field sieve respectively yield $L_p(\frac{1}{3}, (\frac{64}{9})^{\frac{1}{3}})$ and $L_{2^n}(\frac{1}{3}, (\frac{32}{9})^{\frac{1}{3}})$ algorithms.

Later on, Schirokauer in [193] has defined the weight of integer to be the smallest w such that the integer p can be represented as $\sum_{i=1}^{w} \xi_i 2^{a_i}$, with $\xi_1, ..., \xi_w \in \{-1, 1\}$ and $a_i \in Z_p$. He has conducted an analysis of the number field sieve time complexity for integers of low weight. He has demonstrated that a prime field of the order q with weight w yield $L_p(\frac{1}{3}, (\frac{32\tau^2}{9})^{\frac{1}{3}})$, where τ^2 is converging to $\frac{2w-3}{w-1}$. The Solinas primes, considered in this work, have their weight $w = 4$.

In order to generate parameters for different security levels we took into account resistance against aforementioned cryptanalytical methods. Among all the generated pairs: prime divisor r and prime field p, we have selected those with the lowest hamming weight of Barrett's μ parameter (Eq. 4.4). This assumption allows the most efficient computation of the multiplication by the constant μ number from the Alg. 1.

Table 5.1 summarizes the sizes of field, prime divisor, and the exponent value - the most important parameters in case of pairing based on supersingular curves.

5.3.5 Final exponentiation

In regards to the computations of the line 10 of Alg. 2 ($F \leftarrow F^{\frac{q^k - 1}{r}}$), so called, the final exponentiation, Koblitz and Menezes show in [121] that this computation can be significantly simplified. In case of supersingular curves with embedding degree $k = 2$, the expression $\frac{q^2 - 1}{r}$ can be split into two terms: $(q - 1) \cdot \frac{q+1}{r}$ (from the definition of supersingularity of elliptic curves we know that r always divides $q + 1$). Calculating $F' \leftarrow F^{q-1}$ can be easily obtained though a cheap Frobenius computations and an inversion. The second step is to calculate $F'^{\frac{q+1}{r}}$ which is so called, the hard part of the final exponentiation. Due to the fact that the computational cost of inversion (Eq. 5.10) is similar to calculating F^{q-1}, this method is not as effective for embedding degree $k = 2$.

However the final exponentiation, with an exponent in a Solinas form, can be sped up significantly using a simple trick summarized below.

Let F be a complex number and $e = 2^{a_1} + 2^{a_2} - 2^{a_3} + 2^{a_4} - 2^{a_5}$, where a_1, a_2, a_3, a_4, a_5 are integers and $a_1 > a_2 > a_3 > a_4 > a_5$. In particular, a set of $(a_1, a_2, a_3, a_4, a_5)$ corresponds to the (880, 723, 721, 720, 361), a set of powers representing the fixed-exponent e for 80-bit security level (Table 5.1). In order to perform a fixed-exponent exponentiation of a complex number:

$$F^e = F^{2^{a_1}+2^{a_2}-2^{a_3}+2^{a_4}-2^{a_5}} = \frac{F^{2^{a_1}} \cdot F^{2^{a_2}} \cdot F^{2^{a_4}}}{F^{2^{a_3}} \cdot F^{2^{a_5}}} \qquad (5.8)$$

the right-to-left binary method [146] (14.76) has been adopted.

The pseudocode of the final exponentiation method, applicable for different security levels (Table 5.1) is presented in Alg. 7.

The store operations of R_{a1} (Alg. 7 ln.4), R_{a2} (Alg. 7 ln.6), R_{a3} (Alg. 7 ln.8), R_{a4} (Alg. 7 ln.10) and R_{a5} (Alg. 7 ln.12) correspond to the computations of F^{a1}, F^{a2}, F^{a3}, F^{a4}, F^{a5} (Eq. 5.8), respectively. The lines 16 represents the computations of numerator of Eq. 5.8. The line 17 reflects the calculations of denominator of the aforementioned equation.

Algorithm 7 Final Exponentiation for $e = 2^{a_1} + 2^{a_2} - 2^{a_3} + 2^{a_4} - 2^{a_5}$

Require: Complex number F, $e \leftarrow 2^{a_1} + 2^{a_2} - 2^{a_3} + 2^{a_4} - 2^{a_5}$
Ensure: Complex numbers R_u and R_d (partial results of pairing)
1: $F \leftarrow F$, $R \leftarrow 1$
2: **for** $j = 0$ to a_1 **do**
3:     **if** $j = a_1$ **then**
4:        $R_{a_1} \leftarrow F$
5:     **else if** $j = a_2$ **then**
6:        $R_{a_2} \leftarrow F$
7:     **else if** $j = a_3$ **then**
8:        $R_{a_3} \leftarrow F$
9:     **else if** $j = a_4$ **then**
10:       $R_{a_4} \leftarrow F$
11:     **else if** $j = a_5$ **then**
12:       $R_{a_5} \leftarrow F$
13:     **end if**
14:     $F \leftarrow F \cdot F$
15: **end for**
16: $R_u = R_{a_1} \cdot R_{a_2} \cdot R_{a_4}$
17: $R_d = R_{a_3} \cdot R_{a_5}$
18: **return** R_u and R_d

Final F (Eq. 5.2) reconstruction: In case of this work, the final F is proposed to be reconstructed outside of the coprocessor in a post-processing operation. Both R_u and R_d are the complex numbers and can be represented as $xi + y$ and $vi + z$, respectively.

$$F \leftarrow \frac{R_u}{R_d} \leftarrow \frac{x \cdot i + y}{v \cdot i + z} \tag{5.9}$$

The formulae of complex numbers modular inversion are demonstrated in Eq. 5.10.

$$(v \cdot i + z)^{-1} = (v' \cdot i + z') = \begin{cases} v' = \frac{-v}{z^2 + v^2} \\ z' = \frac{z}{z^2 + v^2} \end{cases} \tag{5.10}$$

The final F of the Tate pairing on twisted supersingular Edwards curves over prime fields is a product of $(x \cdot i + y)$ and $(v' \cdot i + z')$.

Hardware coprocessor-related decisions and comments:

The analysis of explicit formulae of algorithms presented above and the parameters choice helped us to draw some conclusions about hardware architecture for Edwards curves-based pairing coprocessor:

- Due to the dependencies between the intermediate values of computations in Alg. 3, Alg. 4 and Alg. 7, the implementation of all the multiplications independently would be inefficient (Most of the circuit would be inactive during most of the pairing computations).

- The number of modular multiplications in lines 3-4 in Alg. 2, and lines 7-8 in Alg. 2 are 20 and 28, respectively. An analysis of internal data dependencies in aforementioned algorithms revealed that it is relatively easy to separate up to four, equally balanced streams of data. At this point two possible scenarios were possible: either hardware architecture based on modular multiplier with four pipelining stages or with four independent modular multiplication units.

- An analysis of the data dependency between consecutive iterations of Alg. 7, led us to the conclusion that pipelining-oriented solution will lead to longer computational

104

time than the alternative solution. Moreover, one more crucial requirement for the multiplier arose - an ability to reduce by factor of 2 (using the double speed mode described in the next section) the multiplication time in case of the availability of twice as many resources compared to the basic mode.

- The most successful modular multipliers, reported in the literature, were based on DSP units (Sec. 4.2). However, the RNS-based unit from [178] utilizes multi-stages pipelining, and therefore the scheduling of Alg. 7 (only results of two multiplications per iteration have to be computed) would always lead to huge number of *idle* states.

  Tripartite module [127] requires enormous number of DSP blocks for the operand sizes from Table 5.1 and the design from [134] is highly optimized for RSA algorithm - it was design for a computations where one of the arguments is not changing and it has not been optimized for interleaving with other operations (like addition or subtraction). A hardware multiplier for Tate pairing on twisted supersingular Edwards curves was inspired by aforementioned designs and it was presented in the previous chapter.

5.4 The coprocessor

In this section, we propose an application, for the previously described modular architectures for Solinas primes, a latency-optimized coprocessor for Tate pairing on Edwards curves.

First, a high-level description of the hardware accelerator will be provided. Then we are going to discuss operation scheduling for the four different operational modes of this circuit: doubling and addition operations in the Miller loop, complex numbers squaring in the Final exponentiation and eventually, the calculation of R_u and R_d (Eq. 5.9).

Top level block diagram of the coprocessor datapath: is demonstrated in Fig. 5.2. Two major group of components in this accelerator are: a bank of memories (memory map in Table 5.2) for the intermediate results of a pairing computations, and the arithmetic modules. In order to enable the basic operations to work on entire length of the arguments the memories were organized in parallel (Fig. 5.2 Pt. 2). Therefore, an argument $R = \{r(n-1), \ ... \ r(0)\}$ can be stored/fetched in a single clock cycle. To start a pairing computation these memories have to be initialized properly. Precomputed constants c_1 (Eq. 5.4), c_2 (Eq. 5.5) and c_3 (Eq. 5.6), coordinates of the point P , initial value of the F have to be introduced from the external environment through the input bus (Fig. 5.2 Pt. 1) and stored in the bank of memories (Fig. 5.2 Pt. 2). The computational resources of our coprocessor consist of four multipliers (Fig. 5.2 Pt. 3), single fully pipelined modular reductor (Fig. 5.2 Pt. 5) and a pipelining modular adder (Fig. 5.2 Pt. 6).

Table 5.4: Scheduling of operations for Alg. 2, when $r_i = 1$

Multiplier 1	Multiplier 2	Multiplier 3	Multiplier 4	Adder
				Continued on next page

Table 5.4 – continued from previous page

Multiplier 1	Multiplier 2	Multiplier 3	Multiplier 4	Adder
$A_{16} \leftarrow A_{11} \cdot A_{11}$, (Alg. 3, ln. 2)	$A_{17} \leftarrow A_{12} \cdot A_{12}$, (Alg. 3, ln. 3)	$A_{21} \leftarrow A_{13} \cdot A_{13}$, (Alg. 3, ln. 5)	$A_{25} \leftarrow A_{25} \cdot A_{25}$, (Alg. 3, ln. 12)	$A_{29} \leftarrow A_{30} - A_{29}$, (Alg. 4, ln. 19) $A_4 \leftarrow A_{37} + A_{38}$, (Alg. 6, ln. 5) $A_7 \leftarrow A_{33} + A_{29}$, (Alg. 4: ln. 19) $A_5 \leftarrow A_{39} + A_{40}$, (Alg. 6, ln. 6)
$A_{15} \leftarrow A_{15} \cdot A_{15}$, (Alg. 3, ln. 1)	$A_{37} \leftarrow A_4 \cdot A_7$, (Alg. 6, ln. 1)	$A_{38} \leftarrow A_5 \cdot A_6$, (Alg. 6, ln. 2)	$A_{12} \leftarrow A_{18} \cdot A_{24}$, (Alg. 3, ln. 10)	$A_{18} \leftarrow A_{16} + A_{17}$, (Alg. 3, ln. 4) $A_{24} \leftarrow A_{16} - A_{17}$, (Alg. 3, ln. 9) $A_{41} \leftarrow A_{17} + A_{21}$, (Alg. 3, ln. 13) $A_{27} \leftarrow A_{21} + A_{21}$, (Alg. 3, ln. 14) $A_{42} \leftarrow A_{18} + A_{18}$, (Alg. 3, ln. 16) $A_{43} \leftarrow A_{16} + A_{16}$, (Alg. 3, ln. 17) $A_{26} \leftarrow A_{25} - A_{41}$, (Alg. 3, ln. 13) $A_{31} \leftarrow A_{15} - A_{18}$, (Alg. 3, ln. 7) $A_{23} \leftarrow A_{18} - A_{27}$, (Alg. 3, ln. 6) $A_{44} \leftarrow A_{27} + A_{26}$, (Alg. 3, ln. 16) $A_{28} \leftarrow A_{27} - A_{26}$, (Alg. 3, ln. 15) $A_{30} \leftarrow A_{26} - A_{43}$, (Alg. 3, ln. 17) $A_{29} \leftarrow A_{42} - A_{44}$, (Alg. 3, ln. 16)
$A_{13} \leftarrow A_8 \cdot A_{23}$, (Alg. 3, ln. 11)	$A_{29} \leftarrow A_{27} \cdot A_{29}$, (Alg. 3, ln. 16)	$A_{30} \leftarrow A_{26} \cdot A_{30}$, (Alg. 3, ln. 17)	$A_{28} \leftarrow A_{28} \cdot A_{31}$, (Alg. 3, ln. 15)	
$A_{11} \leftarrow A_{31} \cdot A_{23}$, (Alg. 3, ln. 8)	$A_{39} \leftarrow A_5 \cdot A_7$, (Alg. 6, ln. 3)	$A_{40} \leftarrow A_4 \cdot A_6$, (Alg. 6, ln. 4)	$A_{17} \leftarrow A_9 \cdot A_{12}$, (Alg. 4, ln. 4)	$A_{33} \leftarrow A_{29} - A_{30}$, (Alg. 3, ln. 19)
$A_6 \leftarrow A_{28} \cdot A_0$, (Alg. 3, ln. 18)	$A_{33} \leftarrow A_{33} \cdot A_1$, (Alg. 3, ln. 19)	$A_{30} \leftarrow A_{30} \cdot A_2$, (Alg. 3, ln. 19)	$A_{14} \leftarrow A_{10} \cdot A_{13}$, (Alg. 4, ln. 1)	$A_{44} \leftarrow A_{10} - A_9$, (Alg. 4, ln. 13) $A_{45} \leftarrow A_{13} + A_{12}$, (Alg. 4, ln. 13)
Continued on next page				

Table 5.4 – continued from previous page

Multiplier 1	Multiplier 2	Multiplier 3	Multiplier 4	Adder
$A_{29} \leftarrow A_{11} \cdot A_9$, (Alg. 4, ln. 16)	$A_{16} \leftarrow A_8 \cdot A_{11}$, (Alg. 4, ln. 3)	$A_{23} \leftarrow A_{44} \cdot A_{45}$, (Alg. 4, ln. 13)	$A_{18} \leftarrow A_3 \cdot A_{17}$, (Alg. 4, ln. 5)	$A_4 \leftarrow A_{37} + A_{38}$, (Alg. 6, ln. 5) $A_5 \leftarrow A_{39} + A_{40}$, (Alg. 6, ln. 6) $A_{34} \leftarrow A_5 - A_4$, (Alg. 5, ln. 2) $A_{35} \leftarrow A_5 + A_4$, (Alg. 5, ln. 3) $A_{44} \leftarrow A_{10} + A_9$, (Alg. 4, ln. 8) $A_{45} \leftarrow A_{11} + A_{12}$, (Alg. 4, ln. 8)
$A_{36} \leftarrow A_4 \cdot A_5$, (Alg. 5, ln. 1)	$A_5 \leftarrow A_{34} \cdot A_{35}$, (Alg. 5, ln. 5)	$A_{21} \leftarrow A_{44} \cdot A_{45}$, (Alg. 4, ln. 8)	$A_{15} \leftarrow A_{14} \cdot A_{14}$, (Alg. 4, ln. 2)	$A_{29} \leftarrow A_{30} - A_{29}$, (Alg. 3, ln. 19) $A_{49} \leftarrow A_{17} - A_{14}$, (Alg. 4, ln. 13) $A_{50} \leftarrow A_8 - A_{10}$, (Alg. 4, ln. 14) $A_{51} \leftarrow A_{11} + A_{13}$, (Alg. 4, ln. 14) $A_{43} \leftarrow A_{16} + A_{17}$, (Alg. 4, ln. 8) $A_{22} \leftarrow A_{17} - A_{16}$, (Alg. 4, ln. 9) $A_7 \leftarrow A_{33} + A_{29}$, (Alg. 3, ln. 19)
$A_{52} \leftarrow A_{11} \cdot A_{10}$, (Alg. 4, ln. 17)	$A_{53} \leftarrow A_9 \cdot A_{13}$, (Alg. 4, ln. 17)	$A_{24} \leftarrow A_{50} \cdot A_{51}$, (Alg. 4, ln. 14)	$A_{26} \leftarrow A_{14} \cdot A_{22}$, (Alg. 4, ln. 9)	$A_4 \leftarrow A_{36} + A_{36}$, (Alg. 5, ln. 4) $A_{29} \leftarrow A_{29} + A_{29}$, (Alg. 4, ln. 16) $A_{23} \leftarrow A_{23} + A_{49}$, (Alg. 4, ln. 13) $A_{29} \leftarrow A_{29} - A_{21}$, (Alg. 4, ln. 16) $A_{47} \leftarrow A_{14} - A_{16}$, (Alg. 4, ln. 14)
$A_{11} \leftarrow A_{21} \cdot A_{14}$, (Alg. 4, ln. 10)	$A_{18} \leftarrow A_{18} \cdot A_{16}$, (Alg. 4, ln. 5)	$A_{37} \leftarrow A_4 \cdot A_7$, (Alg. 6, ln. 1)	$A_{38} \leftarrow A_5 \cdot A_6$, (Alg. 6, ln. 2)	$A_{53} \leftarrow A_{53} + A_{17}$, (Alg. 4, ln. 17) $A_{21} \leftarrow A_{21} - A_{43}$, (Alg. 4, ln. 8) $A_{24} \leftarrow A_{24} + A_{47}$, (Alg. 4, ln. 14) $A_{29} \leftarrow A_{29} - A_{24}$, (Alg. 4, ln. 16)
				Continued on next page

Table 5.4 – continued from previous page

Multiplier 1	Multiplier 2	Multiplier 3	Multiplier 4	Adder
$A_{28} \leftarrow A_{16} \cdot A_{23}$, (Alg. 4, ln. 15)	$A_{29} \leftarrow A_{14} \cdot A_{29}$, (Alg. 4, ln. 16)	$A_{52} \leftarrow A_{52} \cdot A_{23}$, (Alg. 4, ln. 17)	$A_{53} \leftarrow A_{53} \cdot A_{24}$, (Alg. 4, ln. 17)	$A_{19} \leftarrow A_{15} - A_{18}$, (Alg. 4, ln. 6) $A_{20} \leftarrow A_{15} + A_{18}$, (Alg. 4, ln. 7)
$A_{11} \leftarrow A_{11} \cdot A_{19}$, (Alg. 4, ln. 10)	$A_{13} \leftarrow A_{19} \cdot A_{20}$, (Alg. 4, ln. 12)	$A_{12} \leftarrow A_{20} \cdot A_{22}$, (Alg. 4, ln. 11)	$A_{39} \leftarrow A_5 \cdot A_7$, (Alg. 6, ln. 3)	$A_{30} \leftarrow A_{53} - A_{52}$, (Alg. 4, ln. 17) $A_{33} \leftarrow A_{30} - A_{29}$, (Alg. 4, ln. 19)
$A_4 \leftarrow A_{28} \cdot A_0$, (Alg. 4, ln. 18)	$A_{33} \leftarrow A_{33} \cdot A_1$, (Alg. 4, ln. 19)	$A_{30} \leftarrow A_{30} \cdot A_2$, (Alg. 4, ln. 19)	$A_{40} \leftarrow A_4 \cdot A_6$, (Alg. 6, ln. 4)	$A_{15} \leftarrow A_{11} + A_{12}$, (Alg. 3, ln. 1) $A_{25} \leftarrow A_{12} + A_{13}$, (Alg. 3, ln. 12)

Due to the fact that the multiplication circuit works in a sequential fashion, the only possible way to improve the total latency of several, independent (the result of one multiplication is not an argument to the next multiplication), consecutive multiplication is to instantiate multiple such units. In case of tate pairing on super singular Edwards curves the numbers of multiplications per iteration in following cases: Alg. 2 (line 3 and 4), Alg. 2 (line 5 and 6), Alg. 7 (line 14) and Alg. 7 (lines 16-17) are 20, 48, 2, 12, respectively. The greatest common factor of all those numbers is two, and this could be a first choice for the number of multiplication units.

In order to further improve the latency of the pairing computations we have decide to instantiate four such units. This allow us to conduct the computations of a single iteration of Alg. 2 (line 3 and 4), Alg. 2 (line 5 and 6), and and Alg. 7 (lines 16-17) in five, twelve and three phases.

The two multiplication of the single iteration of the final exponentiation doubling operation (Alg. 7 (line 14)) can be computed within one phase. All four multiplication units, used in the double speed mode, are employed for the computations of partial products of aforementioned two multiplications. The final products of them are computed using additional circuit (Fig. 5.2 Pt. 4).
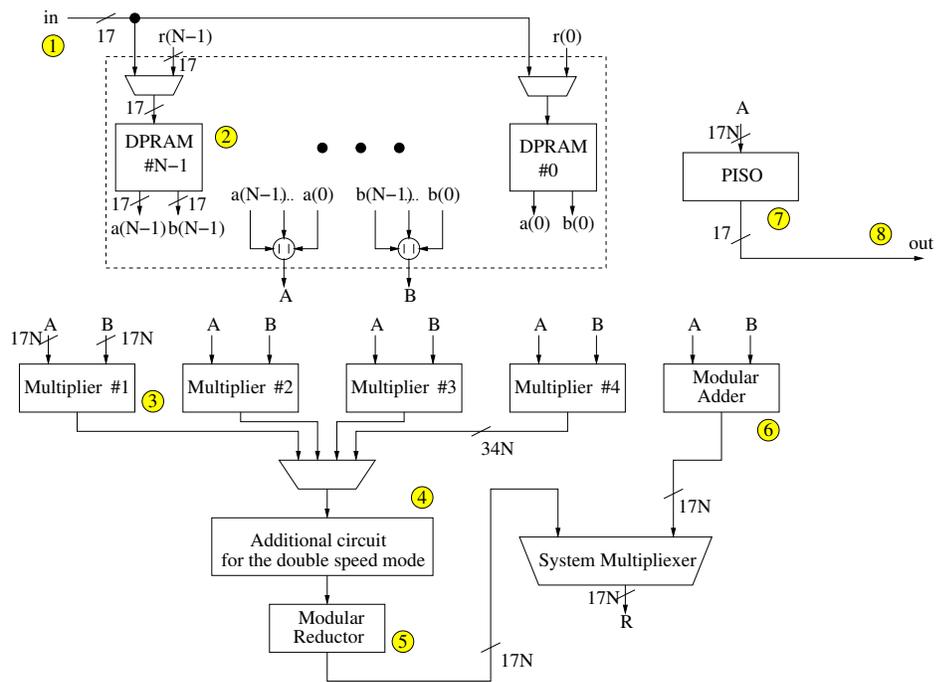
Number of 17−bit words:

N = 31 (80−bit), 75 (120−bit), 88 (128−bit)

A = {a(N−1), ... a(0)}, B = {b(N−1), ...b(0)}, R = {r(N−1), ... r(0)}

Figure 5.2: Top level block diagram of pairing coprocessor

Table 5.2: Memory mapping and initialization

Address	Variable	Init value	Comment
Entire pairing computations			
A_0	c_1	$x_Q \cdot (y_Q^2 - d_E)$	Eq. 5.4 (precomputed constant)
A_1	c_2	y_Q	Eq. 5.5 (precomputed constant)
A_2	c_3	y_Q^2	Eq. 5.6 (precomputed constant)
A_3	d_E	d_E - curve parameter	Eq. 5.1
A_4	f_1	0	Alg. 2 ln. 1, F
A_5	f_2	1	Alg. 2 ln. 1, F
A_6	g_1	-[1]	Alg. 2, G
A_7	g_2	-	Alg. 2, G
A_8	x_P	x_P	Alg. 2 ln. 1
A_9	y_P	y_P	Alg. 2 ln. 1
A_{10}	z_P	z_P	Alg. 2 ln. 1
A_{11}	x_R	x_P	Alg. 2 ln. 1
A_{12}	y_R	y_P	Alg. 2 ln. 1
A_{13}	z_R	z_P	Alg. 2, ln. 1
Miller's loop			
$A_{14} - A_{53}$	$a, b...$	-	Alg. 3, 4, 5, 6 (intermediate values)
Final exponentiation			
A_{14}	R_{a_1} (f_1 part)	-	Alg. 7, ln. 4
A_{15}	R_{a_1} (f_2 part)	-	Alg. 7, ln. 4
A_{16}	R_{a_2} (f_1 part)	-	Alg. 7, ln. 6
A_{17}	R_{a_2} (f_2 part)	-	Alg. 7, ln. 6
A_{18}	R_{a_3} (f_1 part)	-	Alg. 7, ln. 8
A_{19}	R_{a_3} (f_2 part)	-	Alg. 7, ln. 8
A_{20}	R_{a_4} (f_1 part)	-	Alg. 7, ln. 10
A_{21}	R_{a_4} (f_2 part)	-	Alg. 7, ln. 10
A_{22}	R_{a_5} (f_1 part)	-	Alg. 7, ln. 12
A_{23}	R_{a_5} (f_2 part)	-	Alg. 7, ln. 12
[1] do not care			

Table 5.3: Scheduling of operations for Alg. 2, when $r_i = 0$

Multiplier 1	Multiplier 2	Multiplier 3	Multiplier 4	Adder
$A_{16} \leftarrow A_{11} \cdot A_{11}$, (Alg. 3, ln. 2)	$A_{17} \leftarrow A_{12} \cdot A_{12}$, (Alg. 3, ln. 3)	$A_{21} \leftarrow A_{13} \cdot A_{13}$, (Alg. 3, ln. 5)	$A_{25} \leftarrow A_{25} \cdot A_{25}$, (Alg. 3, ln. 12)	$A_{29} \leftarrow A_{30} - A_{29}$, (Alg. 3, ln. 19) $A_4 \leftarrow A_{37} + A_{38}$, (Alg. 6, ln. 5) $A_7 \leftarrow A_{33} + A_{29}$, (Alg. 3: ln. 19) $A_5 \leftarrow A_{39} + A_{40}$, (Alg. 6, ln. 6) $A_{34} \leftarrow A_5 - A_4$, (Alg. 5, ln. 2) $A_{35} \leftarrow A_5 + A_4$, (Alg. 5, ln. 3)
$A_{15} \leftarrow A_{15} \cdot A_{15}$, (Alg. 3, ln. 1)	$A_{36} \leftarrow A_4 \cdot A_5$, (Alg. 5, ln. 1)	$A_5 \leftarrow A_{34} \cdot A_{35}$, (Alg. 5, ln. 5)	$A_{12} \leftarrow A_{18} \cdot A_{23}$, (Alg. 3, ln. 10)	$A_{18} \leftarrow A_{16} + A_{17}$, (Alg. 3, ln. 4) $A_{24} \leftarrow A_{16} - A_{17}$, (Alg. 3, ln. 9) $A_{41} \leftarrow A_{17} + A_{21}$, (Alg. 3, ln. 13) $A_{27} \leftarrow A_{21} + A_{21}$, (Alg. 3, ln. 14) $A_{42} \leftarrow A_{18} + A_{18}$, (Alg. 3, ln. 16) $A_{43} \leftarrow A_{16} + A_{16}$, (Alg. 3, ln. 17) $A_{26} \leftarrow A_{25} + A_{41}$, (Alg. 3, ln. 13) $A_{31} \leftarrow A_{15} - A_{18}$, (Alg. 3, ln. 7) $A_{23} \leftarrow A_{18} - A_{27}$, (Alg. 3, ln. 6) $A_{44} \leftarrow A_{27} + A_{26}$, (Alg. 3, ln. 16) $A_{28} \leftarrow A_{27} - A_{26}$, (Alg. 3, ln. 15) $A_{30} \leftarrow A_{26} - A_{43}$, (Alg. 3, ln. 17) $A_{29} \leftarrow A_{42} - A_{44}$, (Alg. 3, ln. 16)
$A_{13} \leftarrow A_{18} \cdot A_{24}$, (Alg. 3, ln. 11)	$A_{29} \leftarrow A_{27} \cdot A_{29}$, (Alg. 3, ln. 16)	$A_{30} \leftarrow A_{26} \cdot A_{30}$, (Alg. 3, ln. 17)	$A_{28} \leftarrow A_{28} \cdot A_{31}$, (Alg. 3, ln. 15)	$A_4 \leftarrow A_{36} + A_{36}$, (Alg. 5, ln. 4)
$A_{11} \leftarrow A_{32} \cdot A_{24}$, (Alg. 3, ln. 8)	$A_{37} \leftarrow A_4 \cdot A_7$, (Alg. 6, ln. 1)	Neguesha $A_{38} \leftarrow A_5 \cdot A_6$, (Alg. 6, ln. 2)	$A_{39} \leftarrow A_5 \cdot A_7$, (Alg. 6, ln. 3)	$A_{25} \leftarrow A_{12} + A_{13}$, (Alg. 3, ln. 12) $A_{15} \leftarrow A_{11} + A_{12}$, (Alg. 3, ln. 1) $A_{33} \leftarrow A_{29} - A_{30}$, (Alg. 3, ln. 19)
$A_{40} \leftarrow A_4 \cdot A_6$, (Alg. 6, ln. 4)	$A_6 \leftarrow A_0 \cdot A_{28}$, (Alg. 3, ln. 18)	$A_{33} \leftarrow A_1 \cdot A_{33}$, (Alg. 3, ln. 19)	$A_{30} \leftarrow A_2 \cdot A_{30}$, (Alg. 3, ln. 19)	

Table 5.5: Final exponentiation Alg. 7 scheduling.
MSP(x) and LSP(x) - the most and the least significant parts of x-value, respectively.

Multiplier 1	Multiplier 2	Multiplier 3	Multiplier 4	Adder
Alg. 7 ln. 14 is computed using Alg. 5				
				$A_{25} \leftarrow A_5 + A_4$, (Alg. 3, ln. 2) $A_{26} \leftarrow A_5 - A_4$, (Alg. 3, ln. 3)
$a \leftarrow MSP(A_4) \cdot A_5$, (Alg. 3, ln. 1)	$b \leftarrow LSP(A_4) \cdot A_5$, (Alg. 3, ln. 1)	$c \leftarrow MSP(A_{25}) \cdot A_{26}$, (Alg. 3, ln. 4)	$d \leftarrow LSP(A_{25}) \cdot A_{26}$, (Alg. 3, ln. 4)	
				$A_4 \leftarrow A_{24} + A_{24}$, (Alg. 3, ln. 5)
$A_{24} \leftarrow a + b, A_5 \leftarrow c + d$				
Alg. 7 ln. 16-17 is computed using Alg. 6				
$A_{28} \leftarrow A_{14} \cdot A_{17}$, (Alg. 6, ln. 1)	$A_{29} \leftarrow A_{15} \cdot A_{16}$, (Alg. 6, ln. 2)	$A_{30} \leftarrow A_{16} \cdot A_{17}$, (Alg. 6, ln. 3)	$A_{31} \leftarrow A_{14} \cdot A_{15}$, (Alg. 6, ln. 4)	$A_{32} \leftarrow A_{28} + A_{29}$, (Alg. 6, ln. 5) $A_{33} \leftarrow A_{30} + A_{31}$, (Alg. 6, ln. 6)
$A_{28} \leftarrow A_{18} \cdot A_{23}$, (Alg. 6, ln. 1)	$A_{29} \leftarrow A_{19} \cdot A_{22}$, (Alg. 6, ln. 2)	$A_{30} \leftarrow A_{18} \cdot A_{19}$, (Alg. 6, ln. 3)	$A_{31} \leftarrow A_{22} \cdot A_{23}$, (Alg. 6, ln. 4)	$A_{34} \leftarrow A_{28} + A_{29}$, (Alg. 6, ln. 5) $A_{35} \leftarrow A_{30} + A_{31}$, (Alg. 6, ln. 6)
$A_{28} \leftarrow A_{31} \cdot A_{25}$, (Alg. 6, ln. 1)	$A_{29} \leftarrow A_{32} \cdot A_{25}$, (Alg. 6, ln. 2)	$A_{30} \leftarrow A_{31} \cdot A_{32}$, (Alg. 6, ln. 3)	$A_{31} \leftarrow A_{24} \cdot A_{25}$, (Alg. 6, ln. 4)	$A_{32} \leftarrow A_{28} + A_{29}$, (Alg. 6, ln. 5) $A_{33} \leftarrow A_{30} + A_{31}$, (Alg. 6, ln. 6)

Due to the fact that the modular reduction unit (Fig. 5.2 Pt. 5) has more than 4 pipelining stages, regardless the size of operands (Tab. 5.1), it is possible to reuse this unit for every product computed in all four multipliers.

The modular adder unit can process up to 3 and 4 operations at the time for the operands at lower (80-bites) and higher security levels (120-bits and more), respectively. A pairing computation is completed by proper scheduling of these modular operations. More details about it is delivered in the next section. A partial result of pairing calculations: R_u and R_d values are eventually stored into the bank of memories. In order to reconstruct the final F (Eq. 5.2) these R_u and R_d (Alg. 7) have to be stored into parallel-input-serial-output module (Fig. 5.2 Pt. 7) and through output bus (Fig. 5.2 Pt. 8) sent outside of the coprocessor.

Operation scheduling: Table 5.3, 5.4 and 5.5 present the scheduling of basic operations (multiplication, modular reduction, modular addition). Every cell, in those three tables, contains an information about the type of operation and the reference to the line of

a particular algorithm.

Miller's algorithm scheduling. Case $r_i = 0$ in Alg. 2: has been demonstrated in Table 5.4. A calculation of the line 3 and 4 in Alg. 2 incorporate an execution of Alg. 3, 5 and 6. Three, aforementioned algorithms, within one iteration of Alg. 2, require 20 multiplications in total. This fact, together with the analysis of the data dependency, allow us to keep all four multipliers busy almost entire time during the five phases (five rows in Table 5.3) of the doubling computations.

First, we start the computations of intermediate values from lines: 2, 3, 5 and 12 in Alg. 3 (Table 5.3 row 1). In the following phases, more intermediate values are computed. Apart of them, in the second, third and fourth phase of scheduling (Table 5.3 row 2, 3 and 4) for the $r_i = 0$ case, new point's coordinates are calculated. The F (Eq. 5.2) squaring is conducted in the second phase.

Next, the product of F and G is computed in the fourth phase (computation completion of line 4 in Alg. 2).

Finally, in the last row (fifth phase of scheduling) the partial results of the G-value in Alg. 3 (line 18) are computed.

Miller's algorithm scheduling. Case $r_i = 1$ in Alg. 2: has been presented in Table 5.3. A calculation of the lines 3 to 7 in Alg. 2 require an execution of Alg. 3, 4, 5 and 6.

All four before mentioned algorithms, within one iteration of Alg. 2, require 48 modular multiplications total. It helps to keep every multiplier busy almost entire time during the twelve phases (twalve rows in Table 5.4) of the addition computations.

Due to the fact that even in case of $r_i = 1$ the doubling part of the Miller loop is executed, the first five phases of scheduling are designated for the first part of this algorithm. Almost entire multipliers' scheduling for this part is similar to the case of $r_i = 0$. The only exception is the fact that during the doubling operation instead of $F^2 \cdot G$, the $F \cdot G$ computations has to be conducted. It is due to the fact that the doubling and the addition parts of Miller loop are interleaved. The product of F and G from line 7 of Alg. 2 is actually computed in

the second and the fourth phase of the scheduling for $r_i = 1$ case.

The rows seventh to twelfth in Table 5.4 demonstrate the scheduling of the addition part of Miller loop and the operations on F and G values from line 4 in Alg. 2. In particular: a new point R_{i+1} and its coordinates x_3, y_3 and z_3 are computed in 11th phase of the case $r_i = 1$ scheduling (Table 5.4). The operation of squaring F (Eq. 5.2) is conducted in the seventh phase and later on the $F \cdot G$ operations are distributed among nineth, eleventh and twelfth phase of case $r_i = 1$ scheduling.

Finally, in the last row (twelfth phase of scheduling) the partial results of the G-value in Alg. 4 (line 18) are computed.

The final exponentiation: scheduling has been summarized in Table 5.5. The upper part of Table 5.5 corresponds to the Alg. 7 ln. 14 calculations - a complex number squaring. The lower part of this table reflects the Alg. 7 ln. 17 computations - a reconstruction of R_u and R_d values from previously stored (Alg. 7 lines 3-13) partial results.

Due to the fact that square operation of a complex number yield a strong dependency between consecutive computations, any pipelining technique in the multiplier-reductor pair will result in multiple *idle* states. In order to reduce the time of a single square operation of a complex number we have applied a BiPartite-like method of multiplication [125]. The most (Table 5.5: $MSP(A_4)$) and the least significant (Table 5.5: $LSP(A_4)$) part of the first argument are multiplied independently with the second argument (Table 5.5: A_5) in two neighboring multipliers. Eventually, after both parts of the first argument (A_4) are multiplied by the second argument (A_5), their partial results (Table 5.5: a, b) are added and sent to the first reductor. In the remaining part of a given iteration both multipliers will stay *idle*. This way the computation of the line 1 from Alg. 5 is completed. The computation of the line 4 from Alg. 5 is conducted similarily.

Finally, the computation of the line 2 and ln. 3 of Alg. 5 - the arguments for both addition/subtractions are the same, so they can be fetched once and executed fully parallel.

In case of the R_u and R_d computations in Alg. 7 ln. 17 it is possible to keep multipliers working constantly by interleaved computations of $R_u{}^\prime = R_{a1} \cdot R_{a2}$ (Table 5.5: bottom

115

Table 5.6: Latency-related information for building transformations on different security levels for Xilinx (Altera in parentheses)

Security	80-bits	120-bits	128-bits	
Arguments size - n	521	1264	1493	Notation
Number of clock cycles for different basic arithmetic operations				
n-bits modular addition	3	4	4	
basic mode multiplication	22 (15)	53 (36)	63 (42)	C_{bm}
double speed mode multiplication	11 (8(	27 (18)	32 (21)	C_{dm}
basic mode modular reduction	11 (11)	13 (13)	13 (13)	C_{br}
double speed mode modular reduction	12 (12)	14 (14)	14 (14)	C_{dr}
Number of clock cycles per iteration for building algorithms				
Alg. 2 $r_i = 0$	120 (85)	276 (190)	326 (220)	$C_{md} \approx 5 \cdot C_{bm}$
Alg. 2 $r_i = 1$	274 (190)	647 (442)	767 (514)	$C_{mm} \approx 12 \cdot C_{bm}$
Alg. 7 lines 2-15	27 (24)	46 (36)	51 (39)	$C_{fd} \approx C_{dm} + C_{dr}$
Alg. 7 lines 16-17	81 (60)	230 (161)	270 (185)	$C_{fm} \approx 3 \cdot C_{bm} + C_{br}$
Number of iterations of building algorithms				
Alg. 2 $r_i = 0$	156	225	254	I_{md}
Alg. 2 $r_i = 1$	3	32	13	I_{mm}
Alg. 7 lines 2-15	880	2268	2716	I_{fm}
Alg. 7 lines 16-17	3	3	3	I_{fd}
Number of clock cycles per algorithm				
Alg. 2 $r_i = 0$	18720 (13260)	62100 (42750)	82804 (55880)	$C_{m0} = C_{md} \cdot I_{md}$
Alg. 2 $r_i = 1$	822 (570)	20704 (14144)	9971 (6682)	$C_{m1} = C_{mm} \cdot I_{mm}$
Alg. 7 lines 2-15	23760 (21120)	104328 (81648)	138516 (105924)	$C_{f0} = C_{fd} \cdot I_{fd}$
Alg. 7 lines 16-17	243 (180)	690 (483)	810 (555)	$C_{f1} = C_{fm} \cdot I_{fm}$
Sum	43545 (35130)	187822 (139025)	232101 (169041)	$C_p = C_{m0} + C_{m1} + C_{f0} + C_{f1}$

part, first row), then $R_d = R_{a3} \cdot R_{a5}$ (Table 5.5: bottom part, second row) and finally $R_u = R_{a4} \cdot R_u{}'$ (Table 5.5: bottom part, third row).

Latency formulae discussion:

With regard to characterization the speed of the hardware implementation of a pairing, we suggest using Latency, understood as a total time of data transfers in to and out of the circuit and the time of pairing computations. To be exact, we define Latency using the following formula:

$$latency = (C_i + C_p + C_o) \cdot T, \tag{5.11}$$

where C_i, C_p and C_i correspond to the number of clock cycles for fetching arguments, computing pairing operation and storing the result, respectively. T is a clock period, different and characteristic for each hardware implementation of the tate pairing on specific security level.

In order to compute the total number of clock cycles (C_p) required for the pairing computations we have to sum up (Eq. 5.12) number of clock cycles necessary for computations of Alg. 2 ln. 3 and 4 (Miller's loop - doubling) - C_{m0}, Alg. 2 ln. 6 and 7 (Miller's loop addition) - C_{m1}, Alg. 7 ln. 14 (Final exponentiation squaring) - C_{f0}, and Alg. 7 ln. 16 and 17 (Final exponentiation multiplication) - C_{f1}.

$$C_p = C_{m0} + C_{m1} + C_{f0} + C_{f1} \tag{5.12}$$

All the tate pairing supporting algorithms have an iterative nature.

First, the Miller's loop doubling (Alg. 2 ln. 3 and 4) requires I_{md} repetitions. A single iteration of this algorithm is completed after C_{md} clock cycles. Then the product of those two values contributes to the Eq. 5.12 as a C_{m0}.

Since our scheduling scheme for this algorithm, proposed in Table 5.3, determines five phases and the most computationally intensive operation in each of them is the multiplication then we can derive the relation $C_{md} \approx 5 \cdot C_{bm}$. Due to the occasional *idle* states in the multiplication units we could not use the equality sign.

Similarly in case of the Miller's loop addition (Alg. 2 ln. 6 and 7) the product of number of repetitions, denoted by I_{mm}, and the number of clock cycles per each iteration, denoted by C_{mm} constitutes the C_{m0}, a total number of clock cycles for Miller's loop addition. The relation $C_{mm} \approx 12 \cdot C_{bm}$ is a natural consequence of the fact that there are twelve phases

(proposed in Table 5.4) of a single iteration of Alg. 2 ln. 6 and 7.

The final exponentiation, the squaring part, is repeated I_{fd} times. This algorithm has the simplest basic iterative task (scheduling scheme in (in Tab. 5.5 upper part), but the arguments delivered to the i-th iteration are the results of the $(i-1)$-th computation. In such case it is not possible to overlap the multiplication and reduction operations. Due to the fact that there are only two multiplications per final exponentiation squaring operation (Alg. 7 ln. 14) and we have 4 multipliers available the double speed mode can be utilized. The number of clock cycles per each iteration of this algorithm can be described by the relation $C_{fd} \approx C_{dm} + C_{dr}$.

Finally, the number of clock cycles, required for the computation of both lines 16 and 17 of Alg. 7 (in Tab. 5.5 lower part), can be represented by the relation $C_{fm} \approx 3 \cdot C_{bm} + C_{br}$.

Table 5.6 summarizes the detailed, numerical information about the number of clock cycles per given operation, iteration or algorithm.

5.5 Hardware implementation results

The hardware coprocessors for the Tate pairing on twisted supersingular Edwards over prime fields were implemented in two flavors:

- a hybrid 17/24-bits architecture based on DSP48E available in Xilinx devies, and

- a 36-bits architecture based on DSP units in Altera devices.

Each Xilinx Virtex 6 FPGAs DSP48E unit has a two-input multiplier followed by multiplexers and a three-input adder/subtractor/accumulator. The unit can be configured as a 24x17 multiplier (or 25x17 signed) and/or 48-bit adder with up to three inputs [194].

Contrary, Each DSP block in a Stratix device can implement four 18x18-bit multiplications using dedicated multiplier circuitry. Each DSP block can also be configured to support eight 9x9-bit multiplication or one 36x36-bit multiplication for different applications by choosing the appropriate DSP block operation mode in the design software [185],

Table 5.7: Implementation results of the pairing coprocessors for selected FPGA devices

Xilinx Virtex-6 (xc6vhx380tff1924-3)					
Security	Frequency [MHz]	Slices	BRAMs	DSPs	latency [μs]
80-bits	187.4	17214	33	124	232
120-bits	179.5	59482	77	300	1046
128-bits	170.2	73536	90	352	1363
Altera Stratix IV (EP4S100G5H40C2ES1)					
Security	Frequency [MHz]	ALUTs	Memory	DSPs	latency [μs]
80-bits	203.1	39607	552k	240	173
120-bits	197.4	126367	1327k	576	704
128-bits	192.4	144332	1548k	672	879
Altera Stratix V (5SGSMD5H1F35C1)					
Security	Frequency [MHz]	ALUTs	Memory	DSPs	latency [μs]
80-bits	263.1	41471	552k	120	133
120-bits	257.7	120628	1327k	288	541
128-bits	242.3	137484	1548k	336	697

[195].

First, all hardware architectures for 80, 120 and 128-bit security levels, have been first modeled in VHDL-93 and the functionality of the coprocessors was cross-verified with the software implementation in C (based on GMP library [196]) and using Magma scripts [197]. The coprocessors were then synthesized, placed and routed in Xilinx Virtex-6, Altera Stratix IV and V using design software of the respective vendor. The maximum clock frequencies have been determined using static timing analysis tools provided as part of the respective software packages (*quartus_sta* for Altera and *trace* for Xilinx). The tool options were selected in such a way, that the embedded resources, such as block memories or DSP units, were inferred during implementation. Table 5.7 summarizes the results collected after the *Place-and-Route* and *Fitter* in Xilinx and Altera, respectively.

Several conclusions regarding the implementation results of the coprocessor can be made:

- It is very difficult to achieve very high frequency (300MHz+) for s designs which are large in all aspects: number of logic elements, block memories and DSP units. It is due to the fact that routing delay between logic resources and BRAMs or/and DSPs,

119

Table 5.8: Pairing transformations speed records for the range of 120-128-bits security

Publication	Curve Type	Field	Security	Type	FPGA	Latency
This work	**twisted supersingular Edwards**	**GF(p)**	**120-bit**	**Tate**	**Stratix V**	**0.54ms**
Cheung et al. [178]	Barreto-Naehring	GF(p)	126-bit	Opt.-Ate	Virtex-6	0.57ms
This work	**twisted supersingular Edwards**	**GF(p)**	**128-bit**	**Tate**	**Stratix V**	**0.70ms**
This work	**twisted supersingular Edwards**	**GF(p)**	**120-bit**	**Tate**	**Stratix IV**	**0.70ms**
Beuchat et al. [177]	Barreto-Naehring	GF(p)	126-bit	Opt.-Ate	Virtex-6	0.83ms
This work	**twisted supersingular Edwards**	**GF(p)**	**128-bit**	**Tate**	**Stratix IV**	**0.88ms**
This work	**twisted supersingular Edwards**	**GF(p)**	**120-bit**	**Tate**	**Virtex-6**	**1.05ms**
Cheung et al. [178]	Barreto-Naehring	GF(p)	126-bit	Opt.-Ate	Stratix III	1.07ms
Fan et al. [198]	Barreto-Naehring	GF(p)	128-bit	Opt.-Ate	Virtex-6	1.17ms
This work	**twisted supersingular Edwards**	**GF(p)**	**128-bit**	**Tate**	**Virtex-6**	**1.36ms**
Fan et al. [198]	Barreto-Naehring	GF(p)	128-bit	Ate	Virtex-6	1.60ms
Cheung et al. [178]	Barreto-Naehring	GF(p)	126-bit	Opt.-Ate	Cyclone II	1.93ms

very often constitutes the critical path of the design.

- The latency of our design could be further improved by the Karatsuba algorithm [129] on top of the school-book method applied to our multiplier, however in order to speed up twice a single multiplication around 50% more of DSP units have to be added. In such a case the Tate pairing computations for 120 and 128-bit security on Stratix V could have been computed much below 0.4ms and 0.5ms, respectively. In case of Stratix IV they would require less than 0.5ms and 0.6ms, respectively.

- The Karatsuba algorithm can be applied recursively and the depth of this recursion can serve as a basis of the design space exploration of a single multiplication. Both Xilinx (Virtex XT) and Altera (Stratix GS) provide variants of their devices, which focus on DSP-rich and memory-rich applications. Taking into account the rapid growth of the number of such hardwired components in those FPGA devices variants the investigation of even DSP-richer configurations of our multiplier might be possible very soon.

- On Altera Stratix IV and Stratix V devices the computations of the Tate pairing on twisted supersingular Edwards curves over prime fields for 128-bit security level can be computed below 1ms.

Table 5.9: Software implementations of pairing on (single core) Intel Core i7 2.8 GHz

Beuchat et al. [177] Optimal-Ate over Baretto-Naehring						
Security	Multiplication F_p^2	Squaring F_p^2	Miller Loop	Final Exponentiation	Total	Latency [μs]
126-bit	435	342	1330000	1000000	2330000	0.83
Tate pairing over twisted supersingular Edwards curve						
Security	Multiplication	Squaring	Miller Loop	Final Exponentiation	Total	Latency
80-bit	2344	1998	11753280	2493120	14246400	5.09
120-bit	5944	5463	69840602	12518598	82359200	29.41
128-bit	7507	6650	89556628	14337372	103894000	37.11

Table 5.8 demonstrates the fastest to date hardware architectures for pairing computations in the 120-128-bit range of security. The fastest to date coprocessor for the pairing computations on pairing-friendly Barreto-Naehring curves over prime field was reported in [178] (the fastest overall hardware accelerator for pairing at 128-bit security level was reported for binary fields and it was described in [179]). The best variant of the coprocessor from [178] was reported on Stratix III and Virtex-6 and the resource utilization vectors were 4233 ALUTs, 72 DSPs and 7032 slices, 32 DSPs, respectively.

The coprocessors, demonstrated in this work, require much more area. It is primarily due to the fact that in order to provide the same security level the supersingular curves require much larger arguments for any basic arithmetic operation (five to six times for a security level in a range 120-128-bit). The most basic version of the multiplier, demonstrated in this work, optimized for different DSP unit's geometry, offers high computational power and a big flexibility (double speed mode). A single multiplication unit, for 128-bit security level) occupies already 88 DSP48e and 42 DSPs blocks for Virtex-6 and Stratix V, respectively. On the other hand, the biggest advantage of this coprocessor is the fact that even though that the major component, the multiplier is not using even more expensive Karatsuba-like method, still it can compute pairing for the security range 120-128-bit within 541 μs on 28nm Stratix V. This result should be easily improved on any device with bigger number of DSP units.

5.5.1 Note about software implementations

In the paper [177], the authors have presented a software library that implements the optimal ate pairing over a Barreto-Naehrig curve at the 126-bit security level (very similar to the work in [178]). The authors claim, it is "the first (and the fastest so far) to have reported the computation of a bilinear pairing at a level of security roughly equivalent to that of AES-128 in less than one millisecond on a single core of an Intel Core i7 2.8GHz processor".

In this section we are going to provide a results of the software implementation of the Tate pairing over twisted supersingular Edwards curve on prime fields at the 80, 120 and 128-bit security level at the same platform.

Our software library is written in C and can be used on several platforms, including 32/64-bit versions of Windows 7 with Visual Studio 2x Professional, Linux 2.6 and Mac OS X 10.6 with gcc 4.2.1 or later, etc. Our implementation is based on the GMP library, namely the arithmetic operations: modular addition, subtraction and multiplication use the combination of *mpz_mod* together with *mpz_add*, *mpz_sub* and *mpz_mul*, respectively.

Table 5.9 summarizes the average latency in terms of time and clock cycles for full pairing computations. Additionally, we have provided the implementation results for the Miller loop, final exponentiation and basic arithmetic operations: modular multiplication and squaring. For a range of security level 120-128-bit our Tate pairing is slower than the Optimal-Ate pairing over Baretto-Naehring curves in a range of 30-40 times.

Taking into account three facts:

- the number of modular multiplications/squaring for 80, 120 and 128-bit security levels are 5036, 10584 and 11148, respectively, and

- the number of clock cycles per modular multiplication/squaring for aforementioned security levels are (2344, 1998), (5944, 5463) and (7507, 6650), respectively, and

- with a given total number of clock cycles for full pairing operation, summarized in

the column 6 of Table 5.9

we can estimate that those two basic arithmetic operations contribute to the full computations of pairing in a range of 70-80%.

In order to provide a software implementation, being competitive to the implementation results reported in [177], using the optimization techniques described in this chapter, every modular multiplication/squaring have to be conducted below 200 clock cycles (approx. 30-40 times faster than in GMP library). The other possibility would be a multi thread software library for the Tate pairing over twisted supersingular Edwards curves.

5.6   Conclusions

In this chapter, we have demonstrated the very first hardware architecture of pairing on Edwards curves. First, we have proposed, novel, low latency, a hybrid adder based on the high-radix carry save addition and the Kogge-Stone adder. Based on this concept we have developed new hardware architectures, optimized for FPGA devices, for modular addition, subtraction and multiplication for Solinas primes.

We demonstrated that these circuits, together with proper high-level scheduling, is very applicable for the pairing computations. The fastest version computes a Tate pairing at 80, 120 and 128-bit security over prime field in less than 0.13, 0.54 and 0.70 ms, respectively. We must also admit that the proposed circuit seems to be relatively expensive in terms of the area utilization.

For future work, we would like to further investigate the methods of area and latency reduction in Edwards curves based pairings. One of possible direction, an implementation-related, is the usage of hardwired macros instead of inferring embedded components in FPGA devices.

Finally, we would like to investigate even higher security levels, and conduct the practical experiments on Xilinx Virtex-6 and Altera Stratix-IV and V evaluation boards.

Part III

Benchmarking of FPGA-based coprocessors for cryptography

Chapter 6: Benchmarking of hardware architectures for Cryptography

A fair comparison of functionally equivalent digital system designs targeting FPGAs is a challenging and time consuming task. The results of the comparison depend on the inherent properties of competing algorithms, as well as on selected hardware architectures, implementation techniques, FPGA families, languages and tools. In 2010 Cryptographic Engineering Research Group have introduced an open-source environment, called ATHENa for fair, comprehensive, automated, and collaborative hardware benchmarking of algorithms belonging to the same class. In this chapter we are going to demonstrate the heart of ATHENa, the most successful heuristic optimization algorithm the GMU_Optimization_1.

Contents

6.1 Introduction and motivation

In almost every area of science and engineering, the same task can be realized using multiple competing algorithms. This statement is especially true in case of communications, digital

signal processing, and cryptography. The choice of a particular algorithm depends strongly on its efficiency in software and hardware.

In 2010 the Automated Tool for Hardware EvaluatioN (ATHENa) was proposed by Cryptographic Engineering Research Group at George Mason University and originally described in [199]. The improved version, still under development is presented in [200]. One of the primary goals of this environment is to make the comparison of competing algorithms fairer and more comprehensive, especially for the case where reconfigurable hardware is a viable and advantages means of implementation. Although our environment can be used for comparison of algorithms belonging to different fields, it is beneficial to focus first on algorithms belonging to one particular area: cryptography.

6.1.1 Cryptographic Competitions

The reason why this area is appropriate include

- well documented speed-ups and security gains of FPGA implementations over software implementations,

- constantly evolving standards, due to the everlasting struggle between designers of new algorithms and cryptanalysts attempting to break them,

- strong need for fair evaluation associated with the way new cryptographic standards are being developed, namely through open competition of algorithms submitted by groups from all over the world. Starting from the Advanced Encryption Standard (AES) contest organized by NIST in 1997-2000 [51], open contests have become a method of choice for selecting cryptographic standards in the U.S. and over the world. The AES contest in the U.S. was followed by the NESSIE competition in Europe [201], CRYPTREC in Japan [202], and eSTREAM in Europe [203]. Recently, the focus of attention of the entire cryptographic community was on the SHA-3 contest for a new hash function standard, organized by NIST [41].
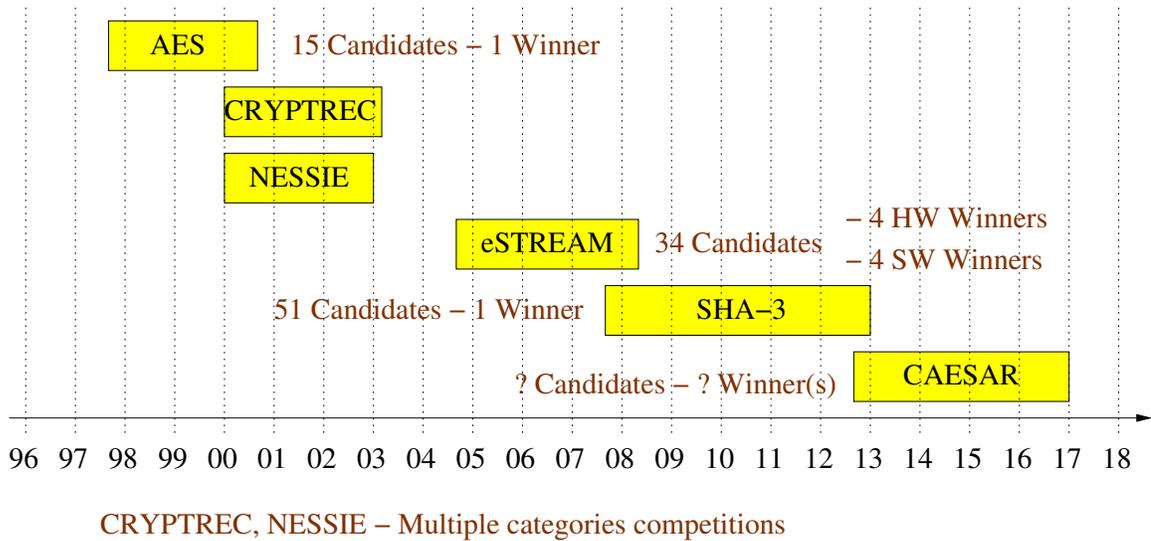
Figure 6.1: Timeline of the major cryptographic competitions

Next in line is going to be the authenticated encryption competition - CAESAR [204]. Figure 6.1 demonstrates the timeline of cryptographic competitions.

Four typical criteria taken into account in the evaluation of candidates are: security, performance in software, performance in hardware, and flexibility. While security is commonly recognized as the most important evaluation criterion, it is also a measure that is most difficult to evaluate and quantify, especially during the relatively short period of time reserved for the majority of contests. The typical outcome is that, after eliminating a fraction of candidates based on security flaws, a significant number of remaining candidates do not demonstrate any easy to identify security weaknesses, and as a result are judged to have adequate security. Interestingly, the differences among the cryptographic algorithms in terms of the hardware performance appeared to be particularly large, and often served as a tiebreaker when other criteria failed to identify a clear winner in AES [205], [206], eSTREAM [207], [208], and SHA-3 [93], [209].

6.1.2 Obstacles to a fair comparison

Saar Drimer in his PhD thesis [210] defined several problems related to benchmarking of FPGA implementations of cryptographic transformations. The most important issues discussed in his dissertation were associated with the difficulties in results replication, selection of the best set of design software options, and apple-to-orange comparison practices (different target technology, software version, etc). In the eve of SHA-3 contest this work was a trigger for the development of automated FPGA benchmarking systems and hardware evaluation methodologies.

Facilitating a fair and comprehensive comparison among competing cryptographic algorithms, implemented in FPGA devices, was investigated in [21] and [211]. Corresponding ASIC-oriented methodologies were proposed in [212], [209] and [213].

In order to conduct a fair comparison several obstacles have to be resolved. Most of them are relatively simple to overcome:

- **an influence of different hardware description languages**: Either of the two languages, VHDL or Verilog, is perfectly suited for the implementation and comparison of cryptographic transformations, as long as all competing algorithms are described in the same language. Using two different languages to describe different candidates may introduce an undesired bias to the evaluation.

- **an influence of the designer skills**: Re-usage of the recurring hardware components and the small team of closely cooperating engineers can reduce significantly, a so called "human factor" in the optimization effort for a given hardware architecture.

- **an influence of the selected platform**: FPGA devices from two major vendors, Xilinx and Altera, dominate the market with about 90% of the market share. Therefore, we assume that it is appropriate to focus on FPGA devices from these two companies.

- **an ambiguity in the definition of our hardware cores**: In order to define

hardware architectures for cryptographic transformations, and in order to make their implementations as practical as possible, we have developed a FIFO-based interface shown in Fig. 1a in [21]. It was proposed for hash functions, however it could be easily adapted to other transformations.

- **selection of performance evaluation metrics**: In most of the cases (hash functions, stream and block ciphers) our choice is the Throughput to Area Ratio, where Throughput is defined as Throughput for long messages, and Area is expressed in terms of the number of basic programmable logic blocks specific to a given FPGA family. Optimizing for the best ratio provides a good balance between the speed and the cost of the solution. However in case of transformations based on modular arithmetic, the major performance related metric is the latency of basic operation. Due to this fact the efficiency is typically defined as the latency · area.

- **the selection of tools, their versions, and a set of the best options**: For the sake of selection of the best set of options for the CAD tools of major vendors, some heuristic algorithms have to be developed.

This chapter demonstrates two algorithms for both Xilinx and Altera tools for the selection of best options for the appropriate tools. To the best of our knowledge these are two the best, to date, heuristic optimization strategies in this area.

The rest of this chapter is organized as follows:

In Section 6.2 we discuss previous work. Section 6.3 is devoted to the description of the heuristic method the *GMU_Optimization_1*. Section 6.4 demonstrates the list of major successes of aforementioned algorithm, finally we draw conclusions in Section 6.5.

6.2   Previous work

FPGA vendors have recently started the development of tools for the exploration of implementation options. The major FPGA vendors Xilinx and Altera publish their version

of exploration tools named ExploreAhead (it is a part of a higher level optimization tool PlanAhead) [214] and Design Space Explorer [215] respectively.

Table 6.1: Benchmarking Tools for Cryptography

Platform	Name	Heuristic Algorithm	Cryptography	Source
Microprocessors	eSTREAM testing framework	list of best options	stream ciphers	[216]
Microprocessors	SUPERCOP	list of best options	stream ciphers, hash functions, public key transformations	[47]
Microcontrollers	XBX	list of best options	hash functions	[217], [48]
Xilinx FPGA	ExploreAhead	predefined strategies	general applications	[214]
Altera FPGA	Design Space	predefined strategies	general applications	[215]
FPGA	ATHENa	GMU_optimization_1	hash functions, modular arithmetic, pairing transformations	[38], [218]

The eSTREAM testing framework was developed by De Cannière [216]. This benchmarking software helped significantly in the European cryptographic project - eSTREAM, which identified a portfolio of promising new stream ciphers.

Bernstein and Lange developed the SUPERCOP [47] benchmarking toolkit for cryptographic software solutions. The SUPERCOP, which stands for System for Unified Performance Evaluation Related to Cryptographic Operations and Primitives, measures the performance of hash functions (eBASH), secret-key stream ciphers (eBASC), public-key encryption systems, public-key signature systems, and public-key secret-sharing systems (eBATS). Both the eSTREAM testing framework and the SUPERCOP conduct benchmarking on general-purpose CPUs.

Recently, Wenzel-Benner and Gräf have developed the eXternal Benchmarking eXtension (XBX) [217] to SUPERCOP, and have successfully used this XBX to benchmark many different hash functions on different microcontrollers.

Table 6.1 aggregates the previous work in the area of benchmarking of cryptographic transformations.
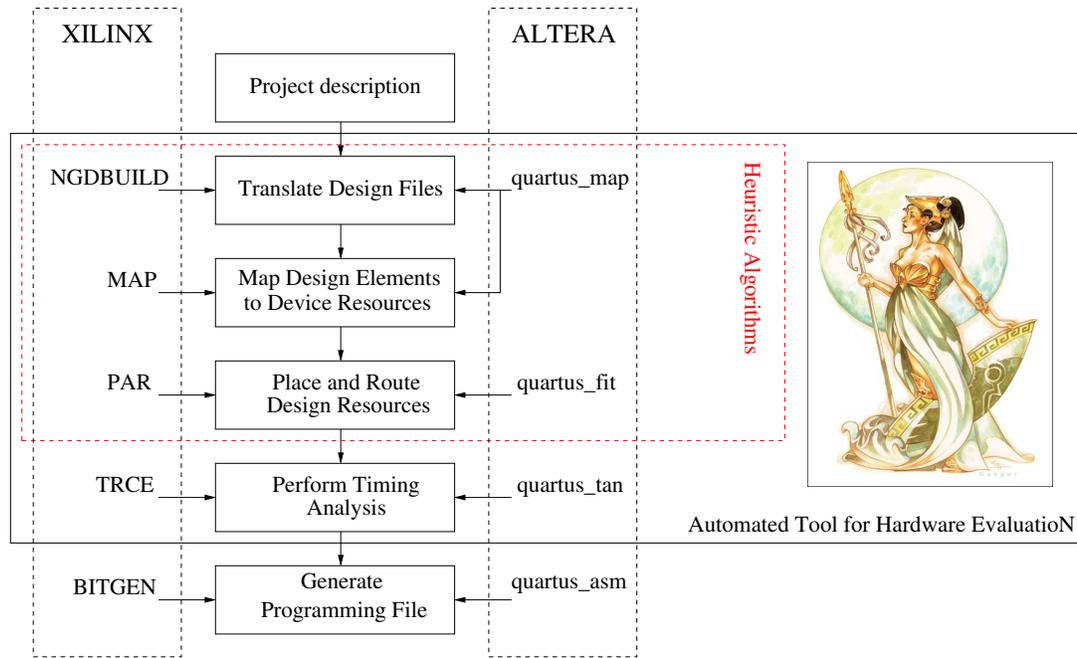
Figure 6.2: Relation between design flows of Altera and Xilinx
and heuristic algorithms in ATHENa

6.2.1 Automated Tool for Hardware EvaluatioN

A very first cross-FPGA platform for hardware benchmarking, Automated Tool for Hardware EvaluatioN - ATHENa, has been proposed at George Mason University in 2010.

The major features of this software are:

- **Running all steps of synthesis, implementation, and timing analysis in batch mode** (Fig. 6.2): This is a very important property, as it allows running time-consuming optimizations, without any user supervision, over long periods of time, such as nights, days, or even weeks.

- **Support for devices and tools of two major FPGA vendors: Xilinx and Altera**: Xilinx and Altera account for about 90% of the FPGA market. Their FPGA devices differ considerably in terms of the structure of a basic building block: configurable logic block (CLB) for Xilinx, and logic element (LE) for Altera. They also differ in terms of dedicated hardwired units, such as blocks of memory, multipliers,

DSP units, etc. As a result, the ranking of algorithms or architectures obtained using devices of one FPGA vendor may not carry to the devices of another vendor.

- **Generation of results for multiple FPGA families of a given vendor,** (e.g. Xilinx: Spartan 3, Virtex 5; Altera: Cyclone III, Aria II, Stratix IV): Our tool allows specifying as target platforms multiple families of FPGA devices of each of the two major vendors.

- **Automated choice of a device within a given family of FPGAs assuming that the resource utilization does not exceed a certain limits**: A maximum clock frequency of a circuit implemented using an FPGA is a function of device resource utilization. When the device utilization reaches 80+% in terms of one of the critical resources, such as configurable logic blocks or Block RAMs, the performance degrades. This effect is caused mostly by the difficulties associated with routing in congested circuits. The utilization threshold at which the performance degradation begins is a function of an FPGA family, an implemented circuit and the version of the design tools.

- **Automated verification of a design through functional simulation, run in batch mode**: Our tool has an additional capability of simulating designs in batch mode in order to verify their correct functionality. The verification is based on a testbench utilizing test vectors stored in a file, and providing a binary answer whether the circuit operates correctly or not.

- Finally, **Automated optimization of results aimed at one of the three optimization criteria: speed, area, and ratio speed to area**: Results generated by the FPGA tools depend highly on the choice of multiple options and the contents of constraint files. Variation of results obtained by changing just a single option may easily exceed 25%. Currently, the most successful heuristic algorithm for throughput and throughput to area ratio optimization is the GMU_optimization_1 method.

6.3 A heuristic optimization algorithm for FPGA-based hardware architectures

6.3.1 A case study and the design rationale for the best ATHENa heuristic algorithm

Out of several hardware architectures of SHA-256, we have selected and implemented an architecture referred to as architecture with rescheduling. It is an optimized architecture, developed by Chaves et al. [219], optimized for the maximum throughput to area ratio. The SHA-2 coprocessor design was adjusted to the evaluation methodology proposed in [21].

The synthesizable source codes, the testbench, and the specification of the generic interface are all available at the ATHENa project web site [218]. For our experiments we have then selected a 65nm Xilinx Virtex-5 device, xc5vlx30ff676-3, the smallest device in this family, with the fastest speed grade (in this proposal we are not going to present our design rationale for Altera devices).

Modern design flow for the FPGA devices is built upon multiple parameterizable steps. The options available for the designer at every stage can be divided into three classes of options:

- options with large space of possible values and their ranges unknown,

- options with large space of possibilities, but within fixed range, and

- the rest of available options with a few possible values - typically 2 or 3.

We have identified that the first group of the design software options is represented by the requested frequency and the setting of a maximum fan-out of a logic gate (which is the total number of gate inputs to which an output of a given gate is connected). The range of possible values depends on the VHDL project description and the target device.

Table 6.2: Influence of design software options on implementation results for the optimized architecture of SHA-256 by Chaves et al.

options	improvement	conclusions
frequency	area:-7%, speed:31%, throughput/area:27%	high correlation between requested and achieved frequency presented in Fig. 6.3
placement	area:-7%, speed:6%, throughput/area:11%	the correlation between placement position and achieved frequency difficult to observe
other	area:-1%, speed:17%, throughput/area:18%	The option: (effort level = high) improves results, but requires more time for execution

The second group is represented by a starting point of a physical implementation. It is denoted as the Cost Table value (1 to 100) in Xilinx *Place and Route* and the Seed value (1 to $2^{32} - 1$) in case of Altera *Quartus Fitter*.

Finally, the remaining options can be very often represented by a simple flag. For instance, the effort level, which particular design software is working on, can be set using three values: HIGH, MEDIUM and NORMAL. Those implementation attempts with different effort levels are based on a simple trade-off between the higher quality results and the execution time of the tools.

In Table 6.2 we have summarized the influence of various software options on the final implementation results in case of each and every group of selected options.

6.3.2 Heuristic optimization algorithms for FPGA design flow

The highest generalization level of the proposed heuristic optimization method was the level of the vendor's specific design tools. Our heuristic strategy was named GMU_Optimization_1 and it performs optimization specific to a Xilinx ISE and Altera Quartus.

For Xilinx, it combines an optimal requested frequency search, and placement search with three different optimization targets (Area, Speed and Balanced), and an effort level selection.

For Altera, only placement search and optimization target are combined together as not much can be gained from frequency search.

The GMU_optimization_1 heuristic method is demonstrated for Xilinx and Altera on
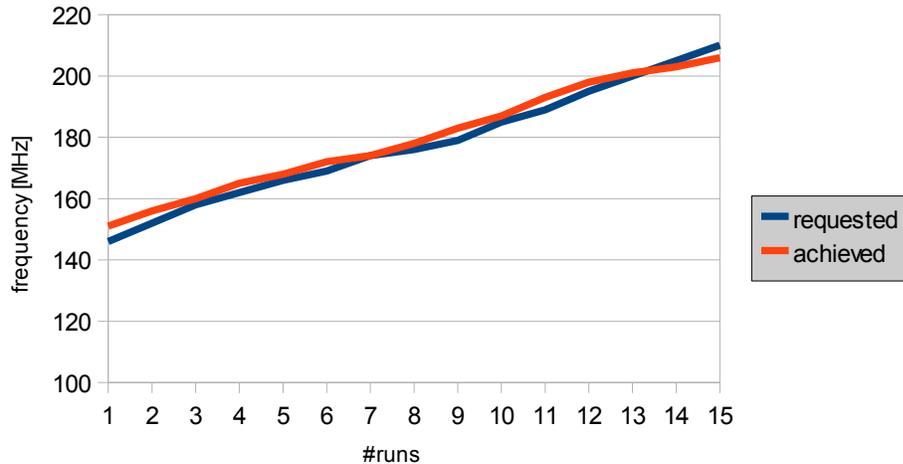
Figure 6.3: Dependency between requested and achieved frequency for combined optimization targets

Figs. 6.4 and 6.5, respectively.

For Xilinx, the GMU_Optimization_1 algorithm works as follows. For each of the optimization targets, an initial run ($Run(F_{req}, Settings)$) with default options of the design tools is generated using the default options. The frequency achieved (F_{ach}) in this initial run determines the starting point of the frequency search. After this initial frequency value is determined, the next run is executed with a requested frequency (F_{req}) equal to the last achieved value increased by the percentage indicated by the first value ($F_{step}(0)$) in the predefined *requested frequency improvement steps list* (the size of this list is denoted as $ord(F_{step})$). The result from this run is used as the starting point for the next run, and this process is continued until either zero or negative improvement is generated by the design software. Once the increases in requested frequency no longer yields a positive effect on the achieved frequency, the highest achieved frequency is used as the requested frequency and the design software options are set to a high effort (Settings=high effort).

The previous incremental improvement process is continued using the high effort options until a positive effect on achieved frequency is no longer attainable. At this point the algorithm will iterate through the placement options to try to accomplish a positive change

135
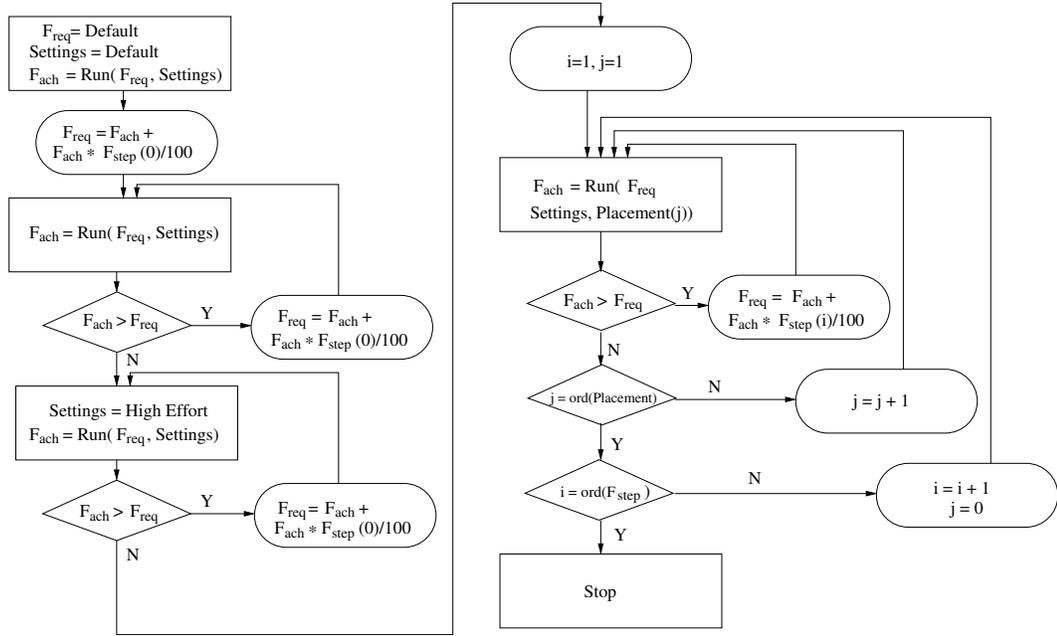
Figure 6.4: ATHENa GMU_optimzation_1 method for Xilinx devices

in the achieved frequency. The placement options are determined by the number chosen for Xilinx *COST TABLE* entry (*Placement*(j) for $j \geq 0$). The initial incremental improvement process is used again until no benefit from the requested frequency increase is observed.

At this point, the highest achieved frequency is used as the basis for incremental improvement, now using the step value indicated as the next value in the predefined *requested frequency improvement step list* ($F_{step}(i)$ for $i \geq 0$). This process continues until all values within the list have been used.

In case of Altera, the GMU_optimization_1 runs through the list of all possible placements (*Placement*(i) for $i \geq 0$) and through the list of all possible optimization targets (*optimization*(b) for b=*speed, area, balanced*). The GMU_optimization_1 is in fact the exhaustive search over a two-dimensional space (placement, optimization target).
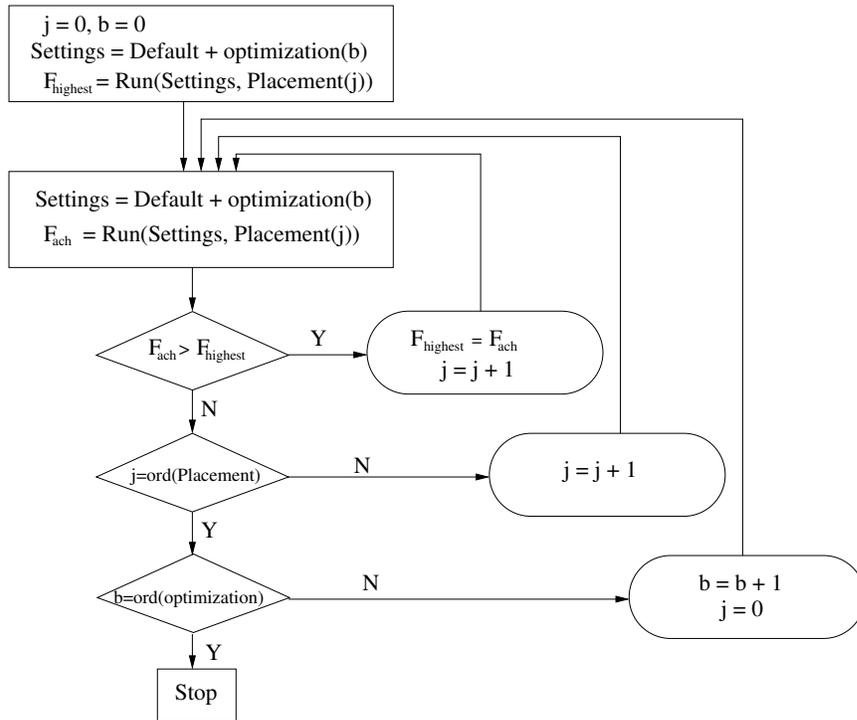
Figure 6.5: ATHENa GMU_optimzation_1 method for Altera devices

6.4 Results

The list of the papers, where the *GMU_Optimization_1* optimization strategy was used for the results generation and optimization is already very long and it is expected to grow quickly.

The first big test of our environment was its application to the evaluation of candidates submitted to the SHA-3 contest for a new hash function standard, organized and coordinated by NIST:

- The hardware architectures, *optimized for throughput/area ratio and based on reconfigurable logic only* for 14 candidates of the 2nd round of the SHA-3 competition have been reported in [21], [220] and [75]. To the best of our knowledge, ATHENa helped to generate 11 out 14 best designs in terms of throughput/area ratio, outperforming other designs reported earlier in the literature.
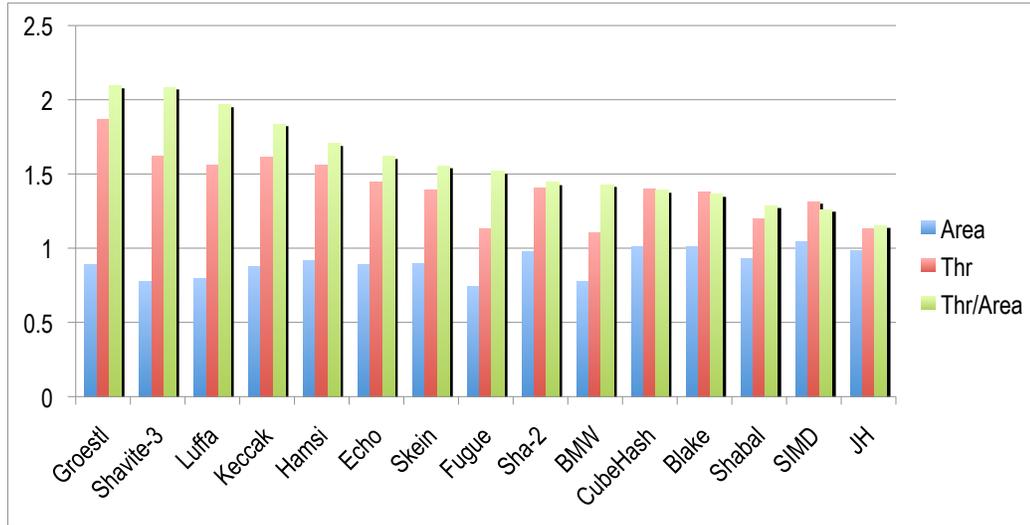
Figure 6.6: Relative improvement of results from using ATHENa Virtex 5, 256-bit variants of hash functions. Ratios of results obtained using ATHENa suggested options vs. default options of FPGA tools. [21]

- Furthermore, it contributed to the improvement of 10 out 14 round two candidates, when *the hardwired components in modern FPGAs* were used. The results presented in [33] and [40] show that in case of AES-like hash functions improvement in terms of the throughput/area ratio was able to reach even 100+%.

- In [221], [93] and [222], we have conducted the hardware architectures *exploration among five finalists of the SHA-3 competition*. The results, reported in [221], are the best reported in the literature for portable source codes (no low level components used, e.g.: Xilinx Unisim library).

- Moreover, in case of the SHA-3 competition our optimization method have been proven to be effective also for the designs, *optimized for low area utilization*, demonstrated in [223] and [224].

Finally, the *GMU_Optimization_1* have been demonstrated to be applicable for different types of transformations:

- *Authenticated encryption* based on the AES-Grøstl coprocessor, presented in [28] and

138

[29].

- *Arithmetic and modular arithmetic cores*, presented in [35] and [36].

- *Pairing accelerators based on embedded resources*, demonstrated in [36].

Typically, it is expected that the *GMU_Optimization_1* optimization algorithm will improve the implementation results between 30 and 100% (Fig. 6.6).

6.5   Conclusions

The ATHENa and its heart, the *GMU_Optimization_1*, optimization strategy, will continue to serve the cryptographic and FPGA community for years to come, providing comprehensive and easy to locate results for multiple cryptographic standards and other classes of algorithms.

Researchers all over the world will benefit from the capability of fairly, comprehensively, and automatically comparing their new algorithms, hardware architectures, and optimization methods against any previously reported work. The designers will benefit from the capability of comparing results of implementing the same algorithm using multiple FPGAs from several major vendors, and will be able to make an informed decision about the choice of the implementation platform most suitable for their particular application. The developers and users of tools will benefit from the comprehensive comparison done across tools from various vendors, and from the optimization methodologies developed and comprehensively tested as a part of this project.

Chapter 7: Conclusions and future research

In this chapter, we will provide a summary for this dissertation as well as several rec-ommendations for future research.

Contents

7.1 Conclusions

In this research, we have made an effort to answer a critical question whether the emerging cryptographic transformations (such as SHA-3 finalists and Tate pairing based on Edwards curves) can be used to develop the most efficient to date hardware architectures of cryptography taking full advantage of special embedded resources present in modern FPGAs.

Hardware architectures investigated in this research contribute to the five, most important cryptographic services: confidentiality, integrity, authentication, non-repudiation, and key exchange. The thesis is divided into three major parts, describing our original contributions to the areas of: high-performance architectures supporting confidentiality, integrity, and authentication, hardware architectures supporting key exchange and non-repudiation, and algorithms for benchmarking and optimization of FPGA-based coprocesors for cryptography.

In the first part, we have discussed new hardware architectures for the emerging hash functions (used as a basis of integrity, authentication, and non-repudiation services) developed during the SHA-3 contest held by NIST in the period 2007-2012. In particular, we

have concentrated on the AES-inspired class of hash functions that advanced to the Round 2 of the competition, including ECHO, Fugue, Grøstl-0, and SHAvite-3. We have proven that these functions can benefit from the special T-box hardware architecture, inspired by a somewhat similar hardware architecture of AES. The proposed architecture has been shown to improve the throughput to area ratio of the four aforementioned hash functions by 49, 173, 424 and 262%, respectively. More importantly, by applying the same technique, the performance of the SHA-3 finalist Grøstl has been improved by 446%, 158% and 58% in Cyclone II, Stratix III, and Virtex 5, FPGAs, respectively. As a second major contribution, we have proposed a new joint architecture for Grøstl and AES, supporting the use of these two algorithms for authentication and confidentiality, respectively, in secure Internet protocols, such as IPSec. This architecture allows substantial resource sharing between Grøstl and AES. Our coprocessor based on this architecture outperforms the best earlier reported design by Jarvinen et al. by 64% for the IP ESP (Encapsulating Security Payload) protocol being a heart of IPSec.

In the second part of the thesis, we focus on new hardware architectures, for emerging public key cryptosystems, such as pairing based schemes. In particular, we investigate in detail the Tate pairing transformation over Edwards curves. To the best of our knowledge, this particular transformation has never been implemented in hardware. In order to support cryptographic services such as confidentiality, non-repudiation, and key exchange, the emerging Pairing-based Cryptography provides unique cryptographic mechanisms, such as Identity-based encryption, Identity-based signatures, and One-Round Tri-Partite key-exchange. Our FPGA-based coprocessor, which can be used directly in any of the afore-mentioned schemes, demonstrates that pairing over Edwards curves is a very promising direction, which should be further investigated from the point of view of standardization and efficient implementations in software and hardware. In particular, we have demon-strated, that even though Edwards curves were not optimized for pairing, they present a valid alternative to pairing friendly Barreto-Naehrig curves. By implementing our new hardware architecture on Altera Stratix V, we have shown that our solution outperforms

all previously reported FPGA-based pairing coprocessors operating over prime fields, for the security level between 120 and 128 bits.

In order to accomplish this result, we have made several important contributions at the intersection of cryptography and computer arithmetic. In particular, we have developed:

- a new, low latency adder based on the use of high-radix carry save representation and Parallel Prefix Networks. We have demonstrated that for long operands, exceeding 1024 bits, this adder takes the best advantage of the special embedded resources supporting fast addition in modern FPGAs called fast carry chains. Our design outperforms the best classical fast adders, Kogge-Stone and Brent-Kung, in terms of the latency · area product by up to 50, 38 and 35% for 1024, 2048 and 4096-bit operands, respectively. At the same time it matches or outperforms these adders in terms of latency.

- a new, low latency modular adder/subtractor based on the aforementioned adder. This modular adder has been shown to significantly outperform all previously known designs in terms of both latency and the product of latency · area. In terms of both of these performance measures an average improvement over the best of the two classical designs was shown to be 15, 40 and 55% for Altera devices, and 50, 45 and 70% for Xilinx devices. The three numbers listed above refer to the results for the 1024, 2048, and 4096-bit operands, respectively. As can be seen from these results, the improvement increases with the increase in the size of operands, which makes this modular adder particularly attractive for the entire field of public key cryptography, in which key sizes and thus operand sizes tend to increase over time to compensate for the constant progress in cryptanalysis and computing power.

- a new, low latency grid multiplier based on the used of DSP units of modern FPGAs. This multiplier incorporates the best features of the previously reported multipliers, removes some of their restrictions (such as a focus on RSA and Diffie-Hellman schemes), and supports the double speed mode of operation for the case when the

number of available multipliers exceeds the number of multiplications that can be scheduled at the same time.

- a new, low latency modular multiplier based on the used of DSP units of modern FPGAs, optimized for the case of special primes used in cryptography called Solinas primes. Our solution takes advantage of the Barrett reduction, which replaces division by multiplication, and of the special form of intermediate operands, which allows replacing multiplication by multi-operand addition. To the best of our knowledge this approach has been applied for the first time to the case of Tate pairing over Edwards curves, and it can be generalized to other related classes of public key cryptosystems.

Finally, in the third part of our thesis, we have described our contribution to the open-source environment, called ATHENa, for fair, comprehensive, automated, and collaborative benchmarking and optimization of digital system designs targeting modern FPGAs. We have developed the heart of ATHENa, the most successful heuristic optimization algorithm: *GMU_Optimization_1*. This algorithm has been shown to allow overall improvements in terms of the throughput to area ratio in the range of 100%. Additionally, this algorithm has been shown to be general enough to apply to several different classes of digital circuits: hash functions, secret key ciphers, modular arithmetic on long operands, pairing transformations, etc. So far, it has served as a back-end tool for the result generation in at least ten publications.

Based on the obtained results and the presented contributions, we may conclude that the emerging cryptographic transformations investigated in this thesis, namely AES-based SHA-3 candidates and the Tate pairing on Edwards curves, are well suited for implementation using modern FPGAs, and can take advantage of special computational units embedded in these FPGAs. Combining the power of new algorithms and the power of new FPGAs leads to some of the most efficient implementations of cryptography reported in the literature to date.

7.2 Future work

There are several possible approaches for the extension of this work. This section is devoted to some of the directions in which the problems can be further explored.

7.2.1 Hardware architectures for pairing on ordinary Edwards curves

The hardware acceleration of pairing on supersingular twisted Edwards curves over prime fields has occurred to be very fast, yet also very demanding in terms of area. Our initial results of the hardware acceleration of pairing on ordinary Edwards curves, defined in [180], has revealed that this algorithm will require approximately fifteen times fewer reconfigurable resource with two times longer computations. Therefore, in terms of the latency · area product, this approach would lead to the improvement by a factor of seven and a half.

Additionally, our early investigation of data dependencies in the scheduling of the basic building operations in pairing on ordinary Edwards curves, showed that it might be impossible to bridge the gap in terms of latency for the pairing computations on supersingular and ordinary Edwards curves. Thus, more research and a new approach might be necessary to overcome this problem.

7.2.2 Hardware architectures for the Edwards Curves Digital Signature

Algorithm based on P25519

The Solinas primes, investigated in Chapter IV and V, were selected in a such a way that their $\mu = \frac{2^{2n}}{p}$ parameter consists of a relatively small number of terms (<30). The prime $2^{255} - 19$ (also called P25519), originally defined by Bernstein in [225], has very similar hardware-friendly properties. Both p and μ parameters for P25519, required in the Barrett reduction [128], consist of relatively small number of terms.

Bernstein et al. [226] have reported the fastest, to date, software implementation of

Digital Signature Algorithm based on Edwards curves (so called EdDSA) and P25519. Due to the similarities, in regards to the Barrett reduction parameters, between the hardware architectures of Solinas primes arithmetic and the P25519 arithmetic, we believe that using our novel architectures for modular arithmetic on large integers it should be possible to build the fastest to date hardware coprocessor for the ECDSA [227].

7.2.3 Hardware architectures for the short digital signatures based on the Barreto-Naehrig curves

Currently, the shortest digital signatures are offered by pairing transformations. The shorter signatures the smaller requirements for the storage and the transmission time of this crucial information. This feature is especially important in resource constrained environments, where the power consumption used for transmission of data is often the most limiting factor [228]. In order to reduce the size of a digital signature by half, without compromising its security a new technology has to be used. One of the first, proposed in the literature short signature schemes is the Boneh-Lynn-Shacham (BLS) scheme [168].

Based on the current state of knowledge, the most suitable, for the short digital signatures, are the Barreto-Naehrig curves [187]. For the 128-bit security level the Barreto-Naehrig-based BLS scheme produces 256-bit digital signatures. Contrary, the BLS scheme, based on supersingular and ordinary Edwards curves, produces 1493 and 401-bit digital signatures, respectively. Thus, the optimal selection for the short digital signatures are the Barreto-Naehrig curves. We believe that the implementation of pairing on the Barreto-Naehrig curves can be still improved using selected architectures presented in this thesis.

7.2.4 Hardware-Software co-design for Public Key Cryptography

A very complex system, which accommodates the functionality of Pairing-based Cryptography, Elliptic Curve Cryptography, classical Public Key Cryptography or even symmetric Cryptography, requires finding the correct balance between flexibility and performance. Principles of a modern approach for such problems, so called, Hardware/Software Co-design are described in [229]. Taking into account this technique, several directions are possible. We name here two of them:

1. Due to the fact that different cryptographic algorithms, in order to provided the same level of security, require different sizes of operands (e.g.: for the 128-bit security level: RSA, pairing on supersingular curves, ECDSA, pairing on ordinary Edwards curves, pairing on BN-curves require 3072, 1493, 512, 401 and 256-bit operands respectively), a hardware/software co-design is a highly attractive solution. A single scalable multiplier, providing support for different sizes of arguments should be the primary hardware element in such a system. All the high-level functionality: scheduling of the arithmetic units for the basic iterative tasks of the aforementioned schemes or even high level protocols and applications could be designed using software approach.

   Such approach would provide, very strong alternative for the purely software or the purely hardware oriented designs. It would inherit the natural software flexibility, but also preserve some fraction of the hardware powerful computational features.

2. Partial Reconfiguration [230] is a technique that allows certain portions of an FPGA device to be re-configured during run-time without affecting the functionality of other portions of the system. This technique, together with an efficient use of hardware-software co-design opens the door to the world of extreme efficiency of systems based on FPGAs. Thanks to the utilization of both methods it might be possible to save a significant portion of hardware resources with a relatively small penalty in terms of performance. The aforementioned arithmetic support for cryptographic services could be extended in a such a way, that instead of utilizing one generic, scalable modular

multiplier, we could have multiple application-optimized versions of arithmetic units. Our joint work with Ahmad Salman and Jens-Peter Kaps [89] has revealed big potential for such systems. Typically, the latency of the cryptographic transformations for the asymmetric cryptography is much larger than for the symmetric transformations at the same security level, thus the overhead from the reconfiguration time contributes less to the total response time in such a system.

Bibliography

Bibliography

[1] K. Järvinen, "Sharing resources between AES and the SHA-3 second round candidates Fugue and Grøstl."

[2] J. Daemen, "Cipher and hash function design. strategies based on linear and differential cryptanalysis," Ph.D. dissertation, Katholieke Universiteit Leuven, 1995.

[3] V. Rijmen, J. Deamen, B. Preneel, A. Bosselaers, and E. De Win, "The cipher shark," in *3rd International Workshop on Fast Software Encryption FSE.*, 1996, pp. 99–111.

[4] J. Daemen, L. Knudsen, and V. Rijmen, "The block cipher square," in *Fast Software Encryption (FSE)*, 1997.

[5] *Advanced Encryption Standard (AES)*, National Institute of Standards and Technology (NIST), FIPS Publication 197, Nov 2001, http://csrc.nist.gov/publications/fips/fips197/fips-197.pdf.

[6] E. Biham, R. Anderson, and L. Knudsen, "Serpent: A new block cipher proposal," in *Fast Software Encryption, FSE 1998*, ser. Lecture Notes in Computer Science (LNCS), vol. 1372.   Springer, January 1998, pp. 222–223.

[7] B. Schneier, J. Kelsey, D. Whiting, D. Wagner, C. Hall, and N. Ferguson, "Twofish: A 128-bit block cipher," Counterpane Systems, Minneapolis, MN, USA, AES Proposal, June 1998.

[8] E. Hong, J.-H. Chung, and C. H. Lim, "Hardware design and performance estimation of the 128-bit block cipher crypton," in *Workshop on Cryptographic Hardware and Embedded Systems - CHES*, 1999.

[9] T. Corp., "Specification of hierocrypt-3," NESSIE.

[10] P. Barreto and V. Rijmen, "The khazad legacy-level block cipher," First open NESSIE Workshop, 2000.

[11] ——, "The anubis block cipher," NESSIE, 2000.

[12] J. Borst, "The block cipher: Grand cru," NESSIE, 2000.

[13] L. McBride, "Q - a proposal for nessie," NESSIE, 2000.

[14] J. Daemen, M. Peeters, G. Van Assche, and V. Rijmen, "Nessie proposal: Noekeon," 2000.

[15] R. Benadjila, O. Billet, H. Gilbert, G. Macario-Rat, T. Peyrin, M. Robshaw, and Y. Seurin, "SHA-3 proposal: ECHO," Submission to NIST (updated), Feb 2009, http://crypto.rd.francetelecom.com/echo/.

[16] S. Halevi, W. E. Hall, and C. S. Jutla, "The hash function Fugue," Submission to NIST (updated), Sep 2009, http://domino.research.ibm.com/comm/research_projects.nsf/pages/fugue.index.html.

[17] P. Gauravaram, L. Knudsen, K. Matusiewicz, F. Mendel, C. Rechberger, M. Schäffer, and T. Søren, "Grøstl - a SHA-3 candidate," Submission to NIST (Round 3), 2011.

[18] E. Biham and O. Dunkelman, "The SHAvite-3 hash function," Submission to NIST (Round 2), 2009, http://www.cs.technion.ac.il/~orrd/SHAvite-3/Spec.15.09.09.pdf.

[19] H. Wu, "The hash function JH," Submission to NIST (round 3), 2011, http://www3.ntu.edu.sg/home/wuhj/research/jh/jh_round3.pdf.

[20] J.-L. Beuchat, "Some Modular Adders and Multipliers for Field Programmable Gate Arrays," in *Parallel and Distributed Processing Symposium*, 2003.

[21] K. Gaj, E. Homsirikamol, and M. Rogawski, "Fair and comprehensive methodology for comparing hardware performance of fourteen round two SHA-3 candidates using FPGA," in *Cryptographic Hardware and Embedded Systems, CHES 2010*, ser. LNCS, S. Mangard and F.-X. Standaert, Eds., vol. 6225. Springer Berlin / Heidelberg, 2010, pp. 264–278.

[22] A. J. Menezes, P. C. van Oorschot, and S. Vanstone, *Handbook of Applied Cryptography*. CRC Press Inc., 1997.

[23] W. Diffie and M. E. Hellman, "New directions in cryptography," *IEEE Transactions on Information Theory*, vol. IT-22, no. 6, pp. 644–654, Nov 1976.

[24] R. L. Rivest, A. Shamir, and L. Adleman, "A method for obtaining digital signatures and public-key cryptosystems," *Commun. ACM*, vol. 21, no. 2, pp. 120–126, Feb 1978.

[25] X. Wang, Y. Yin, and H. Yu, "Finding collisions in the full sha-1," in *Advances in Cryptology - CRYPTO*, 2005.

[26] B. Brumley and N. Tuveri, "Remote timing attacks are still practical," http://eprint.iacr.org/2011/232.pdf.

[27] V. S. Miller, "Short programs for functions on curves," 1985, http://crypto.stanford.edu/miller/miller.pdf.

[28] M. Rogawski and K. Gaj, "A High-Speed Unified Hardware Architecture for AES and the SHA-3 Candidate Grøstl," in *15th EUROMICRO Conference on Digital System Design – DSD'12*, 2012.

[29] M. Rogawski, K. Gaj, and E. Homsirikamol, "A high-speed unified hardware architecture for 128 and 256-bit security levels of aes and grøstl," *Embedded Hardware Design: Microprocessors and Microsystems*, 2013.

[30] S. Drimer, T. Güneysu, and C. Paar, "DSPs, BRAMs and a pinch of logic: Extended recipes for AES on FPGAs," *ACM Trans. Reconfigurable Technol. Syst. (TRETS)*, vol. 3, no. 1, pp. 1–27, 2010.

[31] V. Fisher and M. Drutarovsky, "Two methods of rijndael implementation in reconfigurable hardware," in *Cryptographic Hardware and Embedded Systems CHES*, 2001.

[32] S. Shah, R. Velegalati, J.-P. Kaps, and D. Hwang, "Investigation of DPA resistance of Block RAMs in cryptographic implementations on FPGAs," in *International Conference on ReConFigurable Computing and FPGAs – ReConFig'10*. IEEE, Dec 2010, pp. 274–279.

[33] M. U. Sharif, R. Shahid, M. Rogawski, and K. Gaj, "Use of embedded FPGA resources in implementations of five round three SHA-3 candidates," ECRYPT II Hash Workshop, 2011.

[34] M. Rogawski, "Analysis of implementation of hierocrypt3 algorithm (and its comparison to camellia algorithm) using altera devices," *Biuletyn WAT*, vol. 4, no. 620, Apr. 2004, first version available on http://eprint.iacr.org/2003/258.

[35] M. Rogawski, K. Gaj, and E. Homsirikamol, "Fpga-based adder for thousand bits and more," in *submitted to 2013 International Conference on Field Programmable Technology - FPT*, Dec 2013.

[36] M. Rogawski and K. Gaj, "Hardware acceleration for the tate pairing on supersingular edwards curves," *Journal of Cryptographic Engineering*, 2013, submitted.

[37] M. P. L. Das and P. Sarkar, "Pairing computation on twisted Edwards form elliptic curves," in *Pairing-Based Cryptography*, 2008.

[38] K. Gaj, J.-P. Kaps, V. Amirineni, M. Rogawski, E. Homsirikamol, and B. Y. Brewster, "ATHENa – Automated Tool for Hardware EvaluatioN: Toward fair and comprehensive benchmarking of cryptographic hardware using FPGAs," in *20th International Conference on Field Programmable Logic and Applications - FPL 2010*. IEEE, 2010, pp. 414–421, winner of the FPL Community Award.

[39] E. Homsirikamol, M. Rogawski, and K. Gaj, "Throughput vs. area trade-offs architectures of five Round 3 SHA-3 candidates implemented using Xilinx and Altera FPGAs," in *Workshop on Cryptographic Hardware and Embedded Systems CHES 2011*, ser. LNCS, B. Preneel and T. Takagi, Eds., vol. 6917. Springer Berlin / Heidelberg, Sep 2011, pp. 491–506.

[40] R. Shahid, M. U. Sharif, M. Rogawski, and K. Gaj, "Use of embedded FPGA resources in implementations of 14 Round 2 SHA-3 candidates," in *The 2011 International Conference on Field-Programmable Technology, FPT 2011*, Dec. 2011.

[41] SHA3, "Cryptographic Hash Algorithm Competition," http://csrc.nist.gov/groups/ST/hash/sha3/index.html, 2007.

[42] *Secure Hash Standard (SHS)*, National Institute of Standards and Technology (NIST), Oct. 2008, http://csrc.nist.gov/publications/fips/fips180-3/fips180-3_final.pdf.

[43] SHA3-ZOO, "SHA-3 Hardware Implementations," http://ehash.iaik.tugraz.at/wiki/SHA-3_Hardware_Implementations, 2009.

[44] GMU-CERG, "ATHENa Project website," http://cryptography.gmu.edu/athenadb/, 2010.

[45] G. Bertoni, J. Daemen, M. Peeters, and G. Van Assche, "The Keccak SHA-3 submission," Submission to NIST (Round 3), 2011, http://keccak.noekeon.org/Keccak-submission-3.pdf.

[46] S.-j. Chang, R. Perlner, W. E. Burr, , M. S. Turan, J. M. Kelsey, S. Paul, and L. E. Bassham, "Third-Round Report of the SHA-3 Cryptographic Hash Algorithm Competition," National Institute of Standards and Technology (NIST), Tech. Rep., 2012.

[47] D. J. Bernstein and T. Lange, "System for unified performance evaluation related to cryptographic operations and primitives," ONLINE, 2006, http://bench.cr.yp.to/supercop.html.

[48] C. Wenzel-Benner and J. Gräf, "eXternal Benchmarking eXtension (xbx)," ONLINE, 2010, http://xbx.das-labor.org/trac.

[49] *Advanced Encryption Standard (AES)*, National Institute of Standards and Technology (NIST), FIPS Publication 197, Nov 2001, http://csrc.nist.gov/publications/fips/fips197/fips-197.pdf.

[50] *Data Encryption Standard (DES)*, National Institute of Standards and Technology (NIST), FIPS Publication 46-3, Oct 1999, http://csrc.nist.gov/publications/fips/fips46-3/fips46-3.pdf.

[51] NIST, "Aes archive," http://csrc.nist.gov/archive/aes/, 2000.

[52] TrueCrypt Foundation, "Truecrypt," http://www.truecrypt.org/, 2012.

[53] Weeny Software, "Truecrypt," http://www.weenysoft.com/password-encryption-serpent.html, 2012.

[54] B. Schneier, "Twofish based products," http://www.schneier.com/twofish-products.html, 2000.

[55] R. L. Rivest, "Block encryption algorithm with data-dependent rotations," U.S. Patent 5724428, Mar. 1998.

[56] A. Schorr and M. Lukowiak, "Skein Tree Hashing on FPGA," in *Proc. ReConFig'10*, 2010, pp. 292–297.

[57] K. Guo and H. M. Heys, "A pipelined implementation of the grøstl hash algorithm and the advanced encyption standard," in *Canadian Conference on Electrical and Computer Engineering (CCECE 2013)*, 2013.

[58] N. At, J.-L. Beuchat, and I. San, "Compact Implementation of Threefish and Skein on FPGA," in *Proc. NTMS*, 2012.

[59] N. At, J.-L. Beuchat, E. Okamoto, I. San, and T. Yamazaki, "A low-area unified hardware architecture for the AES and the cryptographic hash function Grøstl," http://eprint.iacr.org/2012/535, Sep 2012.

[60] M. Pelnar, M. Muehlberghuber, and M. Hutter, "Putting together what fits together - græstl," in *11th International Conference, CARDIS 2012,*, 2012.

[61] J.-L. Beuchat, E. Okamoto, and T. Yamazaki, "A low-area unified hardware architecture for the AES and the cryptographic hash function ECHO," *Journal of Cryptographic Engineering*, vol. 1, no. 2, pp. 101–121, 2011.

[62] J. Daemen and V. Rijmen, *The Design of Rijndael.* Springer Verlag, 2002.

[63] RFC-6101, "http://www.ietf.org/rfc/rfc6151.txt," 2011.

[64] RFC-5246, "http://www.ietf.org/rfc/rfc5246.txt," 2008.

[65] RFC-4251, "http://www.ietf.org/rfc/rfc4251.txt," 2006.

[66] RFC-4301, "http://www.ietf.org/rfc/rfc4301.txt," 2005.

[67] RFC-4308, "http://www.ietf.org/rfc/rfc4308.txt," 2005.

[68] RFC-4309, "http://www.ietf.org/rfc/rfc4309.txt," 2005.

[69] P. Gauravaram, L. Knudsen, K. Matusiewicz, F. Mendel, C. Rechberger, M. Schlffer, and S. Thomsen, "Tweaks on grostl," 2011, http://www.groestl.info/Round3Mods.pdf.

[70] P. Gauravaram, L. R. Knudsen, K. Matusiewicz, F. Mendel, C. Rechberger, M. Schäffer, and S. S. Thomsen, "Grøstl – a SHA-3 candidate," Submission to NIST, Oct 2008, http://www.groestl.info/.

[71] M. Rogawski and K. Gaj, "Grøstl Tweaks and their Effect on FPGA Results," Dec. 2011, http://eprint.iacr.org/2011/635.pdf.

[72] S. Tillich, M. Feldhofer, M. Kirschbaum, T. Plos, J.-M. Schmidt, and A. Szekely, "High-speed hardware implementations of BLAKE, Blue Midnight Wish, CubeHash, ECHO, Fugue, Grøstl, Hamsi, JH, Keccak, Luffa, Shabal, SHAvite-3, SIMD, and Skein," Cryptology ePrint Archive, Report 2009/510, Nov 2009, http://eprint.iacr.org/.

[73] L. Dadda, M. Macchetti, and J. Owen, "The design of a high speed ASIC unit for the hash function SHA-256 (384, 512)," in *Proc. DATE'04*, vol. 3, 2004.

[74] M. Macchetti and L. Dadda, "Quasi-pipelined hash circuits," in *Proc. ARITH'17*, 2005, pp. 222–229.

[75] E. Homsirikamol, M. Rogawski, and K. Gaj, "Comparing hardware performance of fourteen round two SHA-3 candidates using FPGAs," Cryptology ePrint Archive, Report 2010/445, 2010.

153

[76] B. Jungk and S. Reith, "On fpga-based implementations of the sha-3 candidate grøstl," in *International Conference on Reconfigurable Computing (ReConFig)*, Dec 2010, pp. 316 – 321.

[77] S. Matsuo, M. Knežević, P. Schaumont, I. Verbauwhede, A. Satoh, K. Sakiyama, and K. Ota, "How can we conduct "fair and consistent" hardware evaluation for SHA-3 candidate?" Second SHA-3 Candidate Conference, Tech. Rep., 2010.

[78] B. Baldwin, N. Hanley, M. Hamilton, L. Lu, A. Byrne, M. O'Neill, and W. P. Marnane, "FPGA implementations of the round two SHA-3 candidates," in *2nd SHA-3 Candidate Conference*, 2010.

[79] K. Kobayashi, J. Ikegami, S. Matsuo, K. Sakiyama, and K. Ohta, "Evaluation of hardware performance for the SHA-3 candidates using SASEBO-GII," http://eprint.iacr.org/2010/010, 2010.

[80] X. Guo, S. Huang, L. Nazhandali, and P. Schaumont, "On the impact of target technology in SHA-3 hardware benchmark rankings," 2010, http://eprint.iacr.org/2010/536.pdf.

[81] K. Gaj, E. Homsirikamol, M. Rogawski, R. Shahid, and M. U. Sharif, "Comprehensive evaluation of high-speed and medium-speed implementations of five sha-3 finalists using xilinx and altera fpgas," Cryptology ePrint Archive, Report 2012/368, 2012, http://eprint.iacr.org/.

[82] Algotronix, "http://www.algotronix-store.com/," 2008.

[83] Helion, "http://www.heliontech.com/," 2011.

[84] M.-Y. Wang, H. C.-T. Su, Chih-Pin, and C.-W. Wu, "An HMAC processor with integrated SHA-1 and MD5 algorithms," in *Proc. ASP-DAC'04*, 2004, pp. 456–458.

[85] K. Järvinen, M. Tommiska, and J. Skytta, "A compact MD5 and SHA-1 co-implementation utilizing algorithms similarities," in *Proc. ERSA'05*, 2005, pp. 48–54.

[86] D. Cao, J. Han, and X.-Y. Zeng, "A reconfigurable and ultra low-cost VLSI implementation of SHA-1 and MD5 functions," in *Proc. ASICON'07*, 2007, pp. 862–865.

[87] T.-S. N. Chiu-Wah Ng and K.-W. Yip, "A unified architecture of MD5 and RIPEMD-160 hash algorithms," in *Proc. ISCAS'04*, vol. 2, 2004.

[88] T. Ganesh, M. Frederick, T. Sudarshan, and A. Somani, "Hashchip: A shared-resource multi-hash function processor architecture on FPGA," *Integration, the VLSI journal*, vol. 40, pp. 11–19, 2007.

[89] A. Salman, M. Rogawski, and J.-P. Kaps, "Efficient hardware accelerator for IPSEC based on partial reconfiguration on Xilinx FPGAs," in *ReConFig'11*, 2011, pp. 242–248.

[90] N. At, J.-L. Beuchat, E. Okamoto, I. San, and T. Yamazaki, "A low-area unied hardware architecture for the aes and the cryptographic hash function grøstl," 2012, report 2012/535, 2012.

[91] J.-L. Beuchat, E. Okamoto, and T. Yamazaki, "A low-area unified hardware architecture for the AES and the cryptographic hash function ECHO," Cryptology ePrint Archive, Report 2011/078, Sep 2012.

[92] P. Gauravaram, L. R. Knudsen, K. Matusiewicz, F. Mendel, C. Rechberger, M. Schäffer, and S. S. Thomsen, "Grøstl – a SHA-3 candidate," Submission to NIST, Oct 2008, http://www.groestl.info/.

[93] K. Gaj, E. Homsirikamol, M. Rogawski, R. Shahid, and M. U. Sharif, "Comprehensive Evaluation of High-Speed and Medium-Speed Implementations of Five SHA-3 Finalists Using Xilinx and Altera FPGAs," Mar 2012, third SHA-3 candidate conference.

[94] G. CERG, "GMU SHA-3 source codes," ONLINE, 2011, http://cryptography.gmu. edu/athena/index.php?id=source_codes.

[95] NIST, *The Keyed-Hash Message Authentication Code HMAC*, National Institute of Standards and Technology (NIST), FIPS Publication 198–1, Jul. 2008, http://csrc. nist.gov/publications/fips/fips198-1/FIPS-198-1_final.pdf.

[96] RFC-2104, "http://www.ietf.org/rfc/rfc2104.txt," 1997.

[97] RFC-6151, "http://www.ietf.org/rfc/rfc6151.txt," 2011.

[98] M. Dworkin, *NIST Special Publication 800-38A: Recommendation for Block Cipher Modes of Operation*, 2001, http://csrc.nist.gov/publications/nistpubs/800-38a/ sp800-38a.pdf.

[99] *Hardware Interface of a Secure Hash Algorithm (SHA)*, v. 1.4 ed., Cryptographic Engineering Research Group, George Mason University, Jan 2010.

[100] K. Parhi, *VLSI digital signal processing systems: design and implementation*. John Wiley & Sons, 1999.

[101] J. E. Bresenham, "Algorithm for computer control of a digital plotter," *IBM Syst. J.*, vol. 4, no. 1, pp. 25–30, Mar. 1965. [Online]. Available: http://dx.doi.org/10.1147/sj.41.0025

[102] X. Wu, "An efficient antialiasing technique," *SIGGRAPH Comput. Graph.*, vol. 25, no. 4, pp. 143–152, Jul. 1991. [Online]. Available: http://doi.acm.org/10.1145/ 127719.122734

[103] *Secure Hash Standard (SHS)*, National Institute of Standards and Technology (NIST), Oct. 2008, http://csrc.nist.gov/publications/fips/fips180-3/fips180-3_final.pdf.

[104] X. Lai and J. L. Massey, "A proposal for a new block encryption standard," in *Advances in Cryptology - EuroCrypt '90*, ser. Lecture Notes in Computer Science (LNCS), I. B. Damgård, Ed., vol. 473. Berlin: Springer-Verlag, 1990, pp. 389–404.

[105] P. Montgomery, "Modular multiplication without trial division," *Math. Comp.*, vol. 44, no. 170, pp. 519–521, 1985.

[106] A. F. Tenca and c. K. Koç, "A scalable architecture for montgomery multiplication," in *Workshop on Cryptographic Hardware and Embedded Systems (CHES99)*, ser. Lecture Notes in Computer Science, C. Paar and c. K. Koç, Eds., vol. 1717. Heidelberg: Springer-Verlag, 1999, pp. 94–108.

[107] D. Harris, R. Krishnamurthy, M. Anders, S. Mathew, and S. Hsu, "An improved unified scalable radix-2 montgomery multiplier," in *Computer Arithmetic*, 2005.

[108] M. Huang, K. Gaj, and T. El-Ghazawi, "New hardware architectures for montgomery modular multiplication algorithm," *IEEE Transactions on Computers*, 2011.

[109] C. McIvor, M. McLoone, and J. McCanny, "Modified Montgomery modular multiplication and RSA exponentiation techniques," in *Computers & Digital Techniques*, ser. IEEE Proceedings, vol. 151, Jul 2004, pp. 402–408.

[110] V. S. Miller, "Uses of elliptic curves in cryptography," in *Advances in Cryptology — CRYPTO '85*, ser. Lecture Notes in Computer Science (LNCS), H. C. Williams, Ed., vol. 218. Berlin: Springer-Verlag, 1986, pp. 417–426.

[111] N. Koblitz, "Elliptic curve cryptosystems," *Mathematics of Computation*, vol. 48, no. 177, pp. 203–209, Jan 1987.

[112] A. Menezes, "An introduction to pairing-based cryptography," *Recent Trends in Cryptography*, vol. 477, pp. 47–65, 2009.

[113] J. G. Earle, "Latched Carry Save Adder Circuit for Multipliers," U.S. Patent 3,340,388, Jul. 1965.

[114] T. Lange and D. J. Bernstein, "ECC Explicit-Formulas Database," http://www.hyperelliptic.org/EFD/index.html.

[115] J.-L. Beuchat and J.-M. Muller, "Automatic Generation of Modular Multipliers for FPGA Applications," *IEEE Transactions on Computers*, vol. 57, no. 12, pp. 1600–1613, 2008.

[116] G. Rosenberger, "Simultaneous Carry Adder," U.S. Patent 2,966,305, Dec. 1960.

[117] R. P. Brent and H. T. Kung, "A regular layout for parallel adders," *IEEE Transactions on Computers*, vol. C-31, no. 3, pp. 260–264, Mar 1982.

[118] P. Kogge and H. Stone, "A Parallel Algorithm for the Efficient Solution of a General Class of Recurrence Equations," *IEEE Transactions on Computers*, 1973.

[119] J. A. Solinas, "Generalized mersenne numbers," National Security Agency, Tech. Rep., 1999.

[120] *Digital Signature Standard DSS*, National Institute of Standards and Technology NIST, FIPS Publication 186-2, January 2000.

[121] N. Koblitz and A. Menezes, "Pairing-based cryptography at high security levels," in *Cryptography and Coding*, vol. 3796, 2005, pp. 13–36.

156

[122] M. Huang, K. Gaj, and T. El Gazawi, "New hardware architectures for montgomery modular multiplication algorithm," *Transactions on Computers*, 2010.

[123] G. T. Alexandre F. Tenca and C. etin K. Koc, "High-radix design of a scalable modular multiplier," in *Workshop on Cryptographic Hardware and Embedded Systems CHES*, 2001.

[124] D. Harris and K. Kelley, "Parallelized very high radix scalable montgomery multipliers," in *Proceedings of the 20th annual conference on Integrated circuits and systems design*, 2005, pp. 306–311.

[125] M. E. Kaihara and N. Takagi, "Bipartite modular multiplication," in *Workshop on Cryptographic Hardware and Embedded Systems—CHES 2005*. Berlin: Springer-Verlag, 2005.

[126] E. Öksüzoğlu and E. Savaş, "Parametric, secure and compact implementation of RSA on FPGA," in *Reconfigurable Computing and FPGAs, 2008. ReConFig '08. International Conference on*, Dec. 2008, pp. 391–396.

[127] K. Sakiyama, M. Knežević, J. Fan, B. Preneel, and I. Verbauwhede, "Tripartite modular multiplication," *Integration, the VLSI Journal*, vol. 44, no. 3, pp. 259–269, Sep 2011.

[128] P. Barrett, "Implementing the rivest shamir and adleman public key encryption algorithm on a standard digital signal processor," in *Advances in Cryptology, CRYPTO'86*, ser. Lecture Notes in Computer Science, A. Odlyzko, Ed., vol. 263. Heidelberg: Springer-Verlag, Jan 1987, pp. 311–326.

[129] A. Karatsuba and Y. Ofman, "Multiplication of multidigit numbers by automata," *Soviet Physics-Doklady*, vol. 7, pp. 595–596, 1963.

[130] S. Kawamura, M. Koike, F. Sano, and A. Shimbo, "Cox-Rower architecture for fast parallel Montgomery multiplication," in *Advances in Cryptology - EUROCRYPT 2000*, ser. Lecture Notes in Computer Science (LNCS), B. Preneel, Ed., vol. 1807. Heidelberg: Springer-Verlag, May 2000, pp. 523–538.

[131] G. Saldamlı, "Spectral modular arithmetic," Ph.D. dissertation, Oregon State University, 2005.

[132] S. Baktır, "Frequency domain finite field arithmetic for elliptic curve cryptography," Ph.D. dissertation, Worcester Polytechnic Institute, 2008.

[133] H. Orup, "Simplifying quotient determination in high-radix modular multiplication," in *Proceedings of the 12th Symposium on Computer Arithmetic*, Jul 1995, pp. 193–199.

[134] D. Suzuki, "How to maximize the potential of fpga resources for modular exponentiation," in *Workshop on Cryptographic Hardware and Embedded Systems—CHES 2007*. Berlin: Springer-Verlag, 2007.

[135] D. Suzuki and T. Matumoto, "How to maximize the potential of FPGA based DSPs for modular exponentiation," *IEICE Trans. Fundamentals*, vol. E94-A, no. 1, January 2011.

[136] A. Toom, "The complexity of a scheme of functional elements realizing the multiplication of integers," *Soviet Matematics - Doklady*, 1963, translation by N.Friedman.

[137] A. Schönhage and V. Strassen, "Schnelle multiplikation großer zahlen," *Computing*, vol. 7, no. 3–4, pp. 281–292, Sep 1971.

[138] M. Fürer, "Faster integer multiplication," in *39th ACM Symposium on Theory of computing STOC*, 2007.

[139] E. A. Michalski and D. A. Buell, "A scalable architecture for RSA cryptography on large FPGAs," in *14th Annual IEEE Symposium on Field-Programmable Custom Computing Machines (FCCM'06)*, 2006.

[140] J.-C. Bajard, L.-S. Didier, and P. Kornerup, "An RNS montgomery modular multiplication algorithm," *IEEE Transactions on Computers*, vol. 47, no. 7, pp. 766–776, Jul 1998.

[141] J.-C. Bajard and L. Imbert, "Brief contributions: a full RNS implementation of RSA," *IEEE Transactions on Computers*, vol. 53, no. 6, pp. 769–774, Jun 2004.

[142] G. Saldamlı and c. Koç, "Spectral modular exponentiation," in *18th IEEE Symposium on Computer Arithmetic*, 2007, (ARITH'07).

[143] D. N. Amanor, "Efficient hardware architectures for modular multiplication," Master's thesis, The University of Applied Sciences Offenburg, Feb. 2005, co-supervisor of this thesis was Christoff Paar.

[144] A. M.AbdelFattah, A. M.Bahaa El-Din, and H. M.A.Fahmy, "Efficient implementation of modular multiplication on fpgas based on sign detection," in *4th International Design and Test Workshop (IDT)*, 2009.

[145] M. E. Kaihara, "Studies on modular arithmetic hardware algorithms for public-key cryptography," Ph.D. dissertation, Nagoya University, 2006.

[146] A. J. Menezes, P. C. van Oorschot, and S. Vanstone, *Handbook of Applied Cryptography*. CRC Press Inc., 1997.

[147] A. D. Booth, "A signed binary multiplication technique," *The Quarterly Journal of Mechanics and Applied Mathematics*, vol. IV, 1950.

[148] *MPC 185 Hardware Reference Manual*, 2nd ed., Freescale, Short, Matthew, Aug. 2003.

[149] D. Stebila and J. Green, "Elliptic curve algorithm integration in the secure shell transport layer," Network Working Group, Tech. Rep., Dec 2009, http://www.openssh.org/txt/rfc5656.txt.

[150] "ESCRYPT embedded security," https://www.escrypt.com/products/.

[151] Certicom, "Security builder crypto," http://www.certicom.com/images/pdfs/sb/ds-crypto-102210.pdf.

[152] N. P. Smart, "The Hessian form of an elliptic curve," in *Proceedings of the 3rd International Workshop on Cryptographic Hardware and Embedded Systems, CHES 2001*, 2001, pp. 118–125.

[153] N. Koblitz, "CM-curves with good cryptographic properties," in *Advances in Cryptology CRYPTO*, vol. 576, 1991, pp. 279–287.

[154] P.-Y. Liardet and N. Smart, "Preventing SPA/DPA in ECC systems using the Jacobi form," in *Proceedings of the 3rd International Workshop on Cryptographic Hardware and Embedded Systems, CHES 2001*, 2001.

[155] P. L. Montgomery, "Speeding the Pollard and elliptic curve methods of factorization," *Mathematics of Computation*, vol. 48, pp. 243–264, 1987.

[156] C. Doche, T. Icart, and D. R. Kohel, "Efficient scalar multiplication by isogeny decompositions," in *9th International Conference on Theory and Practice in Public-Key Cryptography*, 2006, pp. 191–206.

[157] H. M. Edwards, "A normal form for elliptic curves," *Bulletin of the American Mathematical Society*, vol. 44, no. 3, p. 393422, July 2007.

[158] D. J. Bernstein, P. Birkner, M. Joye, T. Lange, and C. Peters, "Twisted edwards curves," in *Progress in Cryptology AFRICACRYPT*, 2008.

[159] D. J. Bernstein and T. Lange, "Inverted Edwards coordinates," in *Proceedings of the 17th international conference on Applied algebra, algebraic algorithms and error-correcting codes*, 2007.

[160] D. J. Bernstein, "Batch binary Edwards," in *Advances in Cryptology Crypto 2009*, 2009.

[161] D. J. Bernstein, T. Lange, and R. R. Farashahi, "Binary Edwards curves," in *Cryptographic Hardware and Embedded Systems, CHES 2008*, Aug. 2008, pp. 244–265.

[162] G. Frey and H.-G. Rück, "A remark concerning m-divisibility and the discrete logarithm in the divisor class group of curves," *Mathematics of Computation*, vol. 62, pp. 865–874, 1994.

[163] A. Menezes, T. Okamoto, and A. Vanstone, "Reducing elliptic curve logarithms to a finite field," *IEEE Transactions on Information Theory*, vol. 39, no. 5, pp. 1639–1645, Sep 1993.

[164] V. S. Miller, "Short programs for functions on curves," May 1986, unpublished manuscript from IBM's Watson Research Center.

[165] A. Joux, "A one round protocol for tripartite Diffie-Hellman," in *Algorithmic Number Theory: 4th International Symposium*, ser. Lecture Notes in Computer Science (LNCS), vol. 1838. Springer-Verlag, 2000, pp. 385–394.

[166] D. Boneh and M. Franklin, "Identity-based encryption from the weil pairing," in *Advances in Cryptology - CRYPTO 2001*, ser. Lecture Notes in Computer Science (LNCS), vol. 2139. Springer-Verlag, 2001, pp. 213–229.

[167] J. Cha and J. Cheon, "An identity-based signature from gap Diffie-Hellman groups," in *Public-Key Cryptography PKC 2003*, ser. Lecture Notes in Computer Science, vol. 2567. Springer, 2003, pp. 18–30.

[168] D. Boneh, B. Lynn, and H. Shacham, "Short signatures from the weil pairing," *Journal of Cryptology*, vol. 17, no. 4, pp. 297–319, Sep 2004.

[169] P. S. L. M. Barreto, S. D. Galbraith, C. O. hÉigeartaigh, and M. Scott, "Efficient pairing computation on supersingular abelian varieties," *Designs, Codes and Cryptography*, 2007.

[170] F. Hess, N. P. Smart, and F. Vercauteren, "The Eta pairing revisisted," 2006, http://eprint.iacr.org/2006/110.

[171] E. Lee, H.-S. Lee, and C.-M. Park, "Efficient and generalized pairing computation on abelian varieties," *IEEE Transaction on Information Theory*, 2009.

[172] F. Vercauteren, "Optimal pairings," *IEEE Transaction on Information Theory*, vol. 56, no. 1, 2010.

[173] J.-L. Beuchat, J. Detrey, N. Estibals, E. Okamoto, and F. Rodrguez-Henrquez, "Hardware accelerator for the tate pairing in characteristic three based on karatsuba-ofman multipliers," in *Workshop on Cryptographic Hardware and Embedded Systems CHES*, 2009.

[174] J. Fan, F. Vercauteren, and I. Verbauwhede, "Faster fp-arithmetic for cryptographic pairings on barreto-naehrig curves," in *Workshop on Cryptographic Hardware and Embedded Systems CHES*, 2009.

[175] N. Estibals, "Compact hardware for computing the tate pairing over 128-bit-security supersingular curves," in *4th International Conference on Pairing-Based Cryptography - Pairing*, 2010.

[176] D. F. Aranha, J.-L. Beuchat, J. Detrey, and E. N., "Optimal eta pairing on supersingular genus-2 binary hyperelliptic curves," 2010, submitted to CT-RSA 2012.

[177] J.-L. Beuchat, J. Gonzlez-Diaz, S. Mitsunari, E. Okamoto, F. Rodriguez-Henriquez, and T. Teruya, "High-speed software implementation of the optimal ate pairing over barretonaehrig curves," in *International Conference on Pairing-Based Cryptography - Pairing*, 2010.

[178] R. C. Cheung, S. Duquesne, J. Fan, N. Guillermin, I. Verbauwhede, and G. X. Yao, "Fpga implementation of pairings using residue number system and lazy reduction," in *Workshop on Cryptographic Hardware and Embedded SystemsCHES 2011*, 2011.

[179] S. Ghosh, D. Roychowdhury, and A. Das, "High speed cryptoprocessor for t pairing on 128-bit secure supersingular elliptic curves over characteristic two fields," in *Workshop on Cryptographic Hardware and Embedded SystemsCHES 2011*, 2011.

[180] C. Arene, T. Lange, M. Naehrig, and C. Ritzenthaler, "Faster computation of the Tate pairing," *Journal of Number Theory*, pp. 842–857, 2010.

[181] *Fact Sheet NSA Suite B Cryptography*, National Security Agnecy, 2008.

[182] *Virtex-6 FPGA Configurable Logic Block*, Feb. 2012.

[183] *Virtex-6 FPGA Memory Resources*, Apr. 2011.

[184] *Virtex-6 FPGA DSP48E1 Slice*, Feb. 2011.

[185] *Stratix IV Device Handbook*, Altera Corp., Sep. 2012.

[186] L. Martin, *Introduction to Identity Based Cryptography.* Artech House, 2008.

[187] P. Barreto and M. Naehrig, "Pairing-friendly elliptic curves of prime order," in *Workshop on Selected Areas in Cryptography*, ser. Lecture Notes in Computer Science,, vol. 3897. Springer, 2006, pp. 319–331.

[188] S. Ghosh, D. Mukhopadhyay, and D. Roychowdhury, "High speed flexible pairing cryptoprocessor on FPGA platform," in *International Conference on Pairing-Based Cryptography - Pairing 2010*, 2010.

[189] D. Kammler, D. Zhang, P. Schwabe, H. Scharwaechter, M. Langenberg, D. Auras, G. Ascheid, and R. Mathar, "Designing an ASIP for cryptographic pairings over Barreto-Naehrig curves," in *Cryptographic Hardware and Embedded Systems*, vol. 5747, 2009, pp. 254–71.

[190] P. C. van Oorschot and M. J. Wiener, "Parallel collision search with cryptanalytic applications," *Journal of Cryptology*, pp. 1–18, 1999.

[191] J. W. Bos, M. Kaihara, T. Kleinjung, A. K. Lenstra, and P. L. Montgomery, "On the security of 1024-bit RSA and 160-bit elliptic curve cryptography," 2009, http://eprint.iacr.org/2009/389.

[192] A. Joux, R. Lercier, N. Smart, and F. Vercauteren, "The number field sieve in the medium prime case," in *Advances in Cryptology - CRYPTO '06*, 2006.

[193] O. Schirokauer, "The number field sieve for integers of low weight," http://eprint.iacr.org/2006/107.

[194] Xilinx, *Virtex-6 Family Overview*, Jan. 2012.

[195] *Stratix V Device Handbook*, Altera Corp., March 2013.

[196] *The GNU Multiple Precision Arithmetic Library*, 5th ed., 2010.

[197] U. of Sydney, "Magma computational algebra system," http://magma.maths.usyd.edu.au/magma/.

[198] J. Fan, F. Vercauteren, and I. Verbauwhede, "Efficient hardware implementation of fp-arithmetic for pairing-friendly curves," *Transaction on Computers*, 2011.

[199] V. Amirineni, "ATHENa – Automated Tool for Hardware EvaluatioN: Software Environment for fair and comprehensive performance evaluation of cryptographic hardware using FPGAs," Master's thesis, George Mason University, July 2010.

[200] B. Brewster, "Distributed computing and orchestration algorithms for fair and efficient benchmarking of cryptographic cores in fpgas," Master's thesis, George Mason University, 2011.

[201] E. ECRYPT, "Nessie archive," https://www.cosic.esat.kuleuven.be/nessie/, 2004.

[202] J. Government, "Cryptrec archive," http://www.cryptrec.go.jp/english/, 2004.

[203] E. ECRYPT, "estream archive," http://www.ecrypt.eu.org/stream/, 2000.

[204] "Caesar archive," http://competitions.cr.yp.to/caesar.html, 2000.

[205] K. Gaj and P. Chodowiec, "Comparison of the hardware performance of the AES candidates using reconfigurable hardware," *Proc. 3rd Advanced Encryption Standard Conference*, pp. pp. 40–54, April 2000.

[206] A. Elbirt, W. Yip, B. Chetwynd, and C. Paar, "An FPGA Implementation and Performance Evaluation of the AES Block Cipher Candidate Algorithm Finalists," in *The Third Advanced Encryption Standard Candidate Conference*, 2000.

[207] D. Hwang, M. Chaney, S. Karanam, N. Ton, and K. Gaj, "Comparison of FPGA-targeted hardware implementations of eSTREAM stream cipher candidates," in *State of the Art of Stream Ciphers Workshop, SASC 2008, Lausanne, Switzerland*, Feb 2008, pp. 151–162.

[208] M. Rogawski, "Hardware evaluation of estream candidates: Grain, lex, mickey128, salsa20 and trivium," in *State of the art of stream ciphers*, 2007.

[209] F. K. Gürkaynak, K. Gaj, B. Muheim, E. Homsirikamol, C. Keller, M. Rogawski, H. Kaeslin, and J.-P. Kaps, "Lessons learned from designing a 65nm ASIC for evaluating third round SHA-3 candidates," Mar 2012, third SHA-3 candidate conference.

[210] S. Drimer, "Security for volatile FPGAs," Ph.D. Dissertation, University of Cambridge, Computer Laboratory, Nov 2009, uCAM-CL-TR-763.

[211] M. Knežević, K. Kobayashi, J. Ikegami, S. Matsuo, A. Satoh, U. Kocabaş, J. Fan, T. Katashita, T. Sugawara, K. Sakiyama, I. Verbauwhede, K. Ohta, N. Homma, and T. Aoki, "Fair and consistent hardware evaluation of fourteen round two SHA-3 candidates," *IEEE Transactions on VLSI*, pp. 827–840, 2011.

[212] S. Tillich, M. Feldhofer, M. Kirschbaum, T. Plos, J.-M. Schmidt, and A. Szekely, "Uniform evaluation of hardware implementations of the round-two SHA-3 candidates," Second SHA-3 Candidate Conference, UCSB, CA, Aug 2010, http://csrc.nist.gov/groups/ST/hash/sha-3/Round2/Aug2010/documents/papers/ TILLICH_sha3hw.pdf.

[213] M. Srivastav, X. Guo, S. Huang, D. Ganta, M. B. Henry, L. Nazhandali, and P. Schaumont, "Design and benchmarking of an asic with five sha-3 finalist candidates," *Microprocessors and Microsystems - Embedded Hardware Design*, vol. 37, no. 2, pp. 246–257, 2013, http://rijndael.ece.vt.edu/schaum/papers/2012micpro.pdf.

[214] R. Shortt, D. Knol, and B. Jackson, *ExploreAhead: A Methodical Approach to Improved QOR through Implementation Tools*, Xilinx Inc., 2007.

[215] "Design space explorer," ONLINE, http://www.altera.com/support/examples/quartus/exm-dse.html.

[216] C. De Canniére, "estream testing framework," 2005, http://www.ecrypt.eu.org/stream/perf/.

[217] C. Wenzel-Benner and J. Gräf, "XBX: eXternal Benchmarking eXtension for the SUPERCOP crypto benchmarking framework," in *Cryptographic Hardware and Embedded Systems, CHES 2010*, ser. LNCS, S. Mangard and F.-X. Standaert, Eds., vol. 6225. Berlin / Heidelberg: Springer, 2010, pp. 294–305.

[218] "ATHENa project website," ONLINE, 2010, http://cryptography.gmu.edu/athena.

[219] R. Chaves, G. Kuzmanov, L. Sousa, and S. Vassiliadis, "Improving sha-2 hardware implementations," in *Cryptographic Hardware and Embedded Systems - CHES 2006*, Oct 2006, pp. 298–310.

[220] K. Gaj, E. Homsirikamol, and M. Rogawski, "Comprehensive Comparison of Hardware Performance of Fourteen Round 2 SHA-3 Candidates with 512-bit Outputs Using Field Programmable Gate Arrays," Aug. 2010, second SHA-3 Candidate Conference.

[221] E. Homsirikamol, M. Rogawski, and K. Gaj, "Comparing hardware performance of round 3 SHA-3 candidates using multiple hardware architectures in Xilinx and Altera FPGAs," ECRYPT II Hash Workshop 2011, May 2011.

[222] K. Gaj, E. Homsirikamol, M. Rogawski, R. Shahid, and M. U. Sharif, "Comprehensive Evaluation of High-Speed and Medium-Speed Implementations of Five SHA-3 Finalists Using Xilinx and Altera FPGAs," Jun. 2012, http://eprint.iacr.org/2012/368.

[223] J.-P. Kaps, P. Yalla, K. K. Surapathi, B. Habib, S. Vadlamudi, S. Gurung, and J. Pham, "Lightweight implementations of SHA-3 Candidates on FPGAs," in *Proc. Indocrypt'11*, 2011, pp. 270–289.

[224] B. Jungk, "Evaluation of compact fpga implementations for all sha-3 finalists," Mar 2012, third SHA-3 candidate conference.

[225] D. J. Bernstein, "Curve25519: new diffie-hellman speed records," in *PKC 2006: 9th International Workshop on Practice and Theory in Public Key Cryptography*, 2006.

[226] D. J. Bernstein, N. Duif, T. Lange, P. Schwabe, and B.-Y. Yang, "High-speed high-security signatures," in *Workshop on Cryptographic Hardware and Embedded SystemsCHES 2011*, 2011.

[227] *Digital Signature Standard, FIPS 186-3*, NIST.

[228] R. Struik, "Cryptography for highly constrained networks," ONLINE, http://www.nist.gov/itl/csd/ct/ceta-2011-agenda.cfm.

[229] P. Schaumont, *A Practical Introduction to Hardware/Software Codesign.* Springer, 2013.

[230] *Partial Reconfiguration Guide*, 12nd ed., Xilinx Inc., Oct. 2010, http://www.xilinx.com/support/documentation/sw_manuals/xilinx12_3/ug702.pdf.

Curriculum Vitae

Marcin Rogawski received his Master of Science Degree in Institute of Mathematics and Cryptology, Faculty of Cybernetics, from Military University of Technology, Poland, in 2003. From 2003 to 2007, he worked as a System Architect in Prokom Software S.A., Poland, where he developed high-speed and low-area cryptographic coprocessors in Freescale PowerPC and Hitachi H8s environments in IPSec supporting family of devices: *IP Nefryt encryptors*. From 2007 to 2008, he work as a Senior Software Engineer in MKS Sp. Z.o.o., Poland, where he worked on commercial antivirus products: *mks_vir 9.0.* and *Awangarda*.

He commenced his Ph.D. studies in the Department of Electrical & Computer Engineering at George Mason University in 8/2008, where he served as a research assistant, developing several digital designs for cryptographic applications, and a teaching assistant for several undergraduate/graduate courses.

His research interests include cryptography and digital security, digital design, hardware/software co-design, and reconfigurable computing for scientific algorithms.

Publications:

1. M. Rogawski - Analysis of Implementation of HIEROCRYPT-3 algorithm using ALTERA devices, *Biuletyn WAT*, Poland, Apr. 2004 **(paper based on the MS thesis awarded first place in the Contest for the best MS Thesis in the area of Cryptography and Information Security defended at a Polish university in the period 2002-2003)**

2. M. Rogawski - Stream ciphers in reconfigurable device, *ENIGMA IX*, Warsaw, Poland, May 2005

3. M. Rogawski - Hardware-oriented stream ciphers, *ENIGMA X* Warsaw, Poland, May 2006

4. M. Rogawski - Hardware evaluation of eSTREAM Candidates: Grain, Lex, Mickey128, Salsa20 and Trivium, *The State of the Art of Stream Ciphers SASC 2007*, Bochum, Germany, Feb. 2007

5. M. Rogawski - Hardware evaluation of eSTREAM Candidate - comprehensive evaluation, *ENIGMA XI*, Warsaw, Poland, May 2007

6. K. Gaj, S. Kwon, P. Baier, P. Kohlbrenner, H. Le, M. Khaleeluddin, R. Bachimanchi, M. Rogawski - Area-Time Efficient Implementation of the Elliptic Curve Method of Factoring in Reconfigurable Hardware for Application in the Number Field Sieve, *IEEE Transactions on Computers*, Dec. 2009

7. K. Gaj, E. Homisirikamol and M. Rogawski - Fair and Comprehensive Methodology for Comparing Hardware Performance of Fourteen Round Two SHA-3 Candidates using FPGAs, *Workshop on Cryptographic Hardware and Embedded Systems 2010 (CHES 2010)*, Santa Barbara, CA, USA, Aug. 2010

8. K. Gaj, E. Homisirikamol and M. Rogawski - Comprehensive Comparison of Hardware Performance of Fourteen Round 2 SHA-3 Candidates with 512-bit Outputs Using Field Programmable Gate Arrays, *The 2nd SHA-3 Candidate Conference*, Santa Barbara, CA, USA, Aug. 2010

9. K. Gaj, J.-P. Kaps, V. Amirineni, M. Rogawski, E. Homsirikamol, B. Y. Brewster - ATHENa - Automated Tool for Hardware EvaluatioN: Toward Fair and Comprehensive Benchmarking of Cryptographic Hardware using FPGAs, *20th International Conference on Field Programmable Logic and Applications*, Milano, Italy, Aug. 2010 - **Best Paper in the category "FPL Community Award"**

10. E. Homsirikamol, M. Rogawski, and K. Gaj - Comparing Hardware Performance of Round 3 SHA-3 Candidates using Multiple Hardware Architectures in Xilinx and Altera FPGAs, *Ecrypt II Hash workshop*, Tallinn, Estonia, May, 2011

11. M. U. Sharif, R. Shahid, M. Rogawski, K. Gaj - Use of Embedded FPGA Resources in Implementations of Five Round Three SHA-3 Candidates *Ecrypt II Hash workshop*, Tallinn, Estonia, May 19-20 2011

12. E. Homisirikamol, M. Rogawski and K. Gaj - Throughput vs. Area Trade-oArchitectures of Five Round 3 SHA-3 Candidates Implemented Using Xilinx and Altera FPGAs, *Workshop on Cryptographic Hardware and Embedded Systems 2011 (CHES 2011)*, Nara, Japan, Sep. 2011

13. A. Salman, M. Rogawski and J.-P. Kaps - Efficient Hardware Accelerator for IPSec based on Partial Reconfiguration on Xilinx FPGAs, *2011 International Conference on ReConFigurable Computing and FPGAs - ReConFig 2011*, Cancun, Mexico, Dec. 2011

14. R. Shahid, M. U. Sharif, M. Rogawski and K. Gaj - Use of Embedded FPGA Resources in Implementations of 14 Round 2 SHA-3 Candidates, *The 2011 International Conference on Field-programmable Technology (FPT 2011)*, New Delhi, India, Dec. 2011

15. F. Gurkaynak, K. Gaj, B. Muheim, E. Homsirikamol, C. Keller, M. Rogawski, H. Kaeslin, J.-P. Kaps - Lessons Learned from Designing a 65nm ASIC for Evaluating Third Round SHA-3 Candidates, *The 3rd SHA-3 Candidate Conference*, Washington DC, USA, Mar. 2012

16. K. Gaj, E. Homsirikamol, M. Rogawski, R. Shahid, M. U. Sharif - Comprehensive Evaluation of High-Speed and Medium-Speed Implementations of Five SHA-3 Finalists Using Xilinx and Altera FPGAs, *The 3rd SHA-3 Candidate Conference*, Washington DC, USA, Mar. 2012

17. M. Rogawski and K. Gaj - A High-Speed Unified Hardware Architecture for the AES and SHA-3 Candidate Grøstl, *15th EUROMICRO Conference on Digital System Design -DSD'12*, Izmir, Turkey, 5-8 September 2012

18. P. Morawiecki, M. Srebrny, E. Homsirikamol and M. Rogawski - Security margin evaluation of SHA-3 contest finalists through SAT-based attacks, *11th International Conference on Information Systems and Industrial Management*, Venice, Italy, Sep. 2012 - **Best Student Paper Award**

19. M. Rogawski, K. Gaj and E.Homsirikamol - A High-Speed Unified Hardware Architecture for 128 and 256-bit Security Levels of AES and Grøstl - *accepted to "Embedded Hardware Design: Microprocessors and Microsystems"*

20. M. Rogawski, K. Gaj, E. Homsirikamol - FPGA-based adder for thousand bits and more - *submitted to FPT'13*

21. M. Rogawski, K. Gaj - Hardware Acceleration for the Tate Pairing on supersingular Edwards Curves - *submitted to "Journal of Cryptographic Engineering"*

Technical Reports:

1. E. Homsirikamol, M. Rogawski, and K. Gaj - Comparing Hardware Performance of Fourteen Round Two SHA-3 Candidates Using FPGAs, *Cryptology ePrint Archive: Report 2010/445*, first version - Aug. 2010

2. M. Rogawski and K. Gaj - Groestl Tweaks and their Effect on FPGA Results, *Cryptology ePrint Archive: Report 2011/635*, first version - Nov. 2011

3. K. Gaj, E. Homsirikamol, M. Rogawski, R. Shahid and M. U. Sharif - Comprehensive Evaluation of High-Speed and Medium-Speed Implementations of Five SHA-3 Finalists Using Xilinx and Altera FPGAs, *Cryptology ePrint Archive: Report 2012/368*, first version - Jun. 2012